INTEGRATION OF POD-DEIM TO FLOW-BASED UPSCALING METHOD IN RESERVOIR SIMULATION MODEL ORDER REDUCTION

A Thesis

by

JINCHENG LI

Submitted to the Office of Graduate and Professional Studies of
Texas A&M University
in partial fulfillment of the requirements for the degree of

MASTER OF SCIENCE

Chair of Committee,	Eduardo Gildin
Committee Members,	Michael King
	Marcelo Sanchez
Head of Department,	Jeffery Spath

May 2021

Major Subject: Petroleum Engineering

ABSTRACT

This thesis proposes a new workflow for mitigating computational effort in reservoir simulation by integrating two methods of complexity reduction used independently in reservoir applications: flow-based upscaling and projection-based reduced-order modeling. The objective of this thesis is to combine the strengths of the discrete interpolation technique (DEIM), such as the selection of few interpolation points, to leverage the permeability calculation and averaging obtained from flow-based upscaling, in order to increase the production rate accuracy of the modified upscaled reservoir model.

The new proposed methodology uses 6 specific one-layer models of the SPE 10 Comparative Project as the base models: (1) Layer 1, 10, 30 from the Tarbert Formation, and (2) Layer 50, 60, and 70 from the Upper Ness formation. Besides, 2 3D models of the SPE 10, layer 1-6, and layer 50-55 is also used for the case study. All cases are two-phase oil-water saturated black oil reservoir model with no gas. A normal 5-spot producing scheme is used with 4 producing wells at four corners and the water injection well located at the center of the reservoir.

To prove the concept and assess the efficiency of the new integrated methodology, the study is divided into three parts. First, solely upscaling is applied by conducting arithmetic, harmonic, and flow-based upscaling. Second, model reduction is performed by applying the Proper-Orthogonal Decomposition POD-DEIM calculation on the residuals of the fine-scale model results and obtain the DEIM index. Lastly, the proposed new method utilized POD-DEIM selection results and incorporated it into the flow-based upscaling permeability modification.

In the 2D cases, 2 by 2 upscaling is utilized to upscale the model. For the 3D cases, a 2 by 2 by 2 upscaling is performed. The flow-based upscaling model has a production error of approximately 20% compared with the original fine-scale model. However, after utilizing different

numbers of DEIM index points to modify the permeability, the new model has a production error decreases of approximately 5% on most of the wells. The remaining wells have a production error similar to the flow-based model.

Overall, the integration of POD-DEIM and flow-based upscaling has been seen to decrease the production error of upscaled model and can be used for decreasing model complexity while maintaining better production matching accuracy than before.

DEDICATION

To my family for their everlasting encouragement and supports.

To the memory of my grandmother and my grandfather.

ACKNOWLEDGEMENTS

I would like to express my deepest gratitude to Dr. Eduardo Gildin, my graduate advisor and the chair of my dissertation committee for his constant kindness, patience, encouragement, and support in guiding and enlightening me through my research work. His time and guidance to me are the most crucial in completion of my research thesis.

I would like to thank Dr. Michael King and Dr. Marcelo Sanchez, the members of my dissertation committee for their valuable suggestions and opinions on my work.

I would like to thank all the professors who have instructed and supported me during my education at Texas A&M University.

CONTRIBUTORS AND FUNDING SOURCES

Contributors

This research thesis is supervised by the dissertation committee consisting of Dr. Eduardo Gildin [chair] and Dr. Michael King [member] of the Harold Vance Department of Petroleum Engineering and Dr. Marcelo Sanchez [member] of the Zachry Department of Civil & Environmental Engineering.

Funding sources

This work is supported by a fellowship from the Department of Petroleum Engineering of Texas A&M University and Gildin Research Fellowship.

NOMENCLATURE

P_o	Reservoir pressure
R	Residual matrix from full model
S_w	Water saturation
$highfraction$	Fraction term computed with k_{high}
$lowfraction$	Fraction term computed with k_{low}
k_a	Arithmetic upscaled permeability
k_{ah}	Wiener bound
k_h	Harmonic upscaled permeability
$\{k_{high}\}$	Fine cells where permeability is greater than flow-based coarse permeability
$\{k_{low}\}$	Fine cells where permeability is lower than flow-based coarse permeability
k_{fine}	Fine cell permeability
k_p	Flow-based upscaled permeability
$k_{pDEIM\ i,j}$	DEIM-modified permeability
X	Snapshots matrix
ϕ_X	Projection matrix from snapshots
ϕ_R	Projection matrix from residual
$\overrightarrow{\wp}$	POD-DEIM indices

TABLE OF CONTENTS

Page

ABSTRACT ii

DEDICATION iv

ACKNOWLEDGEMENTS v

CONTRIBUTORS AND FUNDING SOURCES vi

Contributors vi
Funding Sources vi

NOMENCLATURE vii

TABLE OF CONTENTS viii

LIST OF FIGURES x

LIST OF TABLES xiv

1. INTRODUCTION 1

1.1 Primary Objectives 5
1.2 Thesis Scope 6

2. METHODOLOGY 7

2.1 Reservoir Simulation 7
2.2 Arithmetic and Harmonic Upscaling 9
2.3 Flow-based Upscaling 10
2.4 POD-DEIM 13
2.5 The New Method: Modification of Flow-based Permeability with POD-DEIM Index 16

3. APPLICATION OF THE PROPOSED METHODOLOGY 20

3.1 POD-DEIM 27
3.2 Upscaling and DEIM-modified Upscaling 37
3.3 Flow-Based Upscaling vs DEIM-Modified Upscaling 47
3.4 Time Reduction and Production Rate Error Comparison 73

Page

4. CONCLUSIONS 77

4.1 Summary 77
4.2 Conclusions 78
4.3 Recommendation for Future Work 80

REFERENCES 81

LIST OF FIGURES

FIGURE		Page
1	Representation of the snapshot (solution) matrix. Rows are time evaluation of the pressure and saturation; columns are solution in each time step	8
2	An example of coarse block permeability. A 9 x 9 fine scale block is averaged into a single coarse block	9
3	Illustration of calculating flow-based upscaled permeability in x direction. Here, one imposes a constant pressure boundary condition in each side of the reservoir	12
4	DEIM greedy algorithm pseudocode, input $U\beta$ equivalent for ϕR from SVD of Residual, output $\wp$ is the DEIM index, equivalent as reservoir grid index	15
5	Illustration of $\{khigh\}$ and $\{klow\}$	18
6	Well location configurations for the 3D SPE 10 model. Here, we show 6 layers of the SPE 10 benchmark	21
7	Original model permeability, layer 1 and layer 10	22
8	Original model permeability, layer 30 and layer 50	22
9	Original model permeability, layer 60 and layer 70	23
10	Original model oil rate for the four wells, layer 1, 10 and 30	24
11	Original model oil rate for the four wells, layer 50, 60, and 70	25
12	Original 3D model oil rate for the four wells, layer 1-6 and layer 50-55	26
13	100 by 100 uniform grid oil pressure at the end of simulation	28
14	100 by 100 uniform grid water saturation at the end of simulation	28
15	100 by 100 uniform grid oil and water production rate	29
16	A DEIM index map of 100 by 100 grids oil and water at $nrF = 4000$. Red circles are referenced to the oil front, blue circles are referenced to the water front	30
17	A DEIM index map of 100 by 100 grids oil and water at $nrF = 3000$. Red circles are referenced to the oil front, blue circles are referenced to the water front	30

18 A DEIM index map of 100 by 100 grids oil and water at $nrF = 2000$. Red circles are referenced to the oil front, blue circles are referenced to the water front 31

19 A DEIM index map of 100 by 100 grids oil and water at $nrF = 1000$. Red circles are referenced to the oil front, blue circles are referenced to the water front 31

20 Production rate and error comparison between full model and POD-DEIM reduced case, $nrF = 4000$ 32

21 Production rate and error comparison between full model and POD-DEIM reduced case, $nrF = 3000$ 33

22 Production rate comparison between full model and POD-DEIM reduced case: Not converging production, $nrF = 2000$ 34

23 Not Converging Production Rat Production rate comparison between full model and POD-DEIM reduced case: Not converging production, $nrF = 1000$ 35

24 Time consumption for computing DEIM index as a function of the number of DEIM interpolation points. Y axis is time in log scale 37

25 Layer 1 kx flow-based permeability vs DEIM-modified permeability 39

26 Layer 1 DEIM modified upscaling water saturation map 40

27 Layer 10 kx flow-based permeability vs DEIM-modified permeability 41

28 Layer 10 DEIM modified upscaling water saturation map 41

29 Layer 30 kx flow-based permeability vs DEIM-modified permeability 42

30 Layer 30 DEIM modified upscaling water saturation map 42

31 Layer 50 kx flow-based permeability vs DEIM-modified permeability 43

32 Layer 50 DEIM modified upscaling water saturation map 44

33 Layer 60 kx flow-based permeability vs DEIM-modified permeability 45

34 Layer 60 DEIM modified upscaling water saturation map 45

35 Layer 70 kx flow-based permeability vs DEIM-modified permeability 46

36 Layer 70 DEIM modified upscaling water saturation map 46

37 Layer 1 oil production rate comparison for the four producers 48
38 Layer 10 oil production rate comparison for the four producers 48
39 Layer 30 oil production rate comparison for the four producers 49
40 Layer 50 oil production rate comparison for the four producers 50
41 Layer 60 oil production rate comparison for the four producers 51
42 Layer 70 oil production rate comparison for the four producers 51
43 3D Model Layer 1-6 oil production rate comparison for the four producers 52
44 3D Model Layer 50-55 oil production rate comparison for the four producers 52
45 Layer 1 wells block pressures comparison for the four producers 54
46 Layer 1 wells block water saturation comparison for the four producers..... 55
47 Layer 1 wells water cut comparison for the four producers 56
48 Layer 10 wells block pressures comparison for the four producers 57
49 Layer 10 wells block water saturation comparison for the four producers..... 58
50 Layer 10 wells water cut comparison for the four producers 59
51 Layer 30 wells block pressures comparison for the four producers 60
52 Layer 30 wells block water saturation comparison for the four producers..... 61
53 Layer 30 wells water cut comparison for the four producers 62
54 Layer 50 wells block pressures comparison for the four producers 64
55 Layer 50 wells block water saturation comparison for the four producers..... 65
56 Layer 50 wells water cut comparison for the four producers 66
57 Layer 60 wells block pressures comparison for the four producers 67
58 Layer 60 wells block water saturation comparison for the four producers..... 68
59 Layer 60 wells water cut comparison for the four producers 69

60 Layer 70 wells block pressures comparison for the four producers 70

61 Layer 70 wells block water saturation comparison for the four producers..... 71

62 Layer 70 wells water cut comparison for the four producers 72

LIST OF TABLES

TABLE		Page
1	Flow-based upscaling algorithm	12
2	Workflow of POD-DEIM initialization	13
3	DEIM based upscaled permeability modification workflow	17
4	POD-DEIM Time Reduction	36
5	All case Studies used in the research	38
6	Oil Rate Matching Comparison and Time Reduction: Layer 1, 10, 30 from Tarbet Formation	75
7	Oil Rate Matching Comparison and Time Reduction: Layer 50, 60, 70 from Upper Ness Formation	75
8	Oil Rate Matching Comparison and Time Reduction: 3D cases layer 1-6 and layer 50-55	76

1. INTRODUCTION

Reservoir simulation has always been known as a time-consuming and computationally demanding process especially for large-scale reservoirs involving multiple phases, thermal and geochemical reactions, fracturing and rock mechanics processes. Even with high-end industrial computers – or high performance (HPC) infrastructure – generating multiple simulation scenarios, as in the case of optimization under uncertainty, still depends on countless hours (if not days) of machine time and proper man-power training. Developing alternatives that strive for simplicity and accuracy can lead to better-integrated workflows and reduction of the reservoir development and evaluation cycles.

To tackle this problem, a variety of model order reduction techniques have been developed over the last several decades. Among those techniques there are mainly two branches of model reduction methods, namely local physics-based model reduction and global projection-based model reduction.

In local physics-based model reduction, upscaling and gridding techniques are the main focus, and numerous upscaling techniques have been developed over the years. We cite the work of Christie (1996), Durlofsky (1991, 2005), and King & Mansfield (1997) among others. Upscaling refers to the process of averaging the properties of a group of adjacent geological grid to form one bigger grid. This process aims to reduce the degree of complexity of the whole reservoir system while maintaining reasonable reservoir heterogeneity as in the fine-scale model. For a 3D large model, upscaling techniques can often reduce the complexity of large reservoirs with complexity up to $O(10^8)$ by orders of magnitude.

Simple averaging methods such as arithmetic upscaling, harmonic upscaling, geometric upscaling could be used for low complexity, homogeneous geological model (Tiwary et al, 2009).

These upscaling methods average the permeability of the fine grids directly with arithmetic, harmonic and geometric mean methods. For a more advanced techniques, commercial reservoir simulator such as CMG, Eclipse, and MRST adopted to use sophisticated flow-based upscaling on unstructured grids (Lie 2019). This flow-based upscaling methods solves a locally bounded single phase pressure equation and computed the average coarsen cell permeability as the solution of the pressure solver. It puts more weigh onto the low permeability flow barrier such as shale slates and low permeable layers (He & Durlofsky, 2006).

Novel upscaling techniques such as Control-Relevant Upscaling based on system control (input and output) has also been proposed by Vakili & Jansen (2008) to highlight and emphasize on the level of control we have on a reservoir, which is the bottom hole pressures of the producing wells. In the work of Vakali and Jansen, the coarse-scale permeability is solved by linearizing the non-linear equations and minimizing the distance between input-output behavior of fine scale and coarse scale model. An extensive review of various upscaling techniques is proposed by Durlofsky (2005).

In global non-linear projection-based model reduction, many methods have been proposed, such as the Proper Orthogonal Decomposition (POD) (Van Doren et al, 2006), POD-DEIM (Yang et al., 2016) Trajectory Piecewise Linearization (He & Durlofsky, 2013) and TDEIM (Tan et al, 2019). A review of different model order reduction techniques can be found in (Cardoso 2009).

For the projection-based model order reduction, the proper orthogonal decomposition (Hinze & Volkwein, 2005) has been the method of choice given its simplicity and efficiency applied to reservoir simulators. The method utilizes the states as input, i.e., the state snapshots, and calculates the projection matrix by taking the singular value decomposition (SVD) of the snapshot matrix. The projection matrix only takes a few columns from the left singular vector that corresponds to

the largest singular values of the diagonal matrix. By doing so it retains most of the energy from the state matrix and in turn, can decrease the computational time while maintaining low errors. In reservoir simulation, the non-linear PDE of mass balance and flow equation is discretized into Residual and Jacobian matrices in the Newton solver. The POD method reduces complexity by multiplying the projection matrix onto the Residual and Jacobian. Therefore, the system of non-linear equations is solved in a smaller dimension subspace thus reducing calculation time. The solution is eventually projected back into the full-scale solution by multiplying the states with the transpose of the projection matrix. This adds one more level of complexity as the Jacobians and Residuals needs to be computed back to fine-scale for every Newton step.

As a remedy for this, an interpolation scheme has been proposed in (Chaturantabut & Sorensen, 2010). The strength of the so-called POD-DEIM, stems from the fact that the Jacobian and Residual only needs to be reconstructed on a few points of the simulation domain. POD-DEIM is based on the SVD results of the non-linear residual term in each timestep (Yang et al, 2016). It utilizes a greedy algorithm that calculates reservoir grid index to be used in the projection, which can further reduce the non-linear production subspace from POD. POD-DEIM has been combined with Trajectory Piecewise Linearization Method (TPWL) to form TDEIM, aiming to obtain a better convergence of the simulation (Tan et al, 2019). Both POD and POD-DEIM methods aim at decreasing the size of the non-linear matrices used in Newton solver. They are based on the reservoir state and residual variables, respectively.

The Trajectory Piecewise Linearization method is another useful method that breaks down the high complexity non-linear reservoir problem into multiple segments and are approximated to solve linearly (Cardoso & Durlofsky, 2003). More recently, TPWL are integrated with POD and

DEIM to form POD-TPWL (He & Durlofsky, 2013) and TDEIM (Tan et al, 2019) for much faster model order reduction techniques.

Among two branches of model order reduction techniques, flow-based permeability upscaling, and projection-based model POD based reduction methods have yielded excellent results in many reservoir studies. On the other hand, however, both of those reduction methods have their limitations as well. For example, in flow-based upscaling, a generally accurate coarse grid reservoir model can be achieved to match the reservoir characteristics. However, the well production rate is not quite accurate compared to the fine-scale model, where the production discrepancy can often reach around 10% to 20%. For the projection-based POD method, it can achieve an error of less than 1% but often requires hundreds of training timesteps. POD-DEIM algorithm is the most time-consuming process in terms of offline time, especially as the number of DEIM indices increases, the cost of computing DEIM indices increases in an exponential fashion. Another downside of POD-DEIM algorithm is the convergence issues, where in a heterogeneous reservoir the number of DEIM indices almost often exceeds 30% of the total number of reservoir grids, which requires an equivalent amount of timesteps. For example, a two-phase oil-water saturated reservoir discretized into 100 by 100 grids will have states dimension of 20,000 rows by the number of timesteps of columns. Since the number of timesteps determines the maximum number of DEIM index that can be computed, and a converging POD-DEIM calculation usually requires more than 3000 DEIM index, this will result in computing solution that composed of over 3000 timesteps. The requirements for CPU memory consumption to store and process the large solution and residual matrix make it difficult for POD-DEIM to efficiently works in model order reduction. Nevertheless, POD-DEIM algorithm provides us important

insights as to which grids in the reservoir are the most important and are selected for approximating and interpolating the whole reservoir properties.

Considering the advantages and limitations on each form of MOR methods, the idea of finding a connection between the physical model and projection-based reduction method is worth investigating. This thesis aims at exploring a way to combine the properties from POD-DEIM algorithm and integrate them on modifying flow-based upscaling in hope for a more accurate coarsened model representation. The main upscaling method used in this work is flow-based upscaling, since it is easy to implement, featuring more weight on the flow barrier, and having better production matching accuracy among other simple upscaling methods.

1.1. Primary objectives

This thesis proposes a new workflow for mitigating computational effort and improving production matching accuracy in reservoir simulation by integrating two methods of complexity reduction used independently in reservoir applications: flow-based upscaling and projection-based reduced-order modeling. The main objective of this thesis is to combine the strengths of the discrete interpolation technique (DEIM), such as the selection of few interpolation points, to leverage the permeability calculation and averaging obtained from flow-based upscaling. Specifically, the primary objectives of this thesis are to:

- Assess the use of POD-DEIM and Flow-based upscaling separately to obtain fast simulation models.
- Integrate DEIM selected grid points to the modification of coarse permeability by proposing a new weight-based averaging and assess its efficiency.

- Test the novel approach to generalize permeability modifications using reservoir benchmark (SPE 10) model.

1.2. Thesis scope

In order to have a prove of concept and assess the efficiency of the new integrated methodology, our study is divided into three parts:

1. Projection-based model reduction only: Application of model reduction by applying the POD-DEIM calculation on the residuals of the fine-scale model results.
2. Upscaling only: Application of upscaling by conducting arithmetic, harmonic, and flow-based upscaling to a particular permeability field.
3. Combined Method: Incorporate the DEIM selection process into the flow-based upscaling permeability based on POD-DEIM results.

We apply our new proposed methodology in both 2D and 3D models. For the 2D model, 6 specific layers of SPE 10 Comparative Project are used: (1) Layer 1, 10 and 30 from the Tarbert Formation and (2) Layer 50, 60, and 70 from the Upper Ness formation. For the 3D model, two different formation from SPE 10, layer 1-6, and layer 50-55 are used. In all cases, we implemented a two-phase oil-water saturated black oil reservoir model with no gas. A normal 5-spot producing scheme is used with 4 producing wells at four corners and the water injection well located at the center of the reservoir. The base upscaling schedule used are 2 by 2 upscaling for 2D model; 2 by 2 by 2 upscaling for 3D model.

2. METHODOLOGY

As recalled from the previous chapter, this thesis is composed of three parts: (1) conduct POD-DEIM model reduction on a simple fine scale model; (2) perform arithmetic upscaling, harmonic upscaling, and flow-based upscaling, and (3) modify the flow-based upscaling permeability with DEIM index and test out the new upscaling technique. In this methodology section, we will demonstrate how these parts are implemented separately and in a combined fashion.

2.1 Reservoir Simulation

Before conducting upscaling and POD-DEIM procedures, we first conducted reservoir simulation on the fine scale reservoir model. The solution of the fine scale model is regarded as accurate and will be used for the baseline of assessing the model order reduction accuracy for POD-DEIM, upscaling, and the combined method.

First, the governing equation of two-phase oil-water reservoir simulation is briefed explained here. The fluid transport in porous media can be written as a combination of a mass balance equation for each phase and Darcy's law. For the two-phase black oil simulation with no gas content, the equation is expressed in **Eq. 1** where inertia and temperature effect on fluids flow are neglected for simplicity.

$$\nabla \cdot \left[-\frac{\rho_\alpha k_{r\alpha}}{\mu_\alpha} K(\nabla p_\alpha - \rho_\alpha g \nabla h) \right] + \frac{\partial(\rho_\alpha \emptyset S_\alpha)}{\partial t} - \rho_\alpha q_\alpha = 0 \qquad (1)$$

In the above equation, ∇ is the gradient, $\cdot$ is the divergent operator, K is permeability tensor, μ_α is the fluid phase viscosity, $k_{r\alpha}$ is the fluid relative permeability, p_α is the phase pressure, g is gravity constant, h is depth, ρ_α is fluid density, S_α is fluid saturation and q_α is volumetric sink term.

From Aziz and Settari (1986), the above equation is discretized numerically and solved with Newton Raphson method using finite volume procedures. In each timestep, the state vector is defined as $X = [P_o, S_w]^T$ for a two-phase oil water reservoir simulation, where P_o is oil pressure and S_w is water saturation. **Fig. 1** shows the solution matrix composition, where the rows are composed of number of grid blocks and columns represent number of timesteps. **Eq. 2** describes the newton solver for state vector, where $X_{current}$ is the alteration of solution in the current timestep, J is the full Jacobian term and R is the full residual term. The new solution vector X_{new} is defined as the sum of previous solution X_{old} and current solution changes shown in **Eq. 3**. The detailed formulation of those variable can be found in Aziz and Settari (1986).

$$X_{current} = J\backslash -R \tag{2}$$

$$X_{new} = X_{old} + X_{current} \tag{3}$$

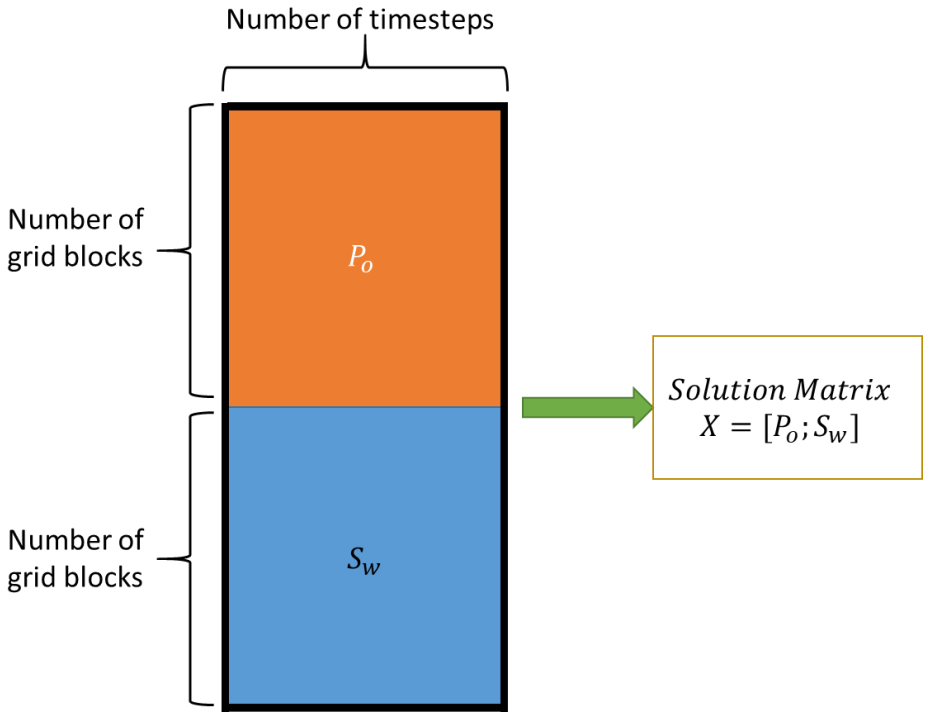

Figure 1 – Representation of the snapshot (solution) matrix. Rows are time evaluation of the pressure and saturation; columns are solution in each time step.

2.2 Arithmetic and Harmonic Upscaling

Arithmetic and harmonic upscaling is one of the simplest ways of conducting upscaling on reservoirs. Arithmetic upscaling refers to the mathematical average of all the fine cell block permeabilities. As shown in **Eq. 4** and **Fig. 2**, for a cartesian gridded reservoir, the arithmetic upscaling permeability of a specific coarse block is calculated by averaging all the fine scale block permeability within it using a weight-based average on the cell area of volume.

$$k_{Coarse,arithmetic} = \frac{\sum_{i=1}^{N} k_i * A_i}{\sum_{i=1}^{N} A_i} \tag{4}$$

Where,

k_i = permeability of fine grid block

A_i = Area of fine grid block

If the reservoir grid blocks have uniform size, then the coarse cell permeability can be expressed as **Eq. 5**:

$$k_{Coarse,arithmetic} = \frac{\sum_{i=1}^{N} k_i}{N} \tag{5}$$

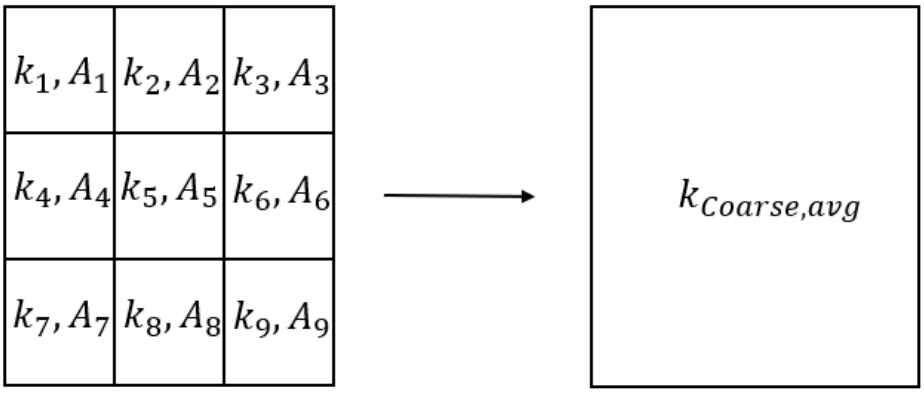

Figure 2 - An example of coarse block permeability. A 9 x 9 fine scale block is averaged into a single coarse block.

The simple harmonic upscaling on the other hand is averaging the permeabilities in reciprocal order. Still taking **Fig. 2** as reference, the simple harmonic upscaling permeability is calculated by **Eq. 6**. If the reservoir is gridded uniformly, simple harmonic upscaling permeability can be simplified into **Eq. 7**.

$$k_{Coarse,harmonic} = \frac{\sum_{i=1}^{N} \frac{1}{A_i}}{\sum_{i=1}^{N} \frac{1}{A_i * k_i}} \tag{6}$$

$$k_{Coarse,harmonic} = \frac{1}{\sum_{i=1}^{N} \frac{1}{k_i}} \tag{7}$$

In this thesis, all the models used in the case study from SPE 10 (Christie & Blunt, 2001) model are uniformly gridded. Each layer has 60 by 220 grid blocks in x and y direction, and it is upscaled into 30 by 110 coarse grid block to preserve as many details of the reservoir as possible. The arithmetic and simple harmonic permeability are calculated first with the above procedures. According to Cardwell and Parsons (1945), the lower and upper bound of upscaled model permeability is obtained from harmonic and arithmetic upscaling, respectively. The Wiener bound (Cardwell & Parsons, 1945) k_{ah} is calculated by the difference between the upper and lower bound of upscaled permeability shown in **Eq. 8**. It is used as an important parameter in the modification of permeability section.

$$k_{ah} = k_a - k_h \tag{8}$$

2.3 Flow-based Upscaling

Flow-based upscaling is a local permeability upscaling method that computes an equivalent coarse cell permeability by solving a single-phase pressure equation shown in **Eq. 9** (Durlofsky,

2005). In a flow-based permeability upscaling shown in **Fig. 3,** the flow-based upscaled permeability is computed by **Eq. 10**, where $k_{x,coarse}$ is the equivalent coarsen scale permeability in x direction, q_{out} is the flux (volume of fluid per total area per time) of the out flowing boundary, L is the length of upscaled coarse grid block in the flow direction, A_{out} is the area of the out flowing face, p_1 is the pressure of the fluid entry side and p_2 is the pressure of the fluid exit side. The equivalent coarse permeability is the sum of flux passing through the outgoing face multiply by the length of the coarse grid in flow direction divided by the area of outgoing boundary and pressure drop.

$$\nabla * (k(x)\nabla p) = 0 \tag{9}$$

$$k_{x,coarse} = \sum \frac{q_{out} * L}{A_{out}} (p_2 - p_1) \tag{10}$$

MRST (Lie, 2019) utilizes the above method with function $incompTPFA$ to solve the single-phase pressure equation in **Eq. 9** and compute single phase flux, then it solves upscaled equivalent permeability with $Upscaleperm$ function with **Eq. 10**. In this thesis, MRST upscaling method is used for performing flow-based upscaling and the workflow is shown in **Table 1**. The upscaled permeabilities in x, y, z directions are computed when going through all the coarse grids index i, j, k with the work flow in **Table 1**. The process emulates a laboratory setup where there is pressure drop in each axial direction and sealing occurs along the other boundaries. Using the same upscaling scheme as in the arithmetic and harmonic upscaling, the fine cell reservoir is upscaled into coarsen cell with the same dimension as the previous two upscaling methods. This permeability obtained will be used as the base coarse scale permeability to be modified by DEIM index in the following stage.

Algorithm: Flow-based upscaling
Data: k_{fine}, $upscaling\ scheme$ **Result**: k_{coarse}, for $i = 1\ to\ N_{coarse}$ do: **1** $Calculating\ flux\ by\ solving\ \boldsymbol{Eq.6}\ using\ incompTPFA\ method$ **2** $Area_{Coarse\ i,j} = \sum Area_{fine\ i,j}$ **3** $L = length\ of\ coarse\ grid\ in\ the\ flow\ direction$ **4** $q = abs(\sum flux)$ **5** $Calculating\ k_{coarse}\ with\ \boldsymbol{Eq.10}$

Table 1 – Flow-based upscaling algorithm

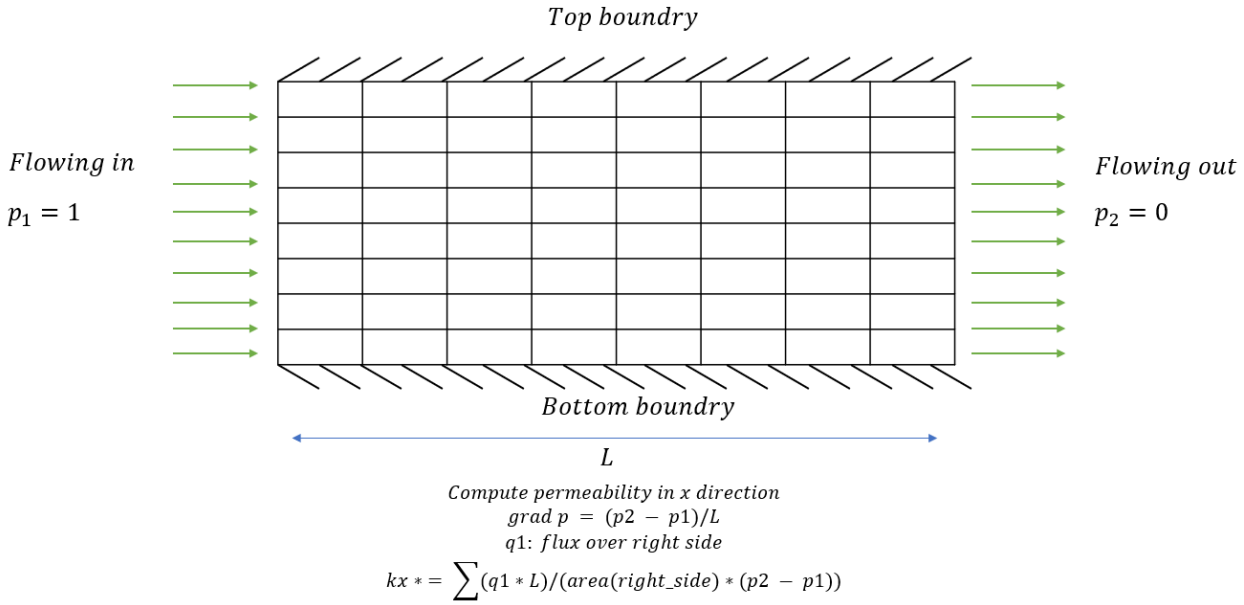

Figure 3 – Illustration of calculating flow-based upscaled permeability in x direction. Here, one imposes a constant pressure boundary condition in each side of the reservoir.

2.4 POD-DEIM

As introduced before, POD-DEIM is a projection-based MOR method that further reduces the sizes of Residual and Jacobian term used in Newton Raphson solver computation. In POD reduction, projection basis is obtained from the singular value decomposition (SVD) of state matrix. It is composed of only the first few columns of the left singular vector correspond to largest eigenvalues in the diagonal matrix for retaining the most energy from the original matrix. POD-DEIM reduces this projection matrix by only retaining rows that correspond to the DEIM index selected by POD-DEIM algorithm (Tan et al, 2019).

Following the work of Tan (Tan et al, 2019), first we collect the states and residual snapshots from the full model reservoir simulation. Then, we compute POD projection matrix from states matrix and DEIM index from residual matrix. The residual term can be expressed as $R = [R_o, R_w]^T$, representing oil residual and water residual. **Table 2** shows the initialization workflow before DEIM index calculation.

Algorithm: Workflow of POD-DEIM initialization	
Data: $states\ matrix: X, residual\ matrix: R$	
Result: ϕ_X, ϕ_R	
1	$Run\ full\ simulation, collecting\ states\ matrix\ X\ and\ residual\ matrix\ R$
2	$Perform\ SVD\ on\ X\ and\ R\ with\ \boldsymbol{Eq.11}\ and\ \boldsymbol{Eq.12}$
3	$Obtain\ projection\ matrix\ \phi_X\ and\ \phi_R\ with\ \boldsymbol{Eq.13}\ and\ \boldsymbol{Eq.14}$

Table 2 – Workflow of POD-DEIM initialization

Eq. 11 and **Eq. 12** shows the singular value decomposition process conducted on states and residual matrix. The resulting left singular vector matrices are $U_{X\beta}$ and $U_{R\beta}$, respectively.

In **Eq. 13**, ϕ_X is the projection matrix for POD, where ${u_{X\beta}}^{(j)}$ is the column of $U_{X\beta}$, $nX\beta$ is the total number of columns retained for high energy. Similarly, in **Eq. 14**, ϕ_R is the projection matrix used for POD-DEIM index calculation, ${u_{R\beta}}^{(j)}$ is the column of $U_{R\beta}$. Contrary to retaining the highest energy from states matrix in POD, since in each column we can compute only 1 DEIM index, and we would like to compute as many DEIM indices as possible, we will use all the columns from decomposition of residual matrix. Therefore, $nR\beta$ is the number of columns in the residual matrix R.

$$\mathrm{X} = U_{X\beta} * \Sigma_{X\beta} * {V^T}_{X\beta} \tag{11}$$

$$\mathrm{R} = U_{R\beta} * \Sigma_{R\beta} * {V^T}_{R\beta} \tag{12}$$

$$\phi_X = [{u_{X\beta}}^{(1)} {u_{X\beta}}^{(2)} \dots {u_{X\beta}}^{(nX\beta)}] \tag{13}$$

$$\phi_R = [{u_{R\beta}}^{(1)} {u_{R\beta}}^{(2)} \dots {u_{R\beta}}^{(nR\beta)}] \tag{14}$$

Following the above workflow, we obtain projection matrix ϕ_R as input. The DEIM index is calculated with the following algorithm shown in **Fig. 4.** Here, $\overrightarrow{\wp}$ is the DEIM index output, representing the index of reservoir grid selected by DEIM. To initialize the process, $\wp_1$ is the index of the maximum absolute value of the first column of the residual projection matrix ${\mathrm{u}_{R\beta}}^{(1)}$. Temporary projection matrix ψ_β is the first column of projection matrix, and P is the selection matrix in **Eq. 15**, where $e_{\wp \mathrm{i}} = [0, \dots 0,1,0, \dots 0]^T$ is the $\wp_{\mathrm{i}} th$ column of the identity matrix $I_{n_b} \in \mathbb{R}^{n_b * n_b}\ for\ i = 1, \dots n_b$.

Then it loops over the 2nd column until the last column. In each column, a temporary constant c is solved with **Eq. 16**, following by a temporary residual term r solved with **Eq. 17**. Then the DEIM index $\wp$ is again computed as the index of the largest absolute value of r. Following that, temporary projection matrix ψ_β will horizontally concatenate the current column of the projection

matrix $\mathrm{u}_\beta{}^{(j)}$, and the selection matrix P appends $e_{\wp \mathrm{i}}$ as the $\wp_{\mathrm{i}} th$ column of the identity matrix. This process is repeated until the last column. In each iteration, temporary projection matrix ψ_β and selection matrix P increases in size, thus increases the time of computing each DEIM index.

$$\mathrm{P} = [e_{\wp \mathrm{i}}, \dots e_{\wp \mathrm{m}}] \in R^{n_b * n_\beta} \tag{15}$$

$$\mathrm{c} = \left(P^T * \psi_\beta\right) \backslash (P^T * \mathrm{u}_\beta{}^{(j)}) \tag{16}$$

$$\mathrm{r} = \mathrm{u}_\beta{}^{(j)} - \psi_\beta * c \tag{17}$$

Algorithm 1 DEIM greedy procedure

Data: $\{\mathbf{u}_\beta{}^{(j)}\}_{j=1}^{n_\beta} \in \mathbb{R}^{n_b}$

Result: DEIM indexes: $\vec{\wp} = \left[\wp_1, \dots, \wp_{n_\beta}\right]^T$

$\left[|\varrho|, \wp_1\right] = \max\left(\mathbf{u}_\beta{}^{(1)}\right)$;
$\boldsymbol{\Psi}_\beta = \left[\mathbf{u}_\beta{}^{(1)}\right]$, $\mathbf{P} = \left[\mathbf{e}_{\wp_1}\right]$, $\vec{\wp} = \left[\wp_1\right]$;
for $j = 2$ *to* n_β **do**
  Solve $\left(\mathbf{P}^T \cdot \boldsymbol{\Psi}_\beta\right)\mathbf{c} = \mathbf{P}^T \cdot \mathbf{u}_\beta{}^{(j)}$ for $\mathbf{c}$;
  $\mathbf{r} = \mathbf{u}_\beta{}^{(j)} - \boldsymbol{\Psi}_\beta \cdot \mathbf{c}$;
  $\left[|\varrho|, \wp_j\right] = \max(\mathbf{r})$;
  $\boldsymbol{\Psi}_\beta = \left[\boldsymbol{\Psi}_\beta \;\; \mathbf{u}_\beta{}^{(j)}\right]$, $\mathbf{P} = \left[\mathbf{P} \;\; \mathbf{e}_{\wp_j}\right]$;
  $\vec{\wp} = \left[\vec{\wp} \;\; \wp_j\right]$;

Figure 4 – DEIM greedy algorithm pseudocode, input U_β equivalent for $\boldsymbol{\phi}_R$ from SVD of Residual, output $\vec{\wp}$ is the DEIM index, equivalent as reservoir grid index.

Following DEIM index calculation, the POD-DEIM model order reduction is achieved with further reduced Residual and Jacobian matrices. Here, $cDEIM$ will substitute the POD projection matrix ϕ_X. R_{DEIM}, and J_{DEIM} is the reduced Residual and Jacobian in newton solver. These three parameters are computed with **Eq. 18** – **Eq. 20**. Noted that in **Eq. 19**, only part of the Residual matrix is utilized in computation depending on the size of DEIM index $\vec{\wp}$. Similarly, in **Eq. 20**,

the Jacobian size is also reduced to $\overrightarrow{\wp}$ numbers of rows. Since the total number of DEIM index $\overrightarrow{\wp}$ is only a fraction of total number of reservoir grids, time saving is achieved in the computation of reduced Residual and Jacobian matrix.

$$cDEIM = \phi_X{}^T * \phi_R / \phi_R(\overrightarrow{\wp}, :) \tag{18}$$

$$R_{DEIM} = cDEIM * R(\overrightarrow{\wp}, :) \tag{19}$$

$$J_{DEIM} = cDEIM * J(\overrightarrow{\wp}, :) * \phi_X \tag{20}$$

Eventually, the newton solver calculates pressure and saturation vectors following **Eq. 21** to **Eq. 22** in a reduced subspace in each timestep and project it back to full scale.

$$X_{DEIM} = J_{DEIM} \backslash -R_{DEIM} \tag{21}$$

$$X = \phi_X * X_{DEIM} \tag{22}$$

2.5 The New Method: Modification of Flow-based Permeability with POD-DEIM Index

In this section, the new proposed workflow of integrating DEIM index into modifying flow-based permeability from upscaling is explained. For the POD-DEIM method from the previous section, the intermediate calculation of each DEIM index involves matrix inversion but the size of those matrix grows linearly as the number of columns. Moreover, in order to converge, the number of DEIM index usually requires more than 30% of the overall number of reservoir grids. Therefore, equally number of timestep is required to perform such reduction, and it would cost an immense amount of time and CPU memory just to store the snapshot matrix in order to calculate DEIM index. To tackle this problem, POD-DEIM was successfully used in a combined fashion with the Trajectory Piecewise Linearization to form POD-TDEIM (Tan et al, 2019) so that POD-DEIM is performed in a generally more linearized, segmented system. This idea reduces the requirements for overwhelmingly large number of DEIM index required and provides better convergence to the

simulation. In this thesis, we will explore a new way to combine few POD-DEIM index onto the modification of flow-based permeability in order to achieve better accuracy as the original model.

In local upscaling techniques, the advantage is the reduction of complexity physically for geological model, but the coarsened model cannot provide an exceptionally good production match. The oil production error is approximately in between 10% to 20% in most cases. It would be desirable to find an alternative method that takes advantage of both methods and integrate them for an improved model reduction workflow. The new proposed workflow here combines the DEIM index selection from POD-DEIM process and integrated to flow-based upscaling permeability modification. We alter the flow-based permeability with POD-DEIM index following the workflow in **Table 3**.

Workflow: DEIM based upscaled permeability modification
Data: k_p, $pDEIM$ **Output**: k_{pDEIM}
1 $for\ i = 1{:}\ CoarseNx$ **2** $for\ j = 1{:}\ CoarseNy$ **3** $for\ j = 1{:}\ CoarseNy$ **4** Obtain ind_1 from $pDEIM$ **5** Find $\{k_{high}\}$ and $\{k_{low}\}$ from **Eq. 23** and **Eq. 24** **6** Calculate $highfraction$, $lowfraction$, and $k_{pDEIM\ i,j}$ from **Eq. 25** – **Eq. 27** **7** end **8** end **9** end

Table 3 – DEIM based upscaled permeability modification workflow.

In the above workflow, i, j, k is used to represent the coarse grid block index, k_{fine}, k_{Coarse} as the fine cell permeability and coarse cell permeability after upscaling, respectively. We denote $\{k_{fine\ i,j,k}\}$ as the collection of fine cells permeability in a coarse cell grid indexed i, j, k. For example, in **Fig. 2**, $k_1, k_2, k_3, \dots, k_9$ are the fine cell permeabilities within coarse grid block $k_{Coarse\ i,j,k}$. Also, we denote k_a, k_h, k_{ah}, k_p as the permeabilities from arithmetic upscaling, harmonic upscaling, wiener bound, and flow-based upscaling, respectively.

For a specific coarse grid block, if there is any DEIM index $\overrightarrow{\wp}$ within that coarse cell grid block, we mark it as ind_1, then denote $\{k_{high}\}$ and $\{k_{low}\}$ in **Eq. 23** and **Eq. 24**as all the fine cell permeabilities selected by DEIM that have values greater and smaller than the corresponding flow-based upscaled permeability $k_{p\ i,j}$. A visual representation of this process is expressed in **Fig. 5**.

$$\{k_{high}\} = \{k_{fine\ i,j}(ind_1)\}\ \forall\ (\{k_{fine\ i,j}(ind_1)\} > k_{p\ i,j}) \tag{23}$$

$$\{k_{low}\} = \{k_{fine\ i,j}(ind_1)\}\ \forall\ (\{k_{fine\ i,j}(ind_1)\} < k_{p\ i,j}) \tag{24}$$

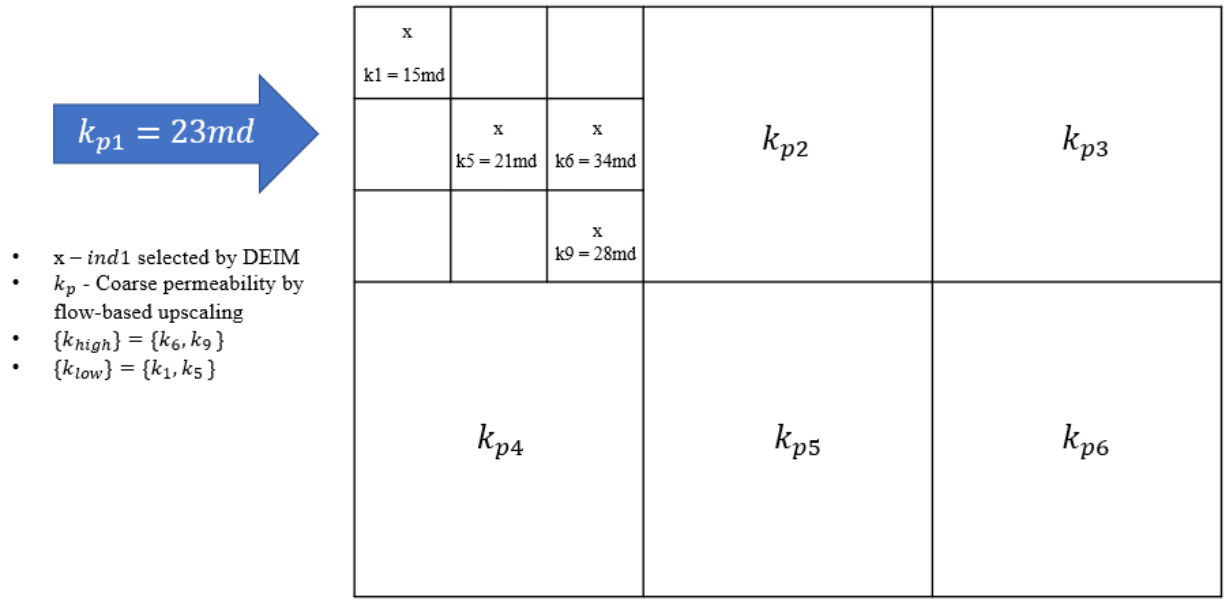

Figure 5 – Illustration of $\{k_{high}\}$ and $\{k_{low}\}$

Following that, we go through all the coarse grid blocks and alter the upscaled flow-based permeability by a weight-based modification from DEIM indices based on **Eq. 25** to **Eq. 27**. The concept here is that each selected grid block by DEIM will influence the overall fluids flow more in the reservoir and have more impact on the overall upscaled permeability. Whereas grid blocks that are not selected by DEIM algorithm are not treated as important, so they should remain as is. Here we denote the new modified permeability by DEIM as $k_{pDEIM\ i,j,k}$ and Ups as the coarsening coefficient. For example, a 3 by 3 by 1 upscaling scheme would have a coarse coefficient of $3 * 3 * 1 = 9$.

$$highfraction = \sum \frac{(\{k_{high}\} - k_{p\ i,j,k}) * (k_{a\ i,j,k} - k_{p\ i,j,k})}{k_{p\ i,j,k} * k_{ah\ i,j,k} * Ups} \tag{25}$$

$$lowfraction = \sum \frac{(\{k_{low}\} - k_{p\ i,j,k}) * (k_{p\ i,j,k} - k_{h\ i,j,k})}{k_{p\ i,j,k} * k_{ah\ i,j,k} * Ups} \tag{26}$$

$$k_{pDEIM\ i,j} = k_{p\ i,j,k} * (1 + highfraction + lowfraction) \tag{27}$$

Eventually, we use the updated coarse cell permeability $k_{pDEIM\ i,j}$ to run the simulation and compare the results with fine scale cases.

3. APPLICATION OF THE PROPOSED METHODOLOGY

In this section, a POD-DEIM standalone case, flow-based upscaling, and the new proposed algorithm is tested out. The 2D models used are SPE10 layer 1, 10, 30, 50, 60, and 70. For the 3D model, we use SPE10 layer 1-6 and layer 50-60. A two-phase oil water saturated black oil model implemented using MRST as the reservoir simulation platform. Initial reservoir pressure is $6000\ psia$ and the production bottom hole pressure for all four wells are set as $2900\ psia$. The injection well injects water at constant rate of $500\ stb/day$. The reservoir undergoes a production scenario of 3000-day time span with dT of 4 days, which yields a total of 750 timesteps. The original heterogeneous porosity is used, and 3D permeability tensor k_x , k_y, and k_z are used in calculations. In order to keep our comparisons consistent, we use a uniform 2 by 2 upscaling for all 2D cases, and 2 by 2 by 2 upscaling for all 3D cases.

We start our experiment with basic reservoir characteristic analysis. First, in **Fig. 6** we illustrate the location of production and injection wells. For all cases, producers are located at the four corners and injector in the center of the reservoir. Then, the original 2D model permeability k_x , k_y, and k_z is plotted shown in **Fig. 7** to **Fig. 9**. The permeability field is plotted in logarithmic scale. The first three models, layer 1, layer 10 and layer 30 features the Tarbet formation, while the layer 50, 60, and 70 model are in the Upper Ness Formation. In **Fig. 7** and **Fig. 8**, the models from the Tarbet Formation shows a higher permeability area in the center of the reservoir. Layer 1 exhibits a vertical distribution of low permeability at the left portion of the reservoir, while layer 10 has low permeability mainly on the right side and layer 30 has a low permeability that takes up most part on the left.

In **Fig. 8** and **Fig. 9**, we observe that Upper Ness Formation (from 36 – 85 layer) has a more distinct channel like features than the Tarbet Formation. The channel direction mainly situated in a NW-SE direction throughout the reservoir for all three cases.

Secondly, we perform a few simulations to evaluate the input-output parameters of the reservoir model. We run the fine scale reservoir simulation with MRST and the oil pressure, water saturation, and residual snapshots is collected and stored. The original oil rate plots of 2D models are shown in **Fig. 10** and **Fig. 11**. The oil rate plots for 3D models are shown in **Fig. 12**. From **Fig. 10** and **Fig. 11** we can see the oil production is quite low, reason being that the thickness of the 2D model is only 2ft, and in the Upper Ness Formation water breakthrough occurs fast due to the channel-like reservoir structures that facilitate fluid transport. Hence some producers have seen very low oil production throughout its production life. In **Fig. 12**, the 3D oil rate increases as expected, but it falls off quickly as the model has only 6 layers, which yields a total thickness of 12 ft.

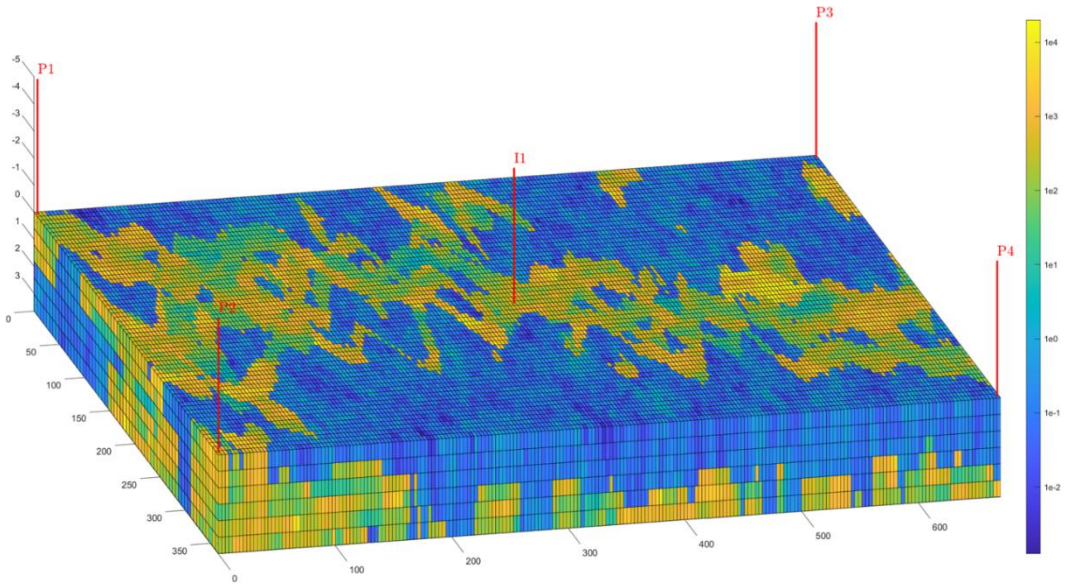

Figure 6 – Well location configurations for the 3D SPE 10 model. Here, we show 6 layers of the SPE 10 benchmark.

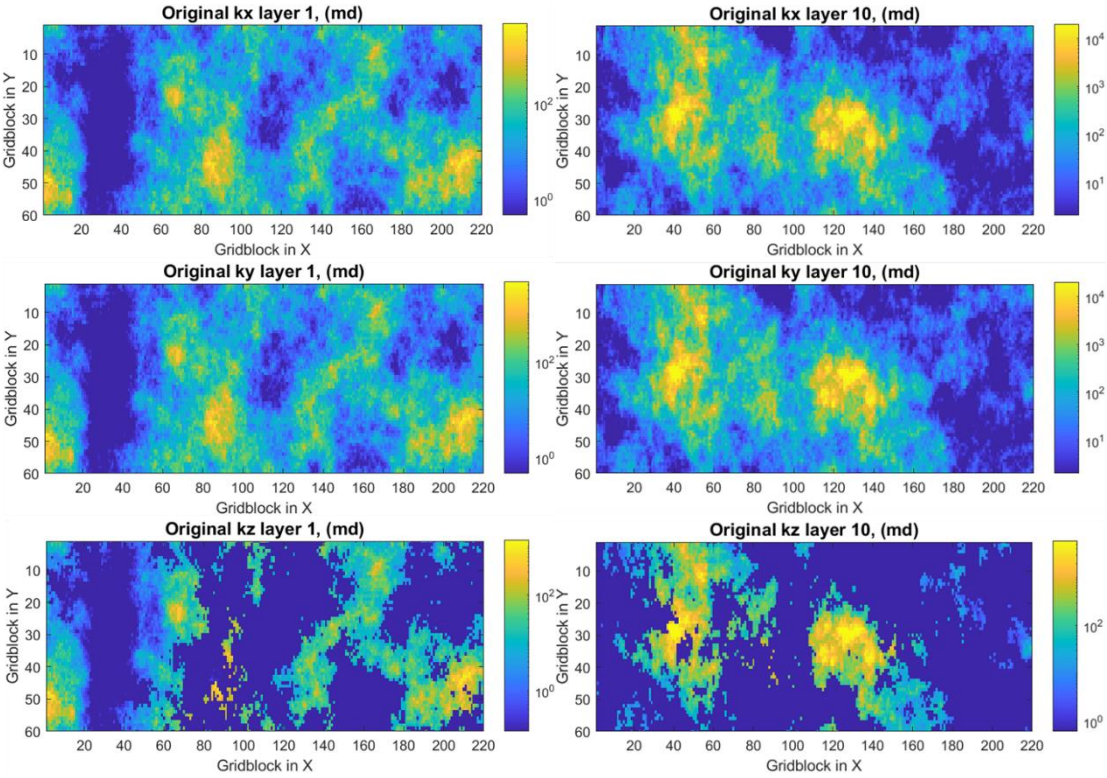

Figure 7 – Original model permeability, layer 1 and layer 10

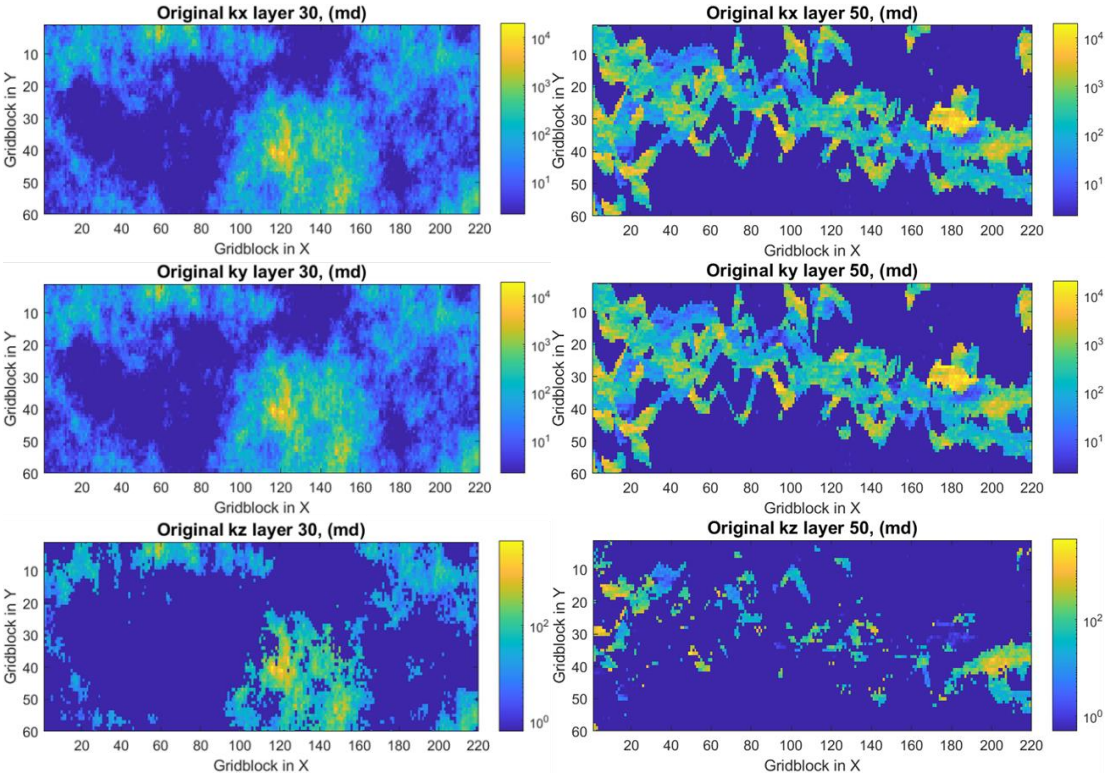

Figure 8 – Original model permeability, layer 30 and layer 50

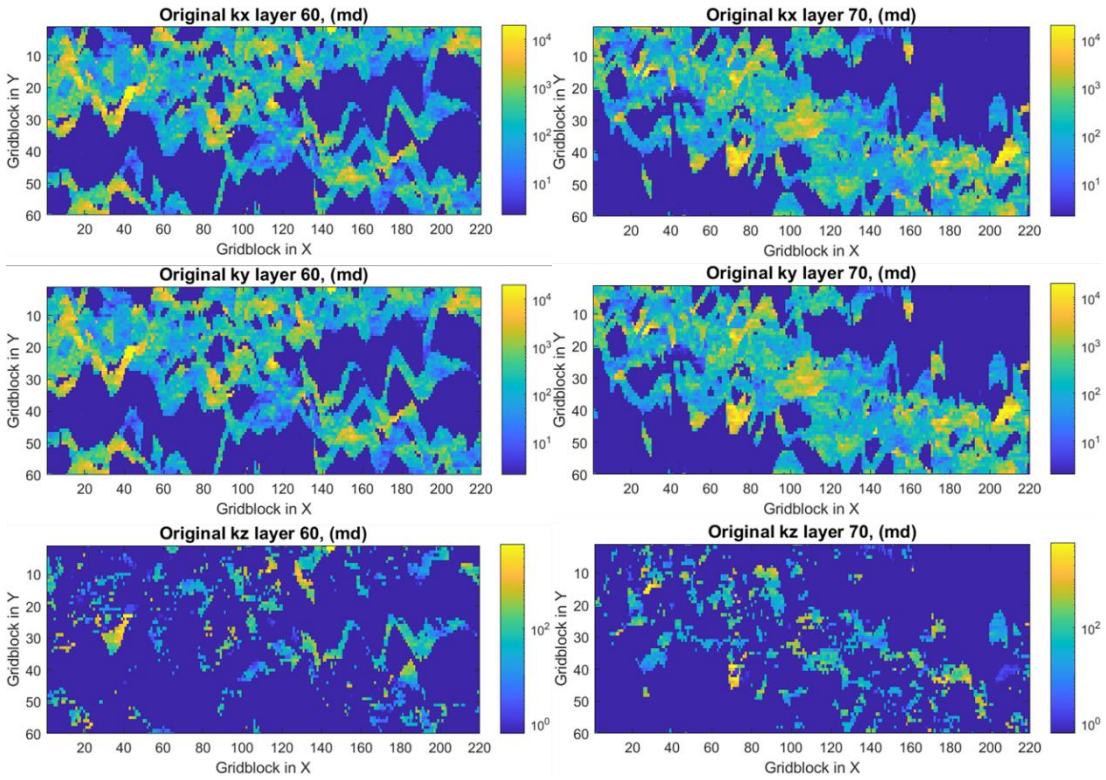

Figure 9 – Original model permeability, layer 60 and layer 70

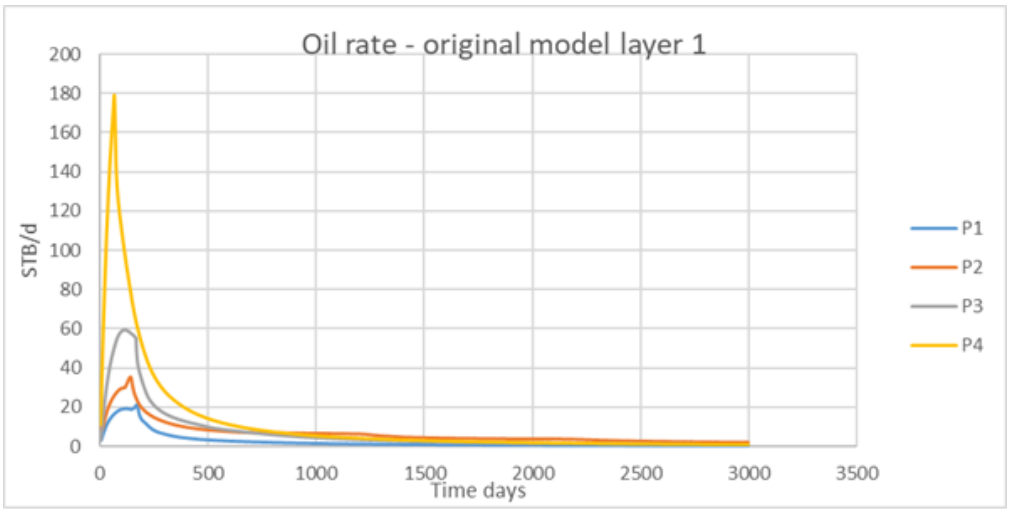

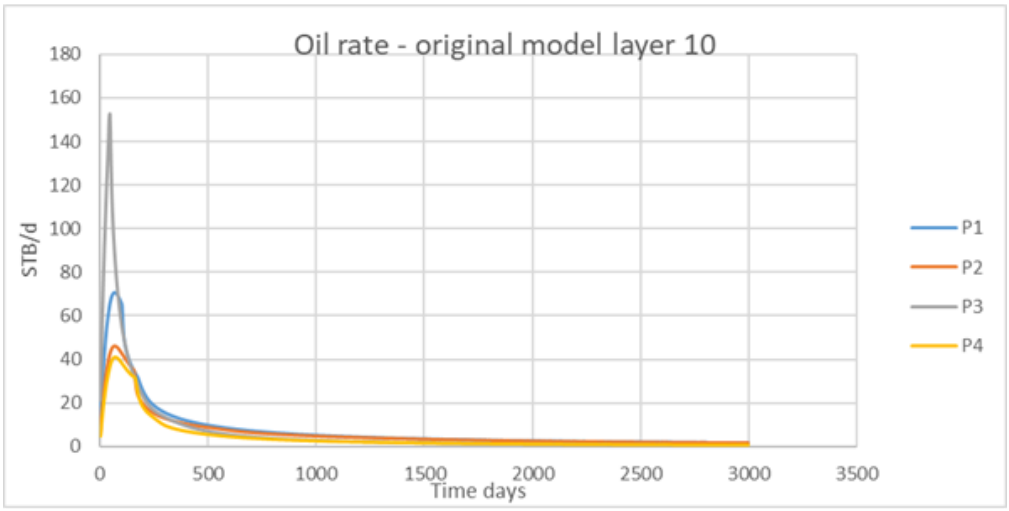

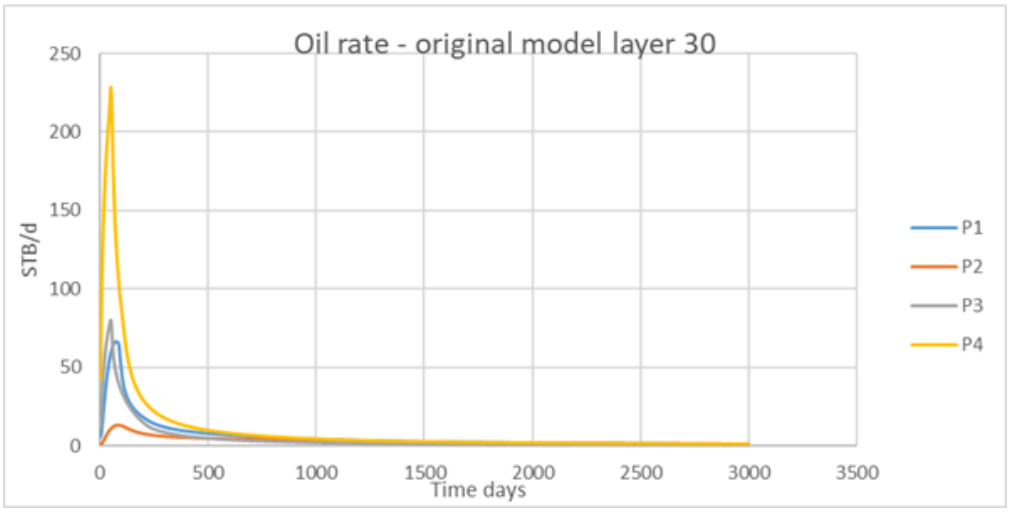

Figure 10 – Original model oil rate for the four wells, layer 1, 10 and 30

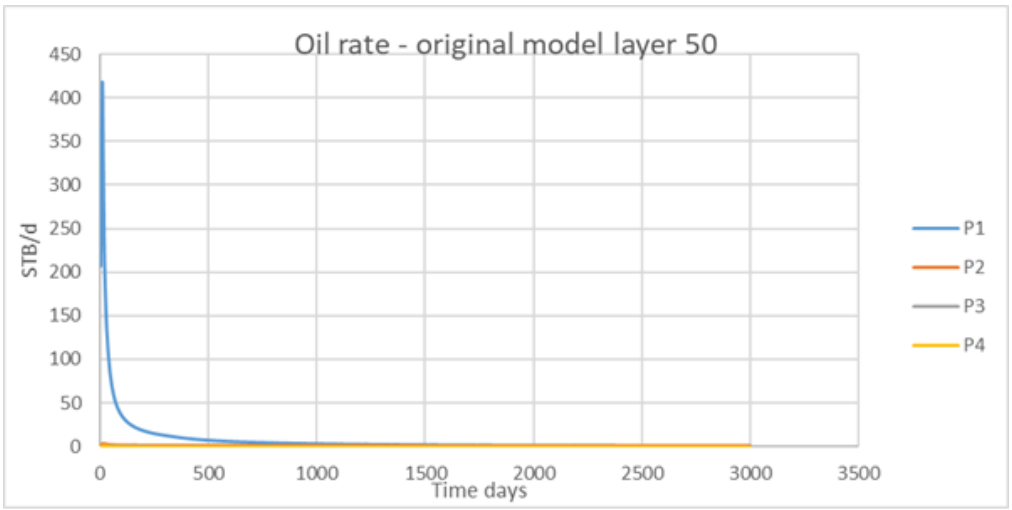

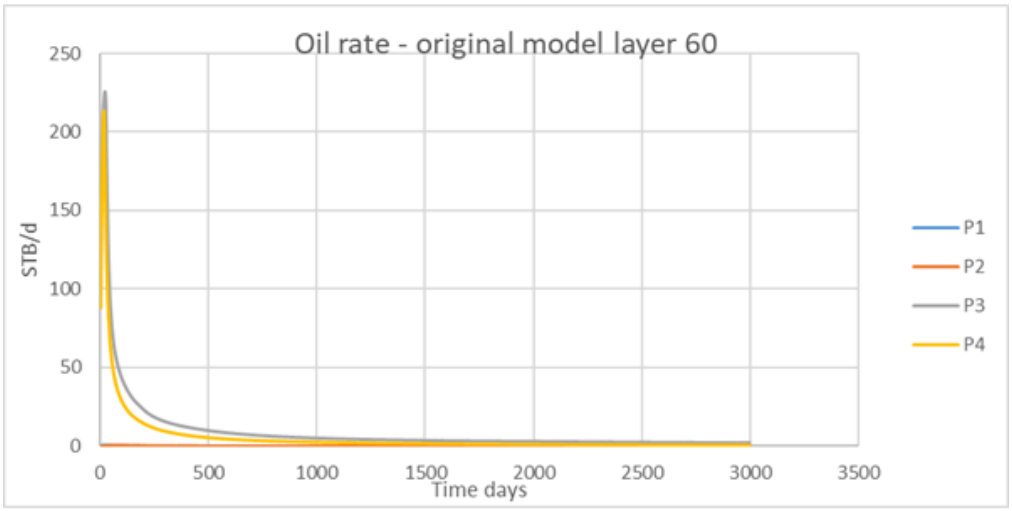

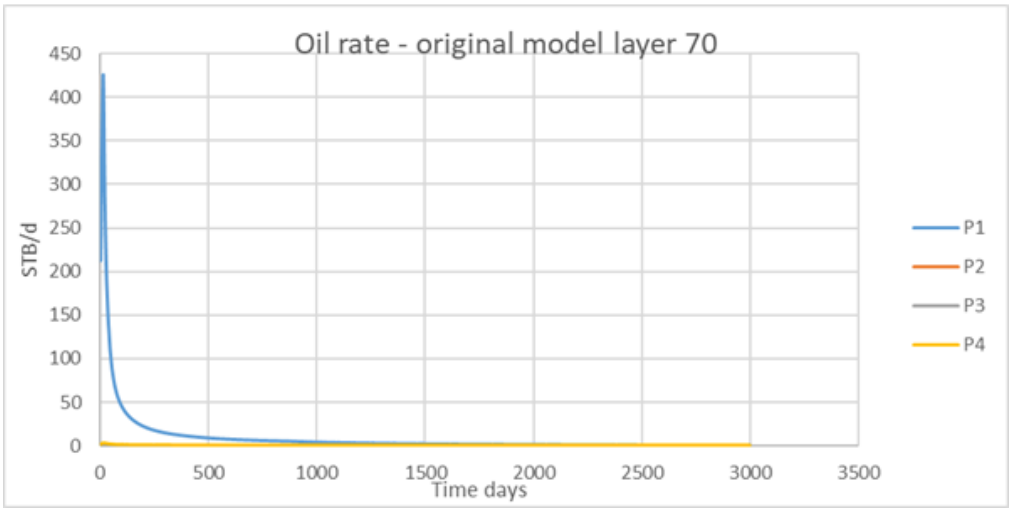

Figure 11 – Original model oil rate for the four wells, layer 50, 60, and 70

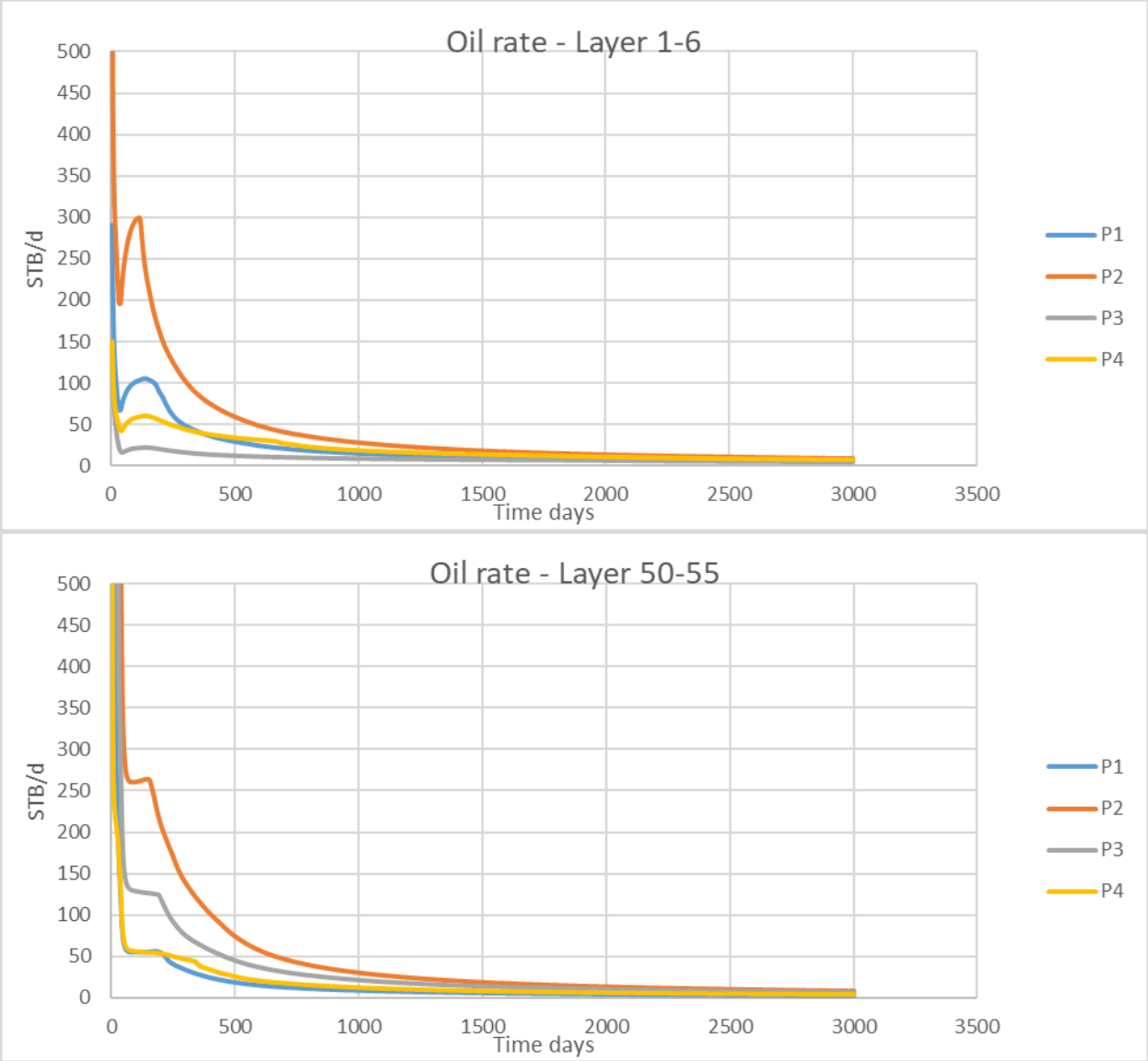

Figure 12 – Original 3D model oil rate for the four wells, layer 1-6 and layer 50-55

3.1 POD-DEIM

In this section, a POD-DEIM standalone case is performed to demonstrate the online simulation time reduction and matching result accuracy with the original model. Due to the computer RAM limitation, our intended performance demonstration of the SPE10 2D model of 60 by 220 grids run with over 6000 timesteps has to be modified. In this case, we adopted to a simpler 2D reservoir of 100 by 100 uniform grids. The dimension of the grid is 32 ft cube square. We also set the 5-spot injection pattern and a uniform porosity of 0.2, two-phase reservoir.

We simulate the fine scale simulation with a 3000-day time span, using a timestep of 0.5 days, eventually yielding a total of 6067 timesteps. We run a huge number of timesteps so that we can have sufficient columns in the residual matrix. We test out different number of DEIM indices used in the POD-DEIM reduction and analyze which one will converge. **Fig. 13** and **Fig. 14** shows the original model oil pressure and water saturation by the end of the simulation. From the plot the water saturation is dissipated out uniformly from the center as it is a uniform homogeneous reservoir. **Fig. 15** shows the oil and water production rates, and since the drawdown pressure we set is only 500 psi, the rate is approximately constant at 200 barrel/day for all four production wells.

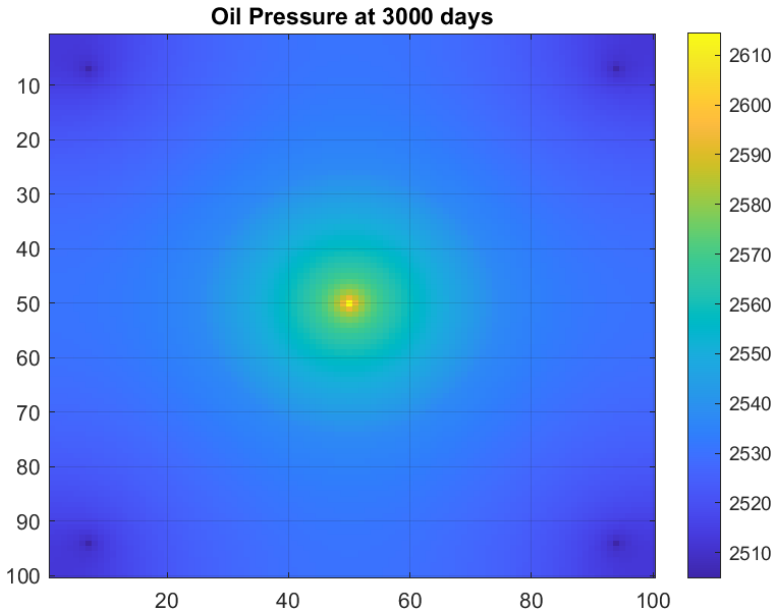

Figure 13 – 100 by 100 uniform grid oil pressure at the end of simulation

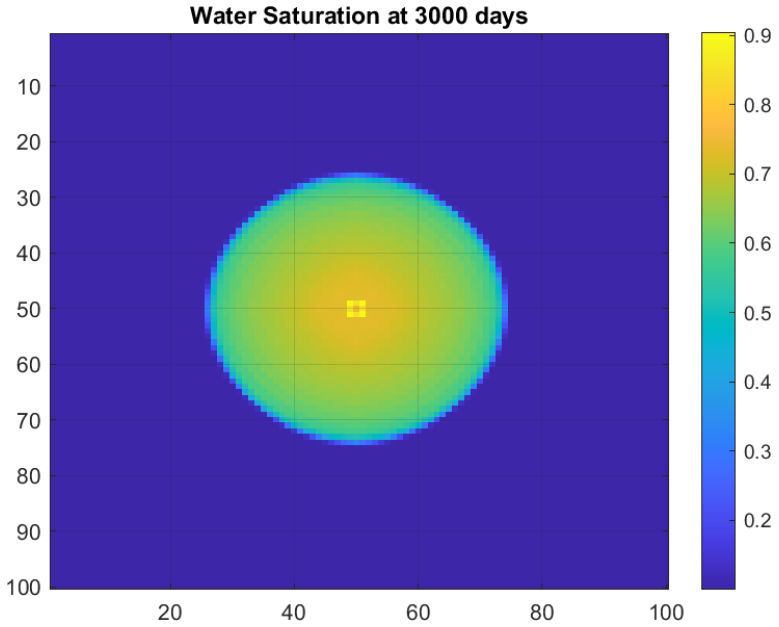

Figure 14 – 100 by 100 uniform grid water saturation at the end of simulation

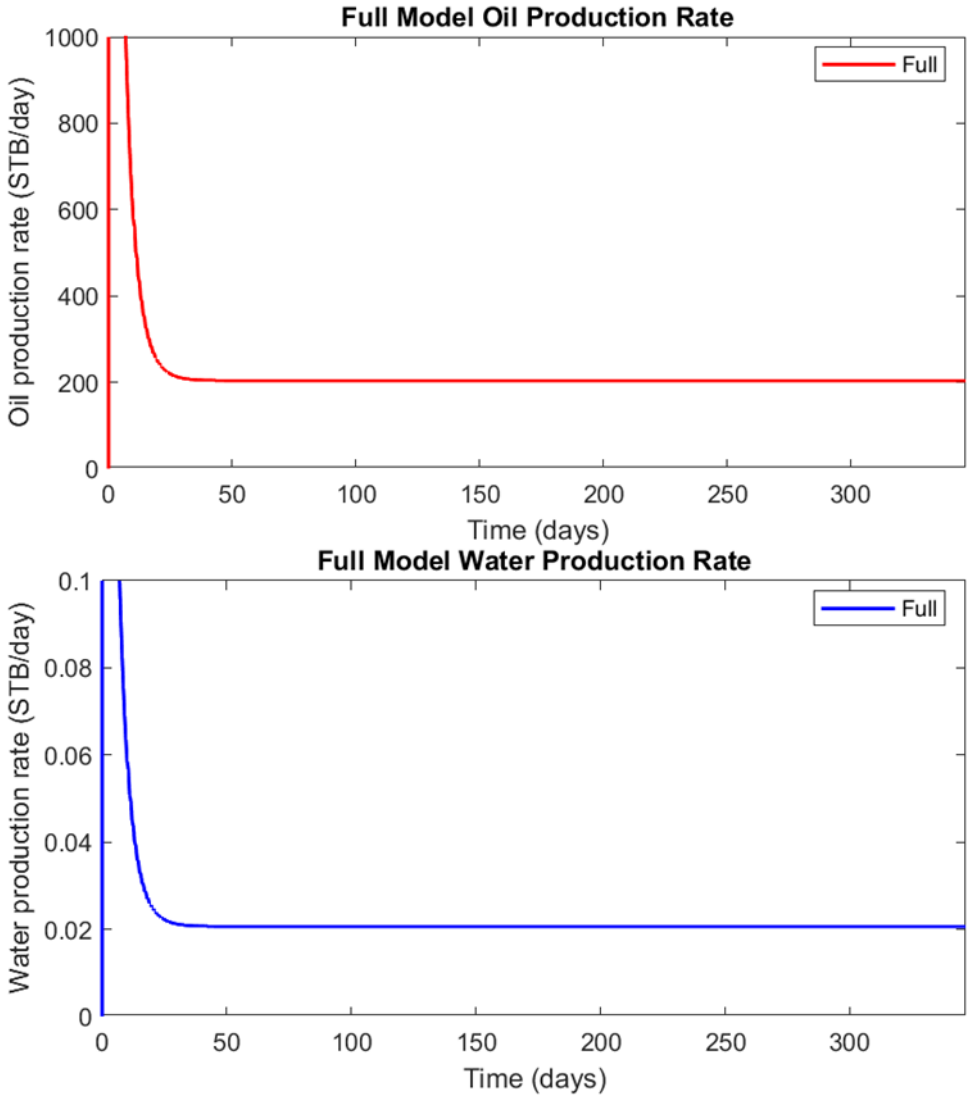

Figure 15 - 100 by 100 uniform grid oil and water production rate

Next, we performed POD-DEIM reduction with various nrF, which is the number of DEIM indices. **Fig. 16** to **Fig. 19** shows the DEIM index map corresponds to different nrF. From all those plots, the DEIM index follows a pattern which is similar to the water front dissipation map. The indices mostly cluster around the outer edge of water saturation at the end of the simulation, and around four production wells. Throughout the remaining area of the reservoir, the DEIM index distribution is more sparsely evenly distributed. As nrF decreases from 4000 to 1000, the DEIM

index appear less in the remaining area of the reservoir and eventually only cluster around the water front area.

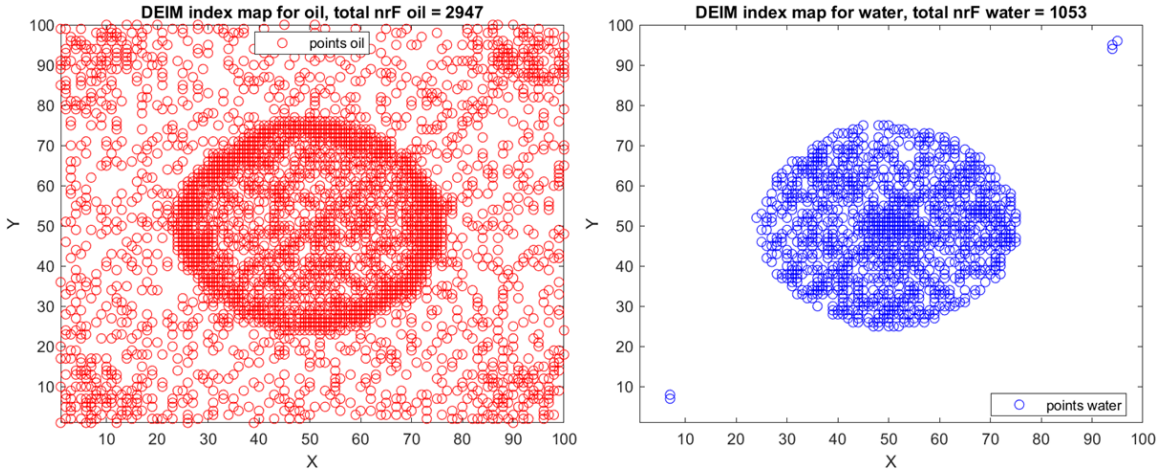

Figure 16 - A DEIM index map of 100 by 100 grids oil and water at $nrF = 4000$. Red circles are referenced to the oil front, blue circles are referenced to the water front.

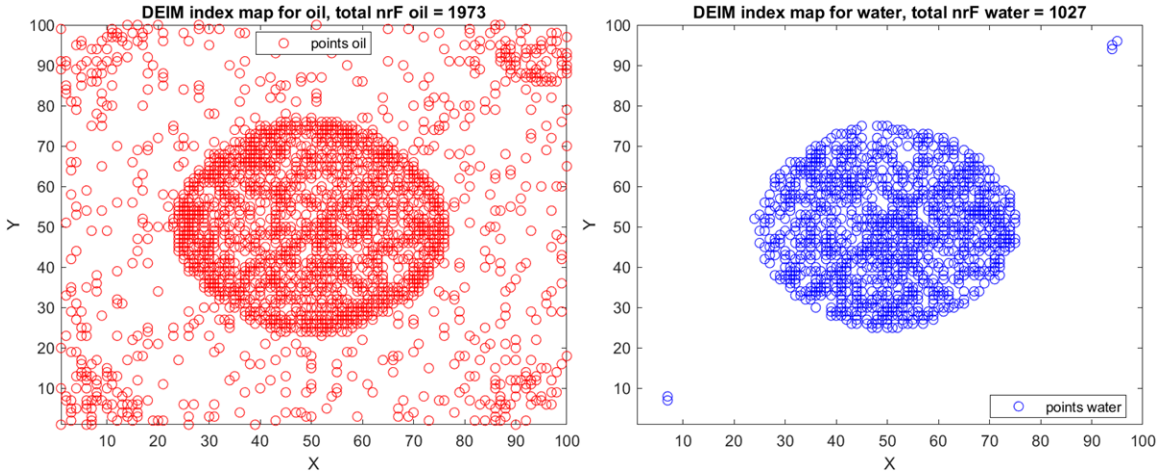

Figure 17 - A DEIM index map of 100 by 100 grids oil and water at $nrF = 3000$. Red circles are referenced to the oil front, blue circles are referenced to the water front.

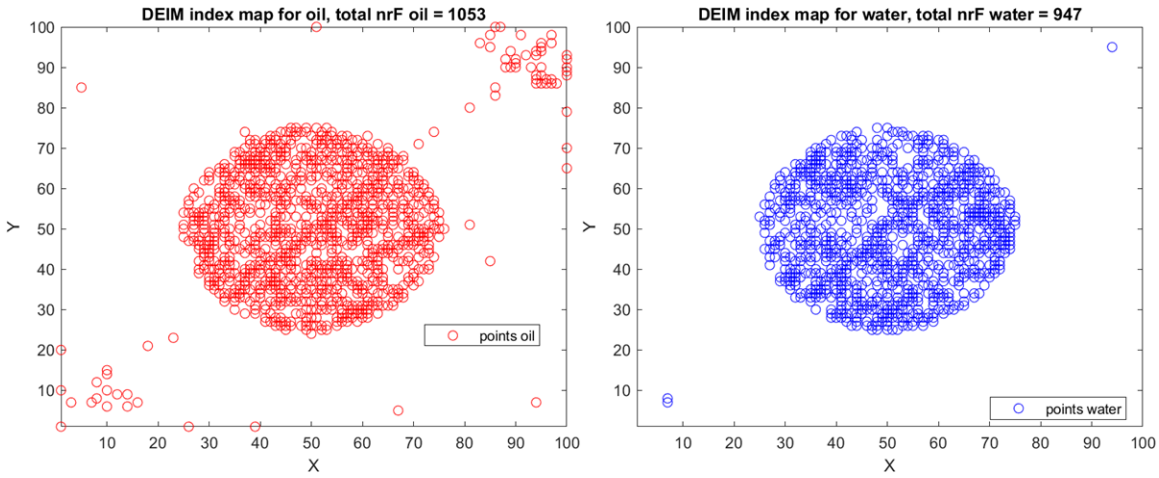

Figure 18 - A DEIM index map of 100 by 100 grids oil and water at $nrF = 2000$. Red circles are referenced to the oil front, blue circles are referenced to the water front.

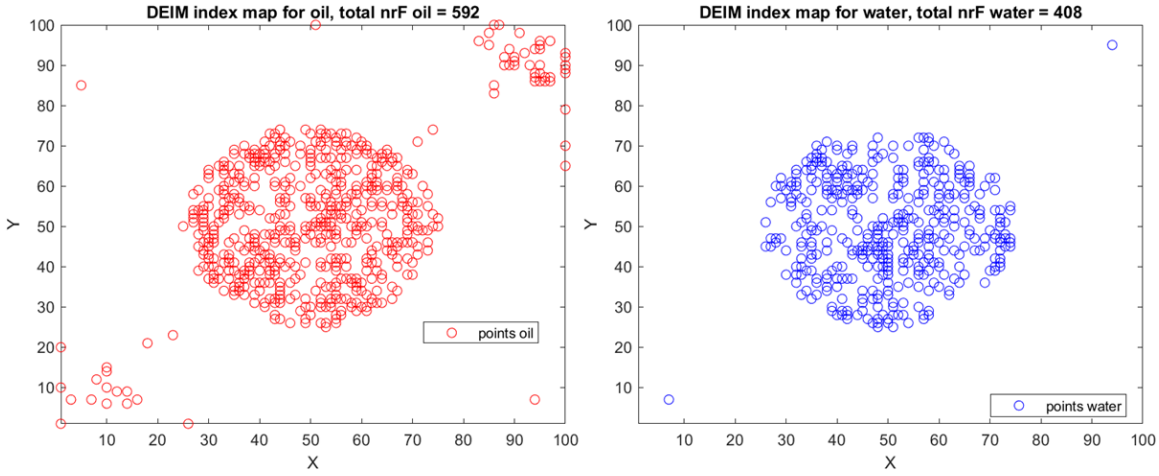

Figure 19 - A DEIM index map of 100 by 100 grids oil and water at $nrF = 1000$. Red circles are referenced to the oil front, blue circles are referenced to the water front.

Based on those different DEIM index, we performed simulation with POD-DEIM. **Fig. 20** and **Fig. 21** shows the absolute oil and water production rate error of the first two cases with $nrF = 4000$ and $nrF = 3000$, respectively.

In **Fig. 20** and **Fig. 21**, the POD-DEIM reduction gives converging results. We observe that the production rate matching of POD-DEIM with 4000 and 3000 DEIM indices follow closely with the original model around 200 STB/day. However, there is oscillation in the POD-DEIM case

production rates. The oscillation in production rate becomes more distinctive as less DEIM indices are utilized. There is also a trend that production rate error is higher in the beginning and at the end of the simulation time, resulting from the fast reservoir changes in the beginning production days and towards the end error accumulating over times.

The oil and water matching error for $nrF = 4000$ case is around 3% during most of the production cycle and around 10% in the beginning and at the end. The second case with $nrF = 3000$ generates about double the error as the first one, with 6% most of the time and 20% error in beginning and the end.

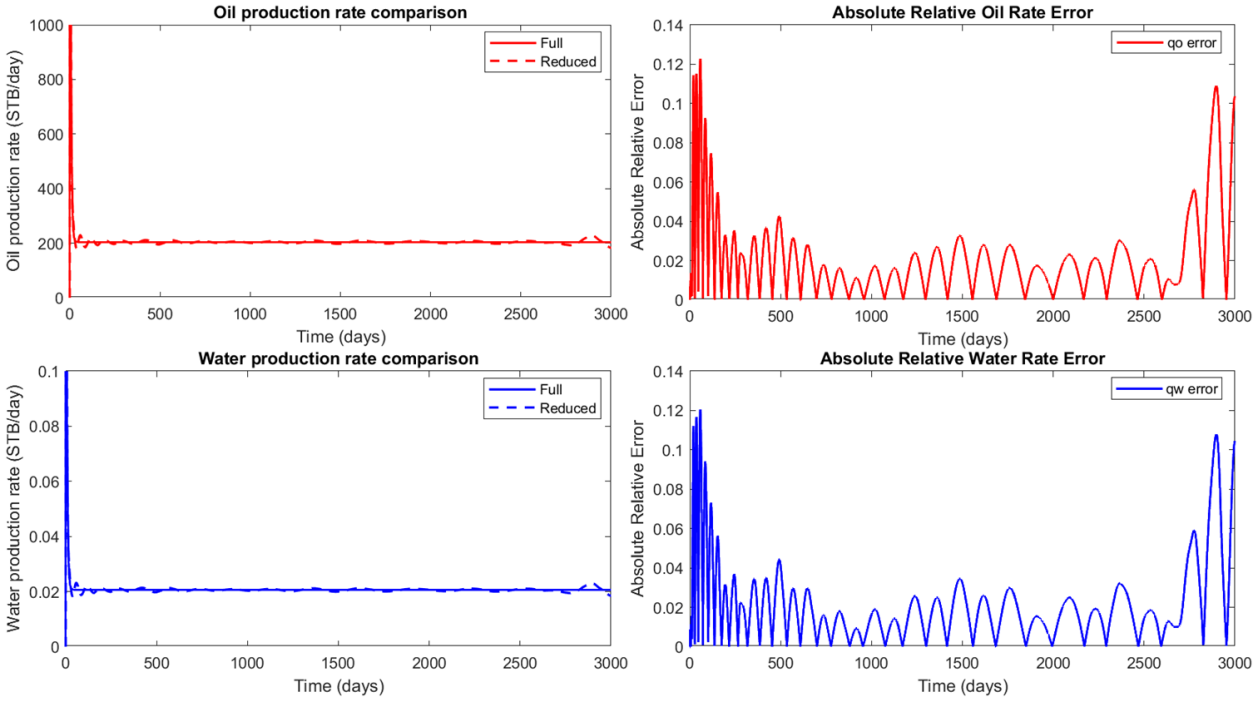

Figure 20 – Production rate and error comparison between full model and POD-DEIM reduced case, $nrF = 4000$

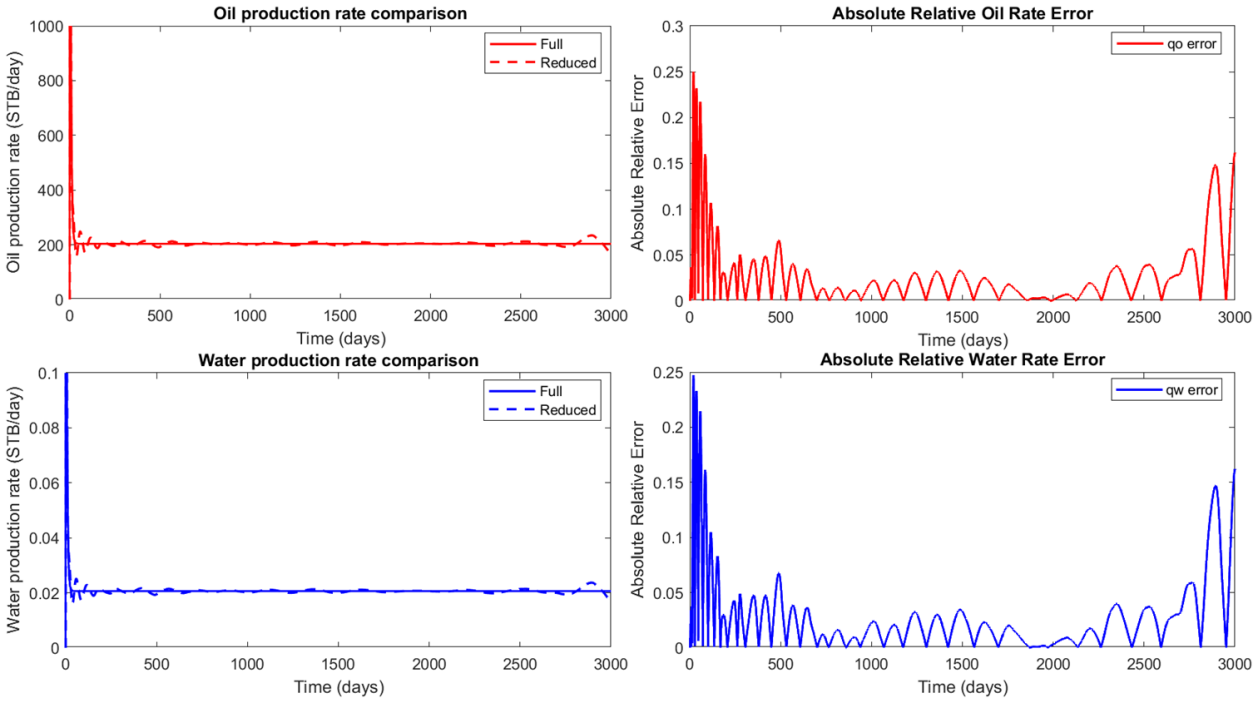

Figure 21 - Production rate and error comparison between full model and POD-DEIM reduced case, $nrF = 3000$

In the simulation using 2000 and 1000 DEIM indices, we do not have a converging reduced model. From **Fig. 22** and **Fig. 23**, both the oil and water production rate changes dramatically, resulting in the non-convergence in newton solver. As the number of DEIM index decreases, the simulation stopped due to non-convergence faster, from around 1900 days to less than 100 days. This abnormality is due to not enough POD-DEIM indices to successfully represent the overall reservoir properties, and the interpolation based on these points generates too much error in the system.

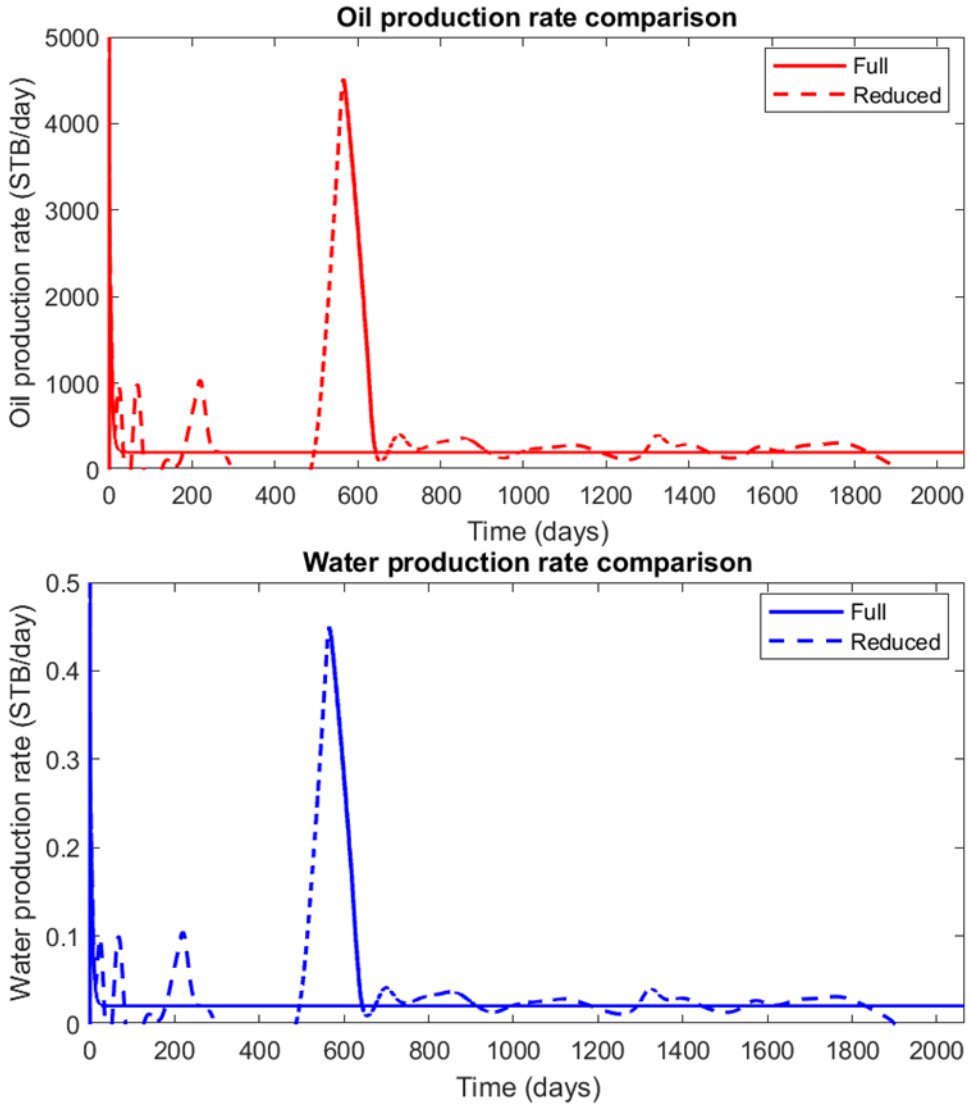

Figure 22 – Production rate comparison between full model and POD-DEIM reduced case:

Not converging production, $nrF = 2000$

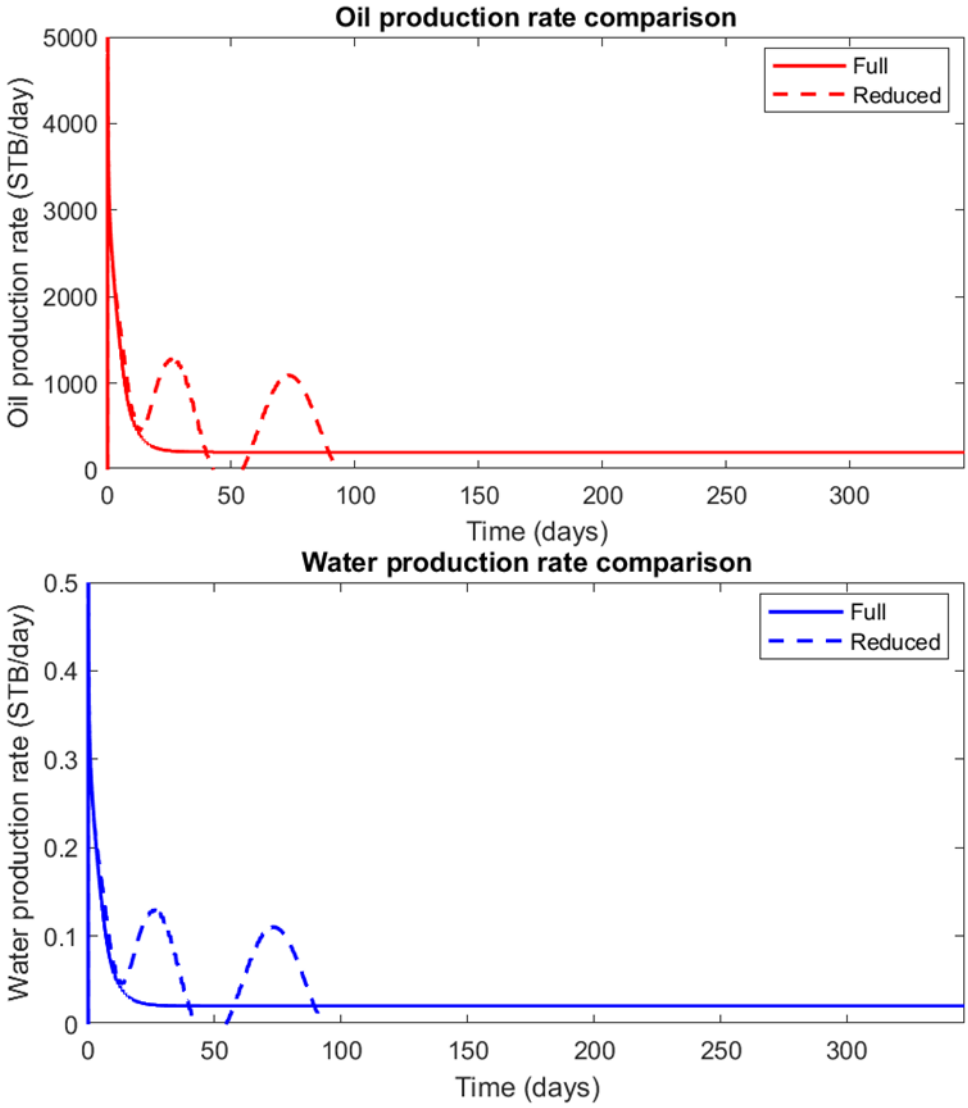

Figure 23 - Not Converging Production Rat Production rate comparison between full model and POD-DEIM reduced case: Not converging production, $nrF = 1000$

Now we investigate the time saving of POD-DEIM method. **Table 4** below shows the reservoir simulation time for full model and POD-DEIM simulation model. We treat the box in green, which is the actual reservoir simulation time, as the online time. This sets a baseline for our comparisons. The yellow box is the offline time which needs to be only computed once for the purpose of calculating the reduced basis. In the first two converging cases, the online simulation time is 921s and 1027s, respectively. The online time reduction is around 65% compared to the full simulation

time of 2843s. Even the number of POD-DEIM indices decreases, the time saving is not seen, this could be resulting from newton solver requires more iteration to converge using less POD-DEIM indices. The time required to calculating POD basis are approximately the same because we are keeping the projection matrix from states matrix consistent. The time required to computing DEIM index starting from 28s for 1000 DEIM index and it increases very fast as more DEIM index is computed, eventually reaches 768 seconds for 4000 DEIM index.

	Full simulation	POD-DEIM simulation			
		nrF = 4000	nrF = 3000	nrF = 2000	nrF = 1000
Reservoir Simulation Time	2843.469226	921.628457	1027.012157	not converged	not converged
Calculating POD basis		81.5259	80.587	79.561	80.982
Calculating DEIM index		768.1217	363.9979	140.7458	28.8095
Reservoir Simulation Time Reduction		67.59%	63.88%	N/A	N/A

Table 4 – POD-DEIM Time Reduction

Fig. 24 shows the CPU time required to calculating each DEIM index. The Y axis shows the time in seconds and the X axis represent the current number of DEIM index being computed. From this plot we can see the time increase is in an approximately exponential fashion. Therefore, if we have a large reservoir and require large amount of DEIM index, the time consumption could be very high.

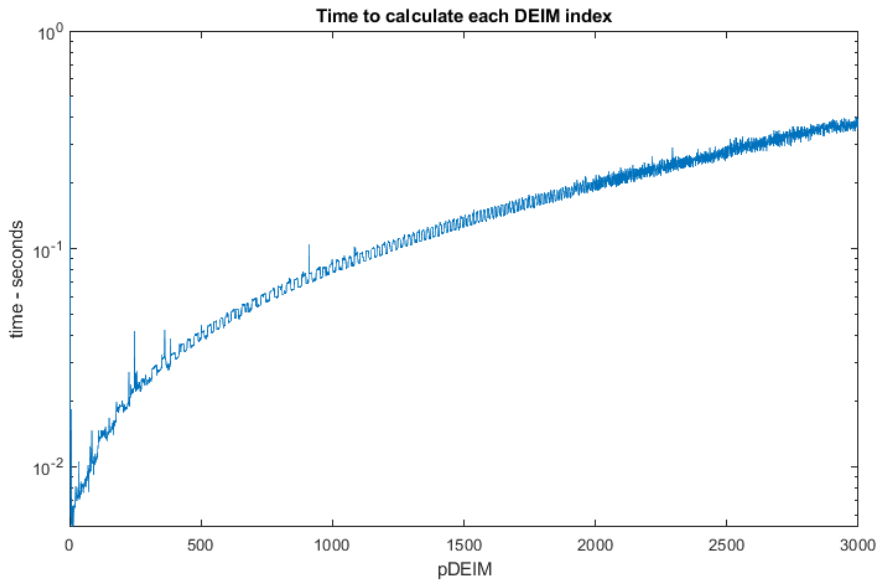

Figure 24 – Time consumption for computing DEIM index as a function of the number of DEIM interpolation points. Y axis is time in log scale.

Another drawback for POD-DEIM reduction is that the minimum number of DEIM index required for a converging simulation is high. In the study test case above, the converging number of DEIM indices is around 3000, which is about 20%-30% of total number of grids. With good conditioning and combination with the use of TPWL, the number of DEIM index could be potentially reduced to 15% of total number of grid blocks. Still, for large reservoir this problem yields large computation time and difficulty in RAM storage. Thus, in the next section, we will show the result using less DEIM index and take advantage of this to modify upscaling permeability.

3.2 Upscaling and DEIM-modified Upscaling

In this section, different model test cases using flow-based upscaling and DEIM-modified upscaling is compared together, so that we can make a direct comparison between these two techniques and assess the advantages of using the new method in a combined fashion.

In the first part of the study, conventional upscaling techniques are applied, including arithmetic, harmonic, and flow-based upscaling. The arithmetic and harmonic upscaling is conducted to obtain Wiener bound as a modification parameter. Here our focus is on the comparison of flow-based upscaling and DEIM-modified upscaling. **Table. 5** shows all the upscaling schemes conducted in the test cases for 2D and 3D models.

Case Studies					
Model Dimension	**Case**	**Upscaling Scheme**	**Production Scheme**	**Production Pressure**	**Injection Scheme**
2D	Layer 10	2 by 2	Normal 5-spot injection	Pwf = 2900 constant	Qinj = 500 STB/day constant
	Layer 25	2 by 2	Normal 5-spot injection	Pwf = 2900 constant	Qinj = 500 STB/day constant
	Layer 30	2 by 2	Normal 5-spot injection	Pwf = 2900 constant	Qinj = 500 STB/day constant
	Layer 50	2 by 2	Normal 5-spot injection	Pwf = 2900 constant	Qinj = 500 STB/day constant
	Layer 60	2 by 2	Normal 5-spot injection	Pwf = 2900 constant	Qinj = 500 STB/day constant
	Layer 70	2 by 2	Normal 5-spot injection	Pwf = 2900 constant	Qinj = 500 STB/day constant
3D	Layer 1-6	2 by 2 by 2	Normal 5-spot injection	Pwf = 2900 constant	Qinj = 500 STB/day constant
	Layer 50-55	2 by 2 by 2	Normal 5-spot injection	Pwf = 2900 constant	Qinj = 500 STB/day constant

Table 5 – All case Studies used in the research.

Next, we computed 750 DEIM indices in each of the model based on 750 timesteps. The flow-based permeability is modified with weight-based averaging using those DEIM indices.

In the following plots, we present the side-by-side comparison charts of upscaled k_x using the flow-based upscaling technique, DEIM-modified permeability, differences between two permeabilities, and the DEIM index maps. Here, we utilized only the DEIM index map of oil to modify the overall upscaling permeability because when we evaluate the upscaled model, oil rate is the most important parameter to take into consideration. Besides, in the previous section we see that DEIM index of water saturation mostly overlap with DEIM index of oil. Therefore, using DEIM index from oil pressure and evaluating oil rate matching with the original model is our main focus. In addition, the water saturation migration map throughout the production life of each reservoir is plotted, and we will analyze the pattern between DEIM index map and the water saturation map.

In **Fig. 25** – **Fig. 30**, we plotted the upscaled permeability of the first 3 layer from the Tarbet Formation, layer 1, layer 10, and layer 30, respectively. In all cases, the DEIM-modified permeability changes only at the location of the DEIM index as expected. Most of the grid block permeabilities alteration is within 50% range from the flow-based permeability. Also, we noticed that in **Fig. 25**, the DEIM index mostly located in the left bottom area of the reservoir, where the permeability and water saturation at the end of the simulation is relatively low. The index also cluster around the bottom right corner of the reservoir, where in **Fig. 26** there is a distinct water break through path from the center injector to Producer 4 located at the bottom right corner.

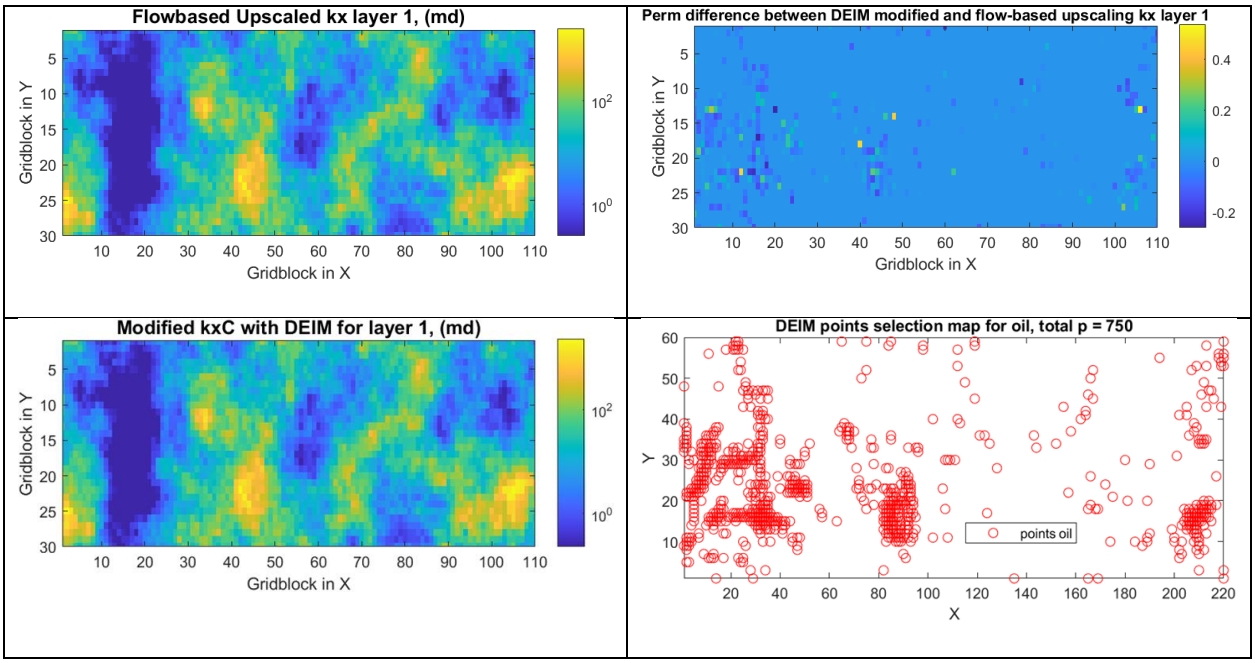

Figure 25 – Layer 1 k_x flow-based permeability vs DEIM-modified permeability

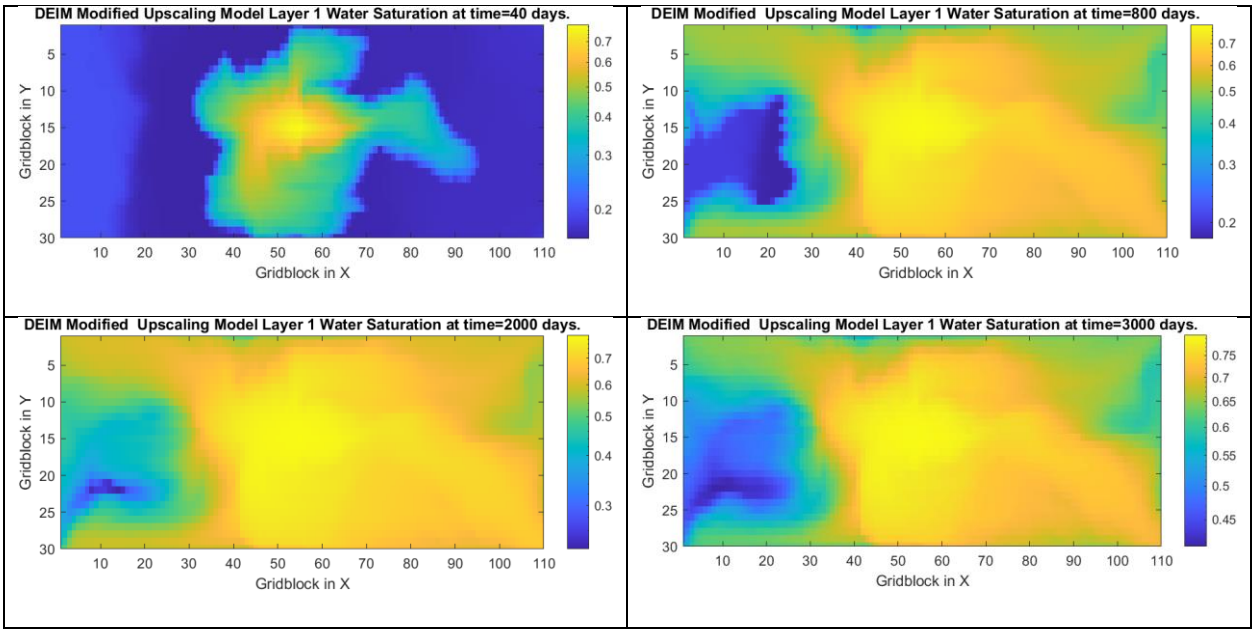

Figure 26 – Layer 1 DEIM modified upscaling water saturation map

In **Fig. 27**, the DEIM index is mostly located in the lower area where water flow does not reach. It also clusters around center of the reservoir in **Fig. 28** where permeability is very high and water saturation is highest since the injector is placed in the middle.

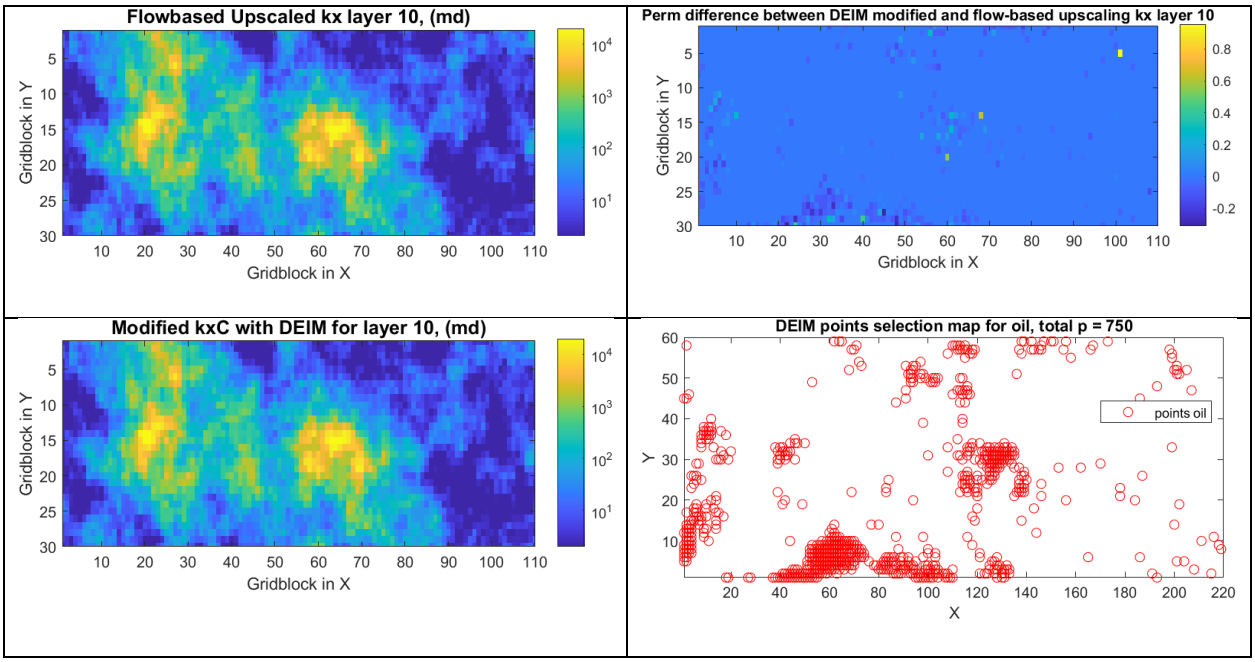

Figure 27 – Layer 10 k_x flow-based permeability vs DEIM-modified permeability

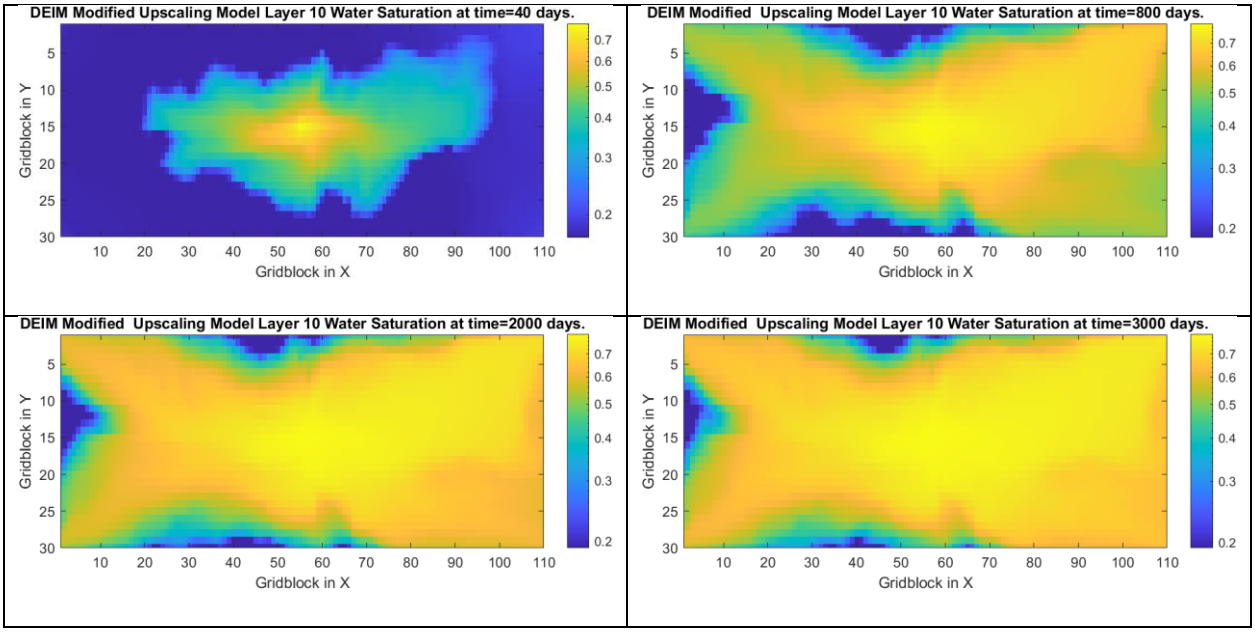

Figure 28 – Layer 10 DEIM modified upscaling water saturation map

From **Fig. 29** and **Fig. 30**, we noticed the DEIM index distribution are located around bottom left corner of the reservoir, where the water saturation is still low at the end of production life. This is also result from a low permeability barrel located in that section of the reservoir that impedes fluid flows into that section, eventually leading to low production rate for that well.

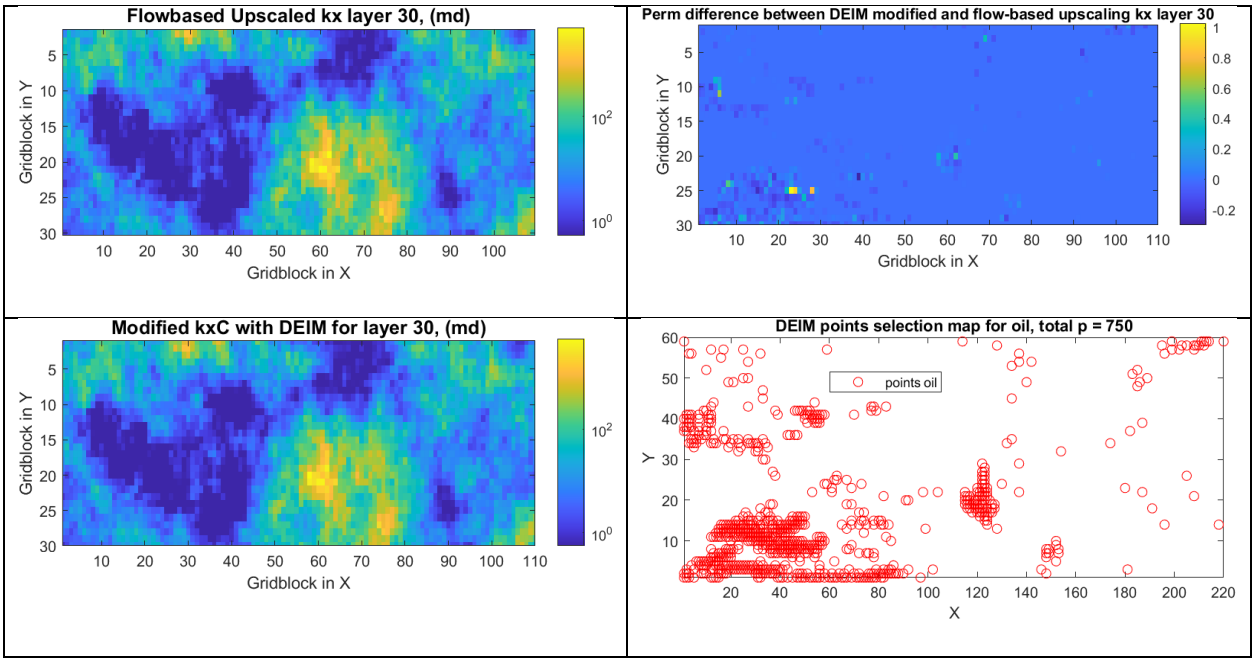

Figure 29 – Layer 30 k_x flow-based permeability vs DEIM-modified permeability

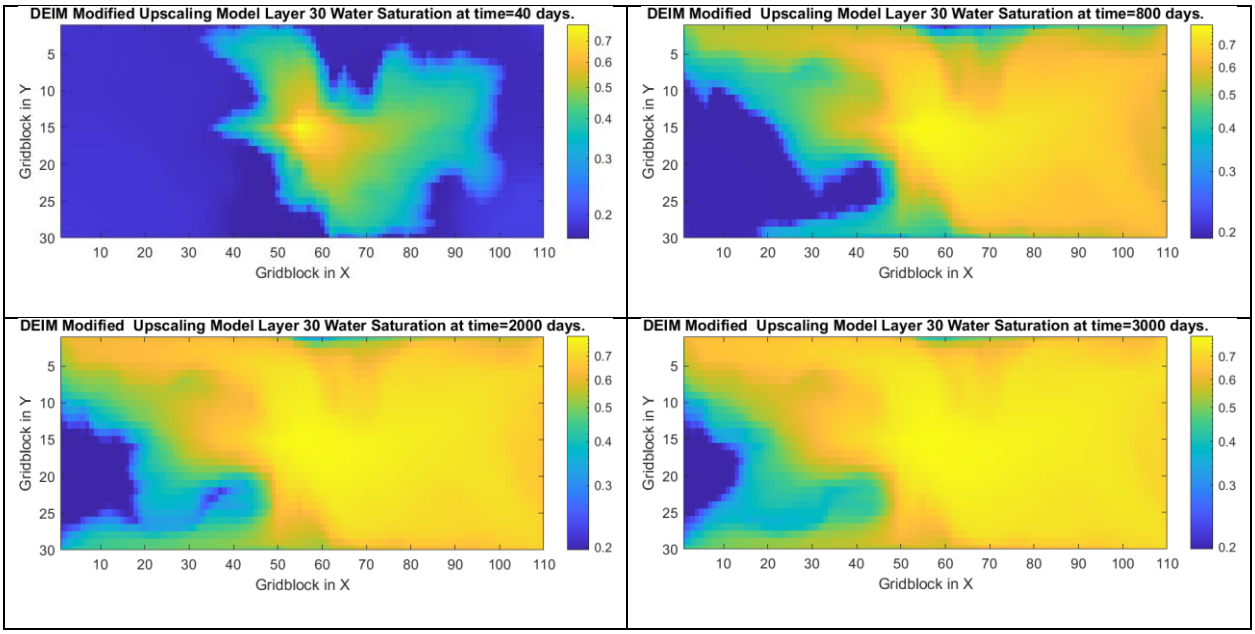

Figure 30– Layer 30 DEIM modified upscaling water saturation map

Next, we show the upscaling, and DEIM index map for layer 50, 60, and 70, which is the Upper Ness Formation. **Fig. 31** shows the channel feature in top left to bottom right direction, and **Fig. 32** shows the water flow paths go from center to the top left and bottom left. In this case, the DEIM index map overlaps very well with the water migration pattern, whereas in the right side of the reservoir there is hardly any DEIM index presents.

Since at the end of the simulation the water saturation at the top right and top bottom corner has very little alterations, and the fluid is not flowing towards those sections, oil production rate for those 2 wells is extremely low, and we see no DEIM index at those locations.

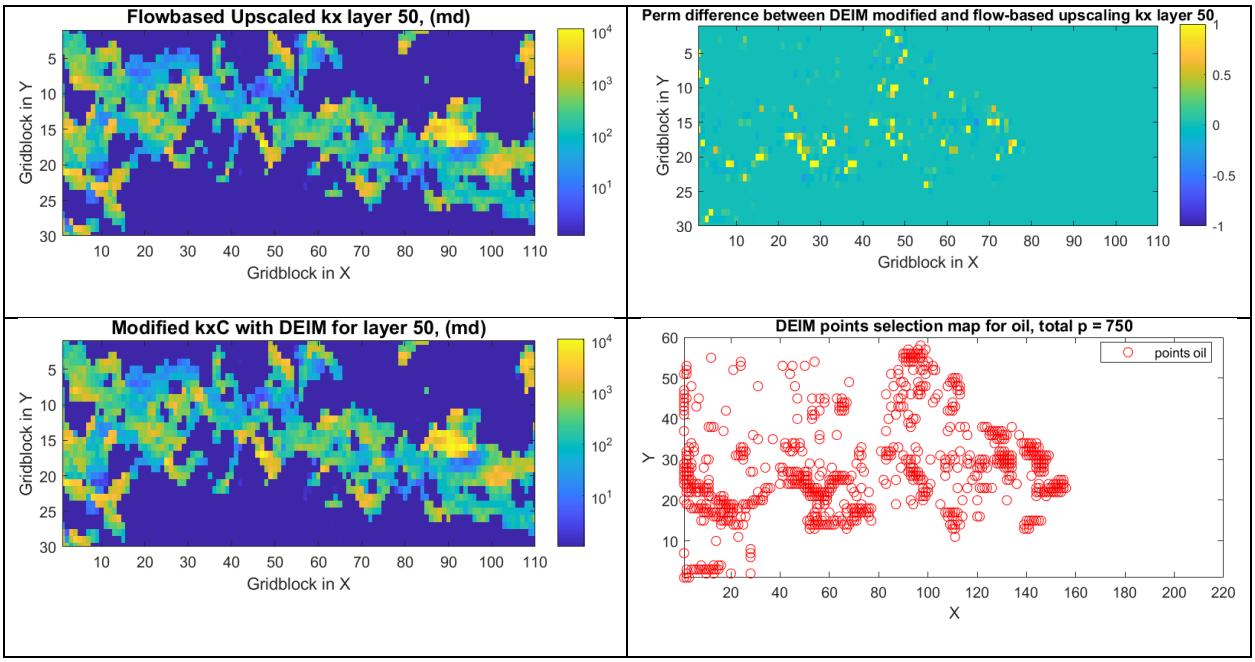

Figure 31 – Layer 50 k_x flow-based permeability vs DEIM-modified permeability

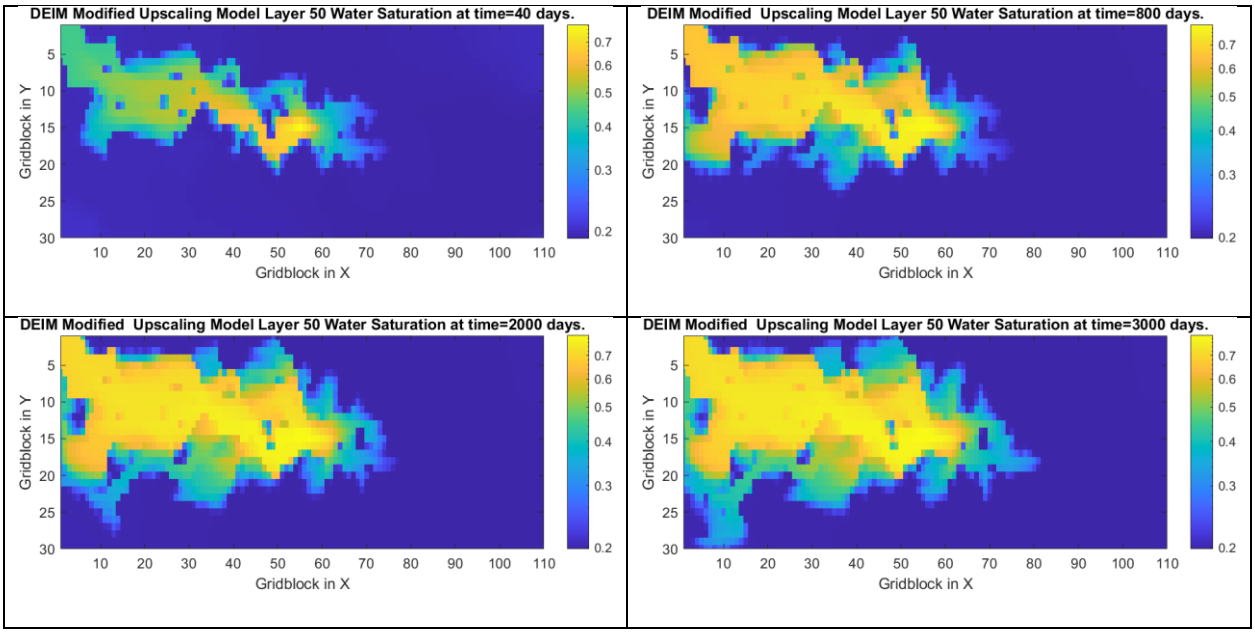

Figure 32– Layer 50 DEIM modified upscaling water saturation map

In **Fig. 33** – **Fig. 36**, DEIM index distribution map follows the same pattern as the water saturation map towards the end of simulation. In these reservoirs, the presence of high permeability channels makes water breakthrough path forms very easily towards the high permeability area. Once the water breakthrough path forms, it is difficult for fluids to flow through other area. Therefore, production rate at wells located at low permeability zone has extremely low production and DEIM index only clusters at those high permeability/ high water saturation paths.

Overall, in various test cases for the 2D reservoir, we conclude that the DEIM index map distribution follows these patterns:

- High permeability zone around injector
- Waterfront and water breakthrough/ migration path
- Near high production well with high permeability
- Near low production well with low permeability

Thus, these areas present most portion of the reservoir where most or least fluid dynamics occurs. In the next section we present the oil rate, water cut, well block pressure and water

saturation comparison between the flow-based upscaling and DEIM-modified permeability upscaling.

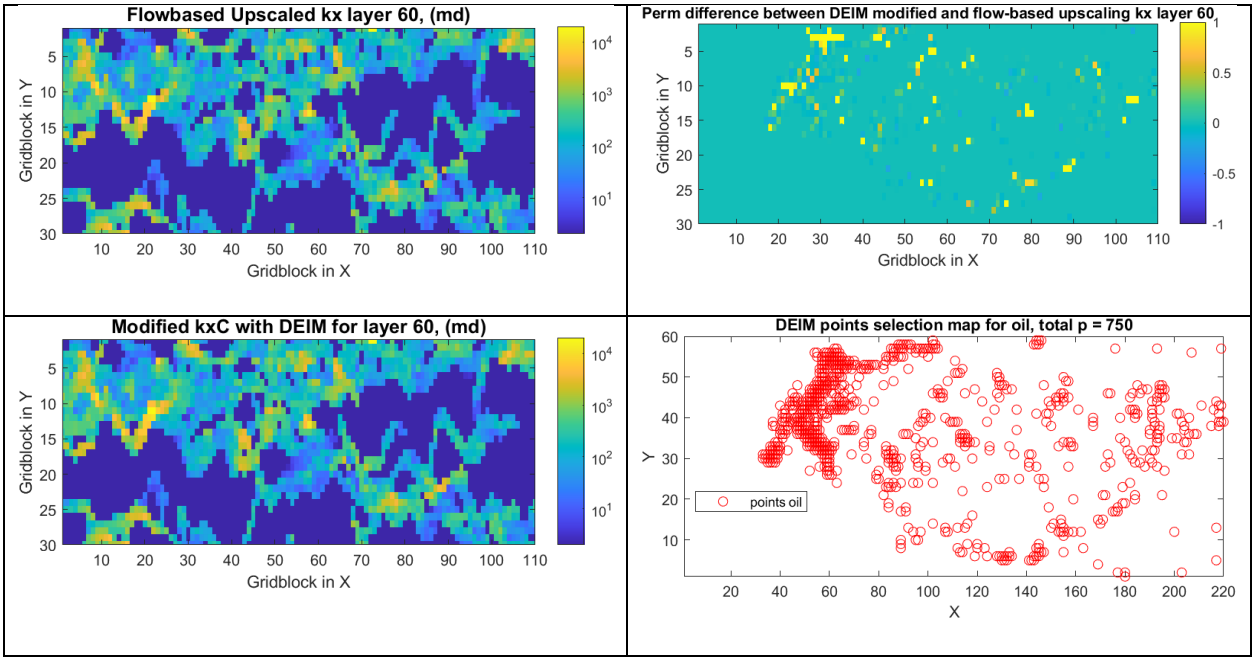

Figure 33 – Layer 60 k_x flow-based permeability vs DEIM-modified permeability

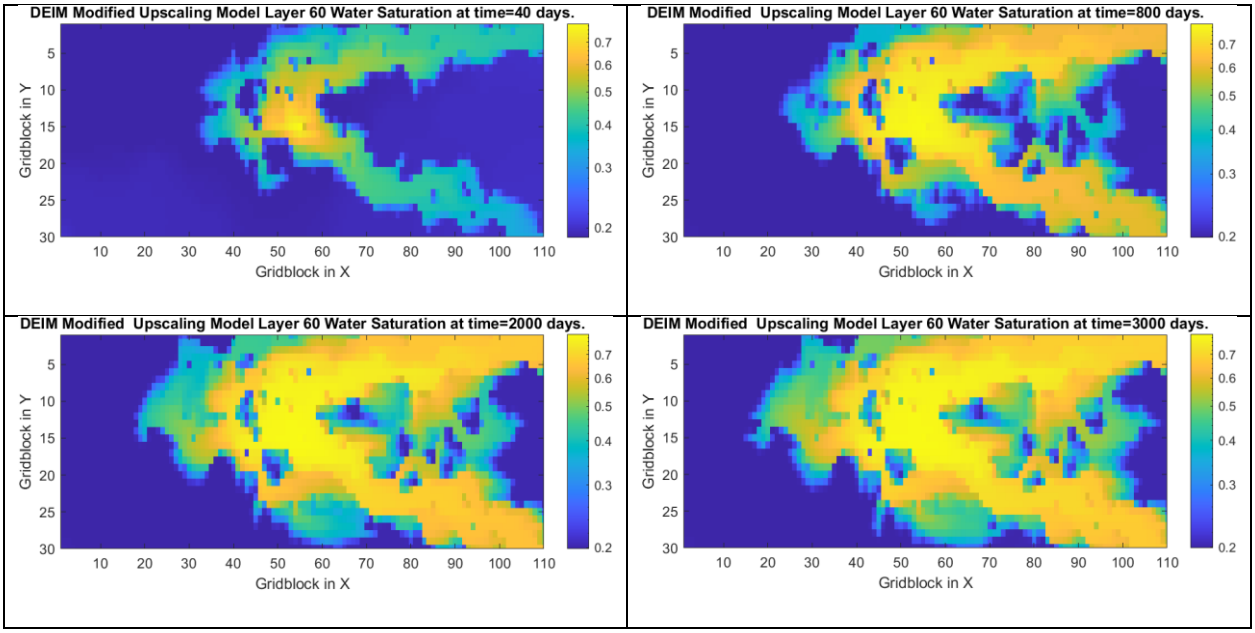

Figure 34– Layer 60 DEIM modified upscaling water saturation map

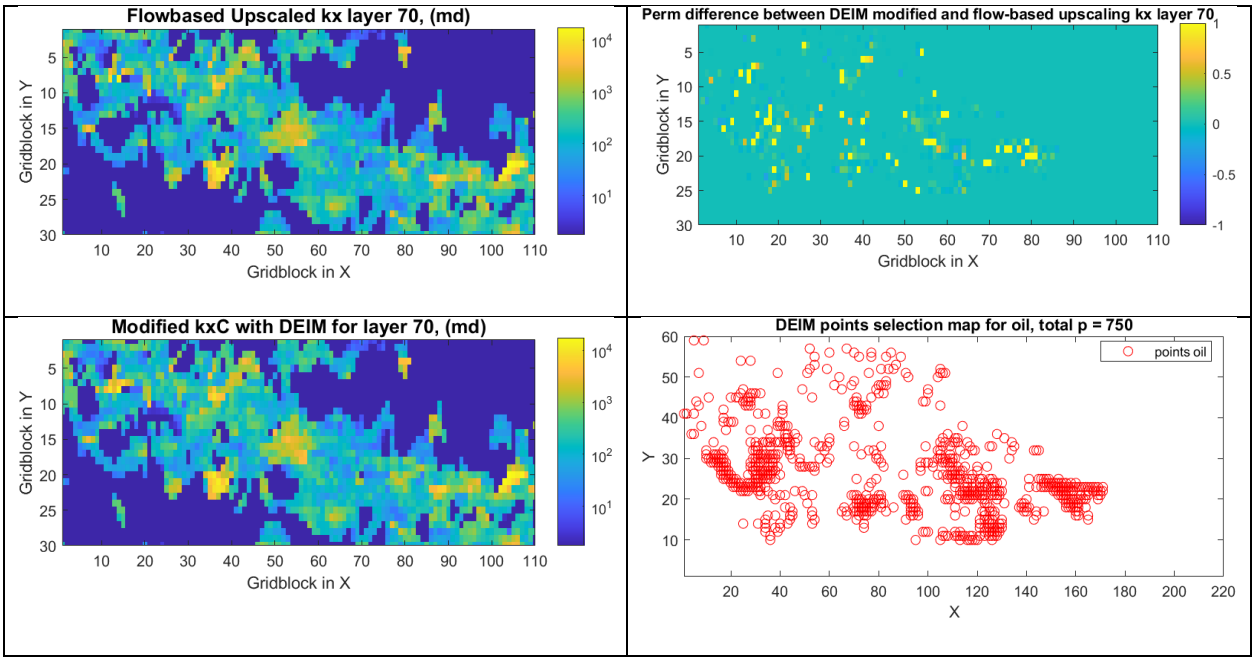

Figure 35 – Layer 70 k_x flow-based permeability vs DEIM-modified permeability

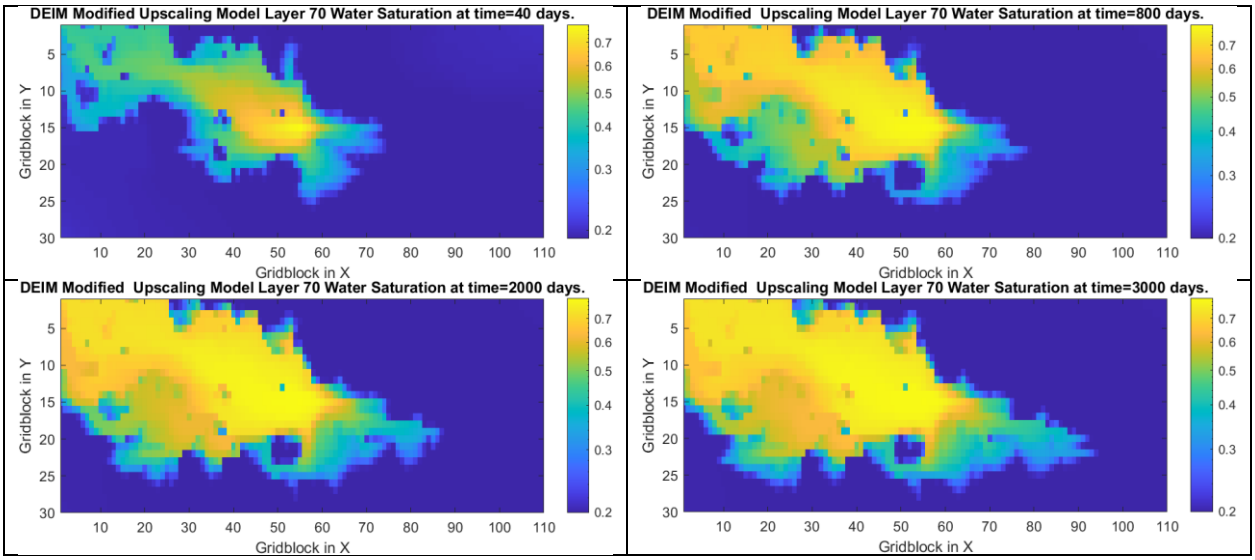

Figure 36– Layer 70 DEIM modified upscaling water saturation map

3.3 Flow-Based Upscaling vs DEIM-Modified Upscaling

To assess the performance of the upscaled model as compared with the original model, several parameters are mostly used for evaluation: oil production rate, well block pressure, well block water saturation and water cut. In the following plots, flow-based upscaling and upscaling with POD-DEIM index modification is compared using those parameters. The relative errors of those two methods are evaluated, and eventually we compare the time reduction between two methods and summarize the benefits of the proposed new methodology.

First, we compare the relative oil production rate between flow base upscaling and the new method. The error shown in **Eq. 28** is relative to the full model results, which we simulated in the beginning of our test cases. **Fig. 37** to **Fig. 39** shows the relative oil production rate errors for models in Tarbet Formation. In **Fig. 37**, layer 1 has very mild error rate improvement in Producer 2 and Producer 3, where the production rate errors in other producers are basically the same. In **Fig. 38**, we observe a mild error reduction in Producer 2, located at the bottom left corner. Referring to **Fig. 27**, the DEIM index clustering around Producer 2 contributes to the permeability changes in that area and leads to production rate improvements. Similarly, in **Fig. 38**, Producer 3 and Producer 4 has a descent error reduction due to the DEIM index mainly clustering at the bottom left and top left corners referring to **Fig. 27**.

$$Absolute\ relative\ error = \frac{\left|Q_{upscaled} - Q_{original}\right|}{\left|Q_{original}\right|} \tag{28}$$

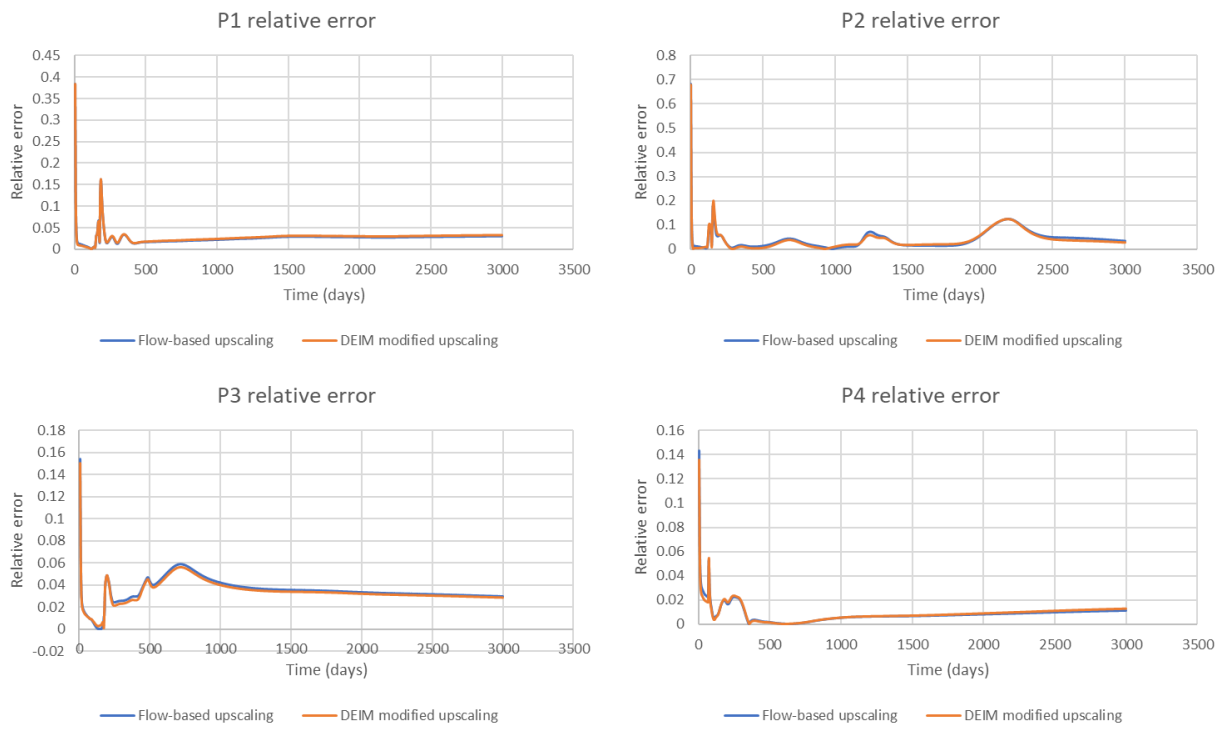

Figure 37 – Layer 1 oil production rate comparison for the four producers.

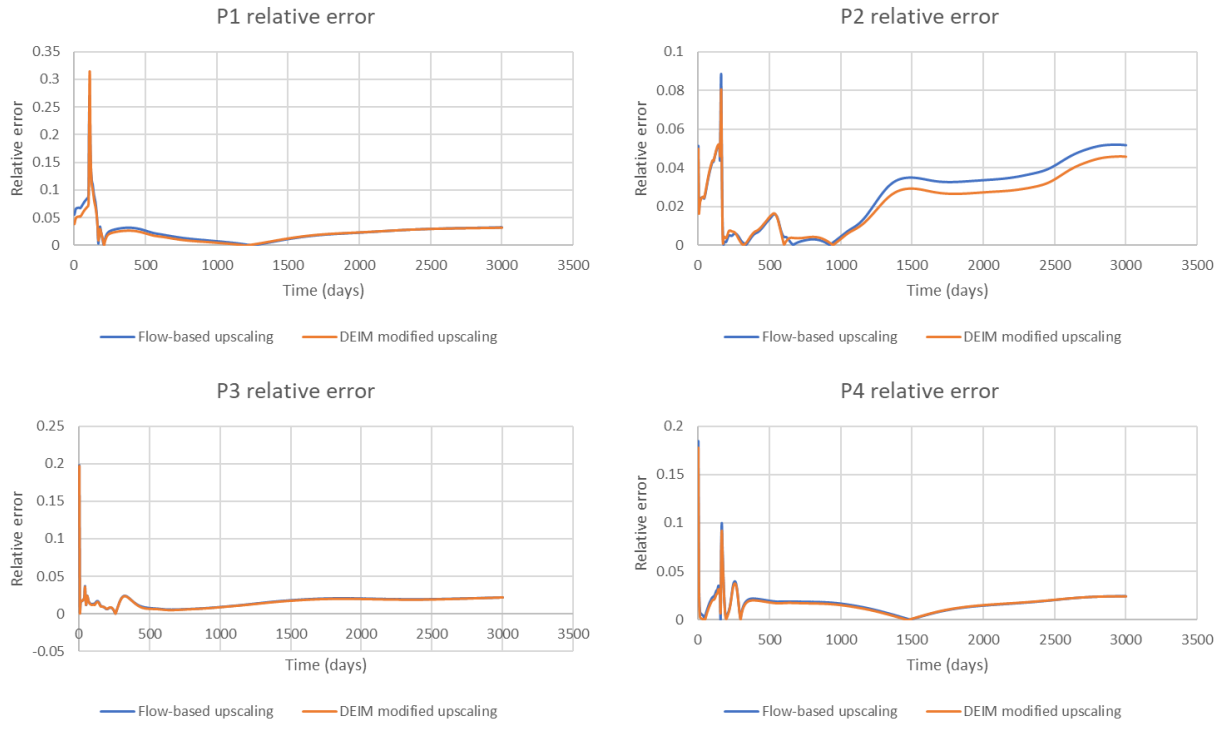

Figure 38 – Layer 10 oil production rate comparison for the four producers.

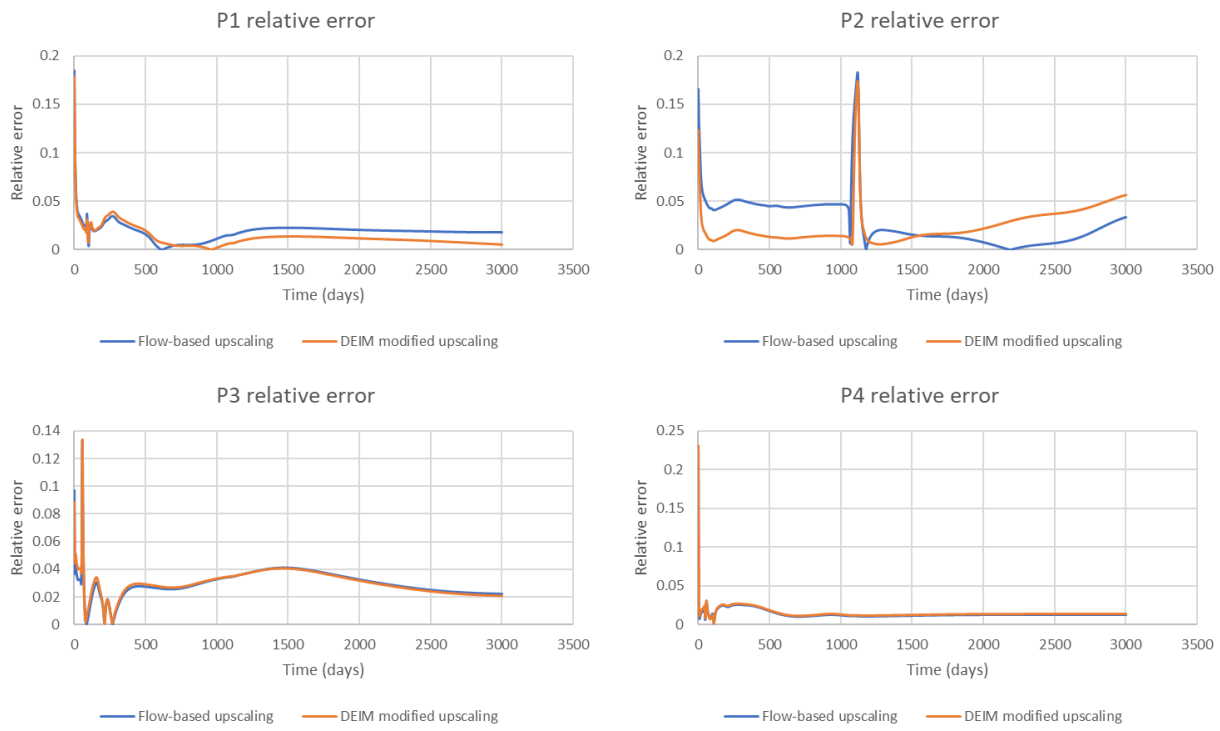

Figure 39 – Layer 30 oil production rate comparison for the four producers.

In **Fig. 40** to **Fig. 42**, layer 50, 60, and 70, we observe that the relative error rate decreases much more for reservoir in Upper Ness Formation which has predominantly high permeability channel structures. In **Fig. 40**, Producers 1, 3, 4 all have a reasonable error reduction, around 5% in each case. This reduction results from DEIM indices in **Fig. 31** are populated on the fluid flow paths of that connect these wells. Even though upscaling on these complex geological structures has erased some of the channel features and yields errors, the process of reevaluating that permeability selected by POD-DEIM algorithm has counter that effect and improve production rate accuracy. As experimented previously, grids that are selected by DEIM algorithm are where most fluid dynamics happens in the reservoir. Therefore, highlighting the influence of those grid block permeability in overall upscaling permeability results in a better reservoir characteristic matching and production rate matching improvement.

In **Fig. 41** and **Fig. 42**, three our of four producing wells have some oil rate error reduction. The side effect is that 1 well out of all 4 has a mild error increase as in the case of P3 in layer 60 and P1 in layer 70. This could be the result of too less or too much permeability modification based on the DEIM indices distribution. But overall, these results show a positive effect of upscaling model oil rate matching improvements.

Besides the 2D cases, in **Fig. 43** and **Fig. 44**, we observe similar error rate changes for layer 1-6 and layer 50-55 model. In both cases, 3 wells have error reduction around 5% to 10% and 1 well, P1 from the first model has error increment that is over 15%. Nevertheless, this result is coming from modification using 750 DEIM indices only, whereas the number of grids in those 3D reservoirs is 79200. If more DEIM indices is computed based on large number of timesteps, we will expect more permeability alterations in the reservoir and overall better error rate reduction.

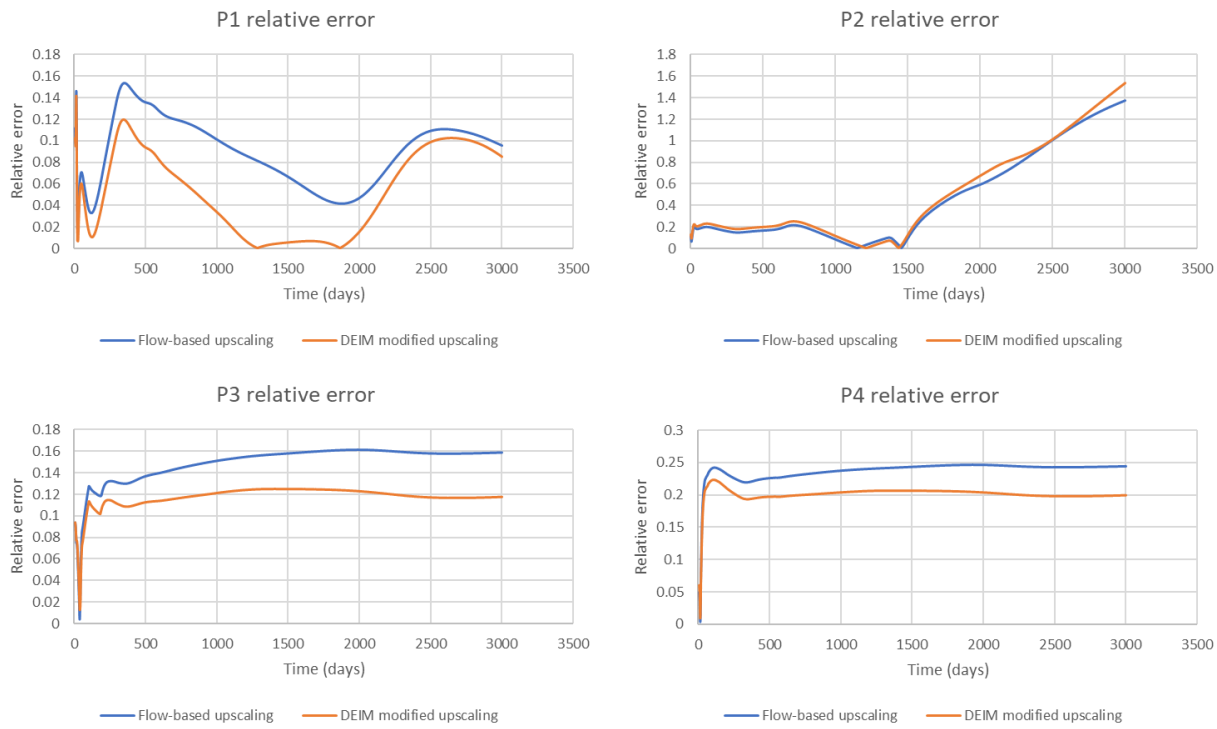

Figure 40 – Layer 50 oil production rate comparison for the four producers.

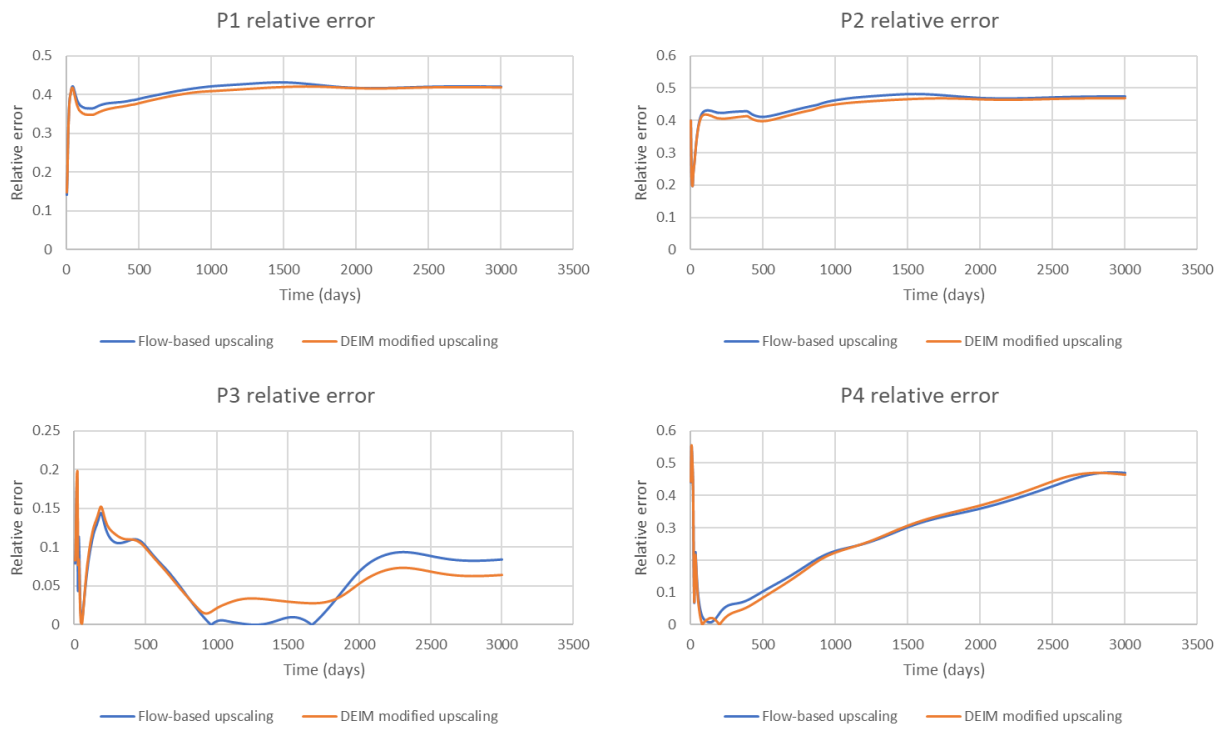

Figure 41 – Layer 60 oil production rate comparison for the four producers.

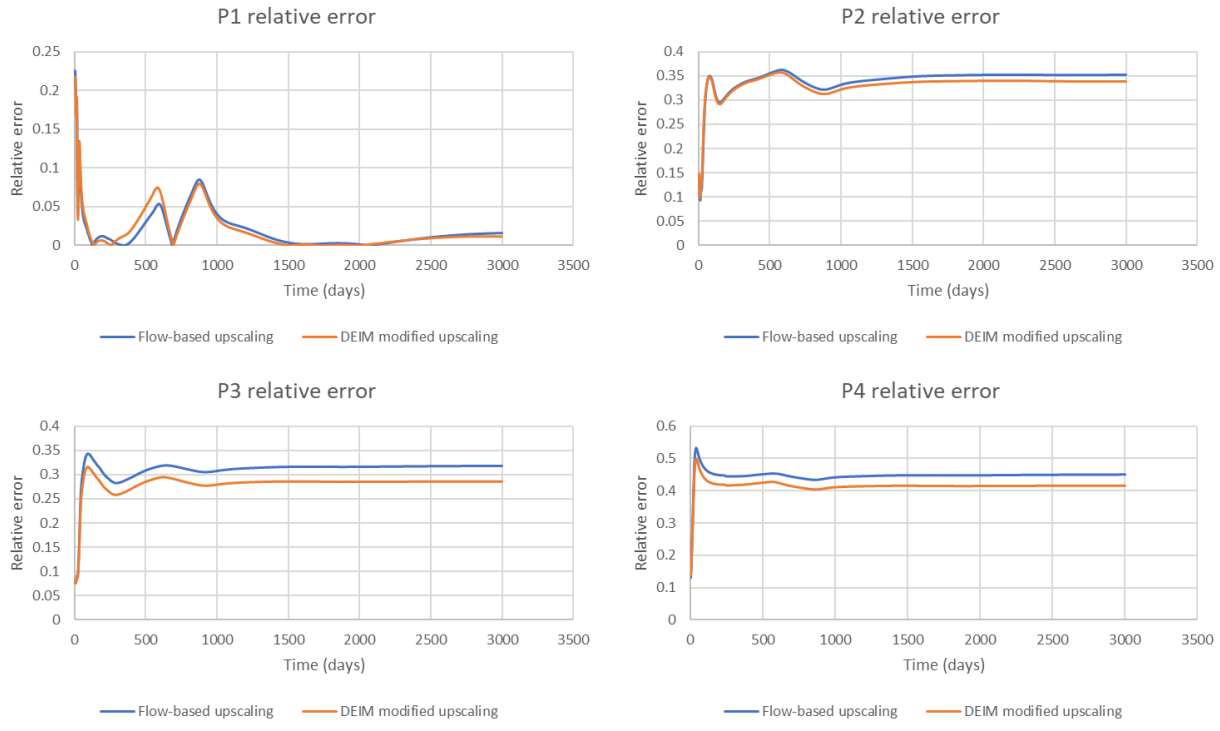

Figure 42 – Layer 70 oil production rate comparison for the four producers.

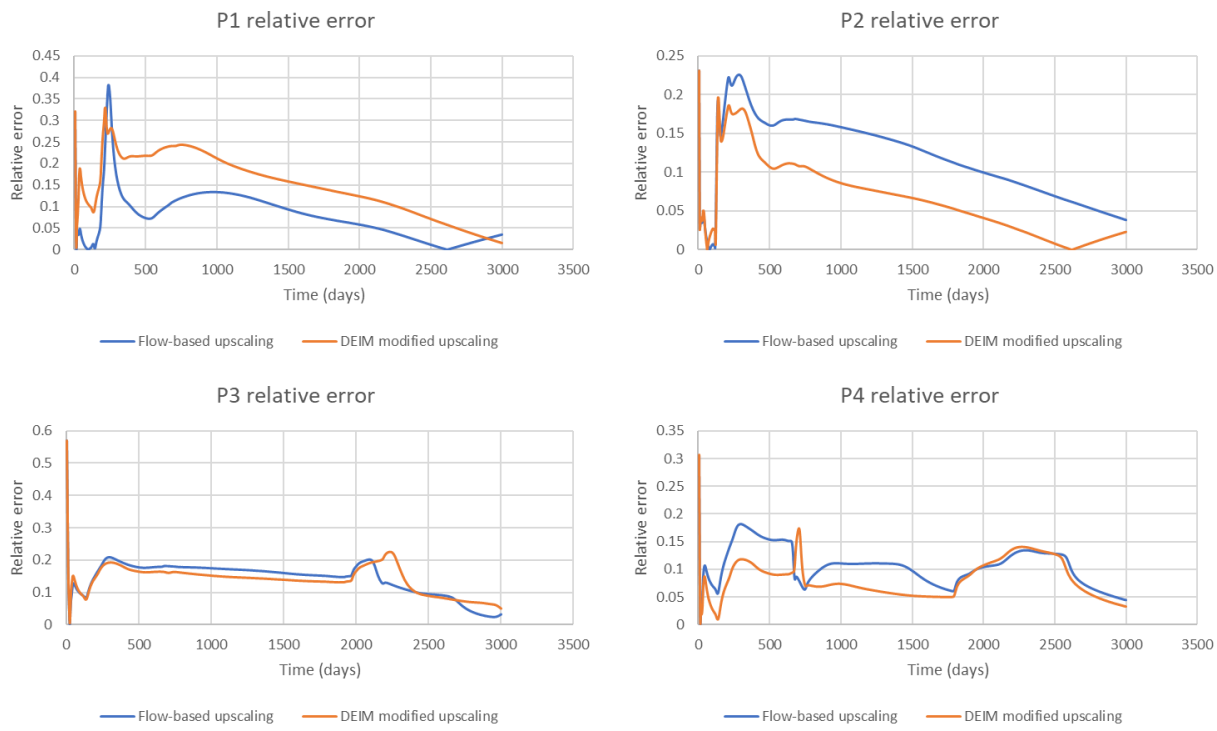

Figure 43 – 3D Model Layer 1-6 oil production rate comparison for the four producers.

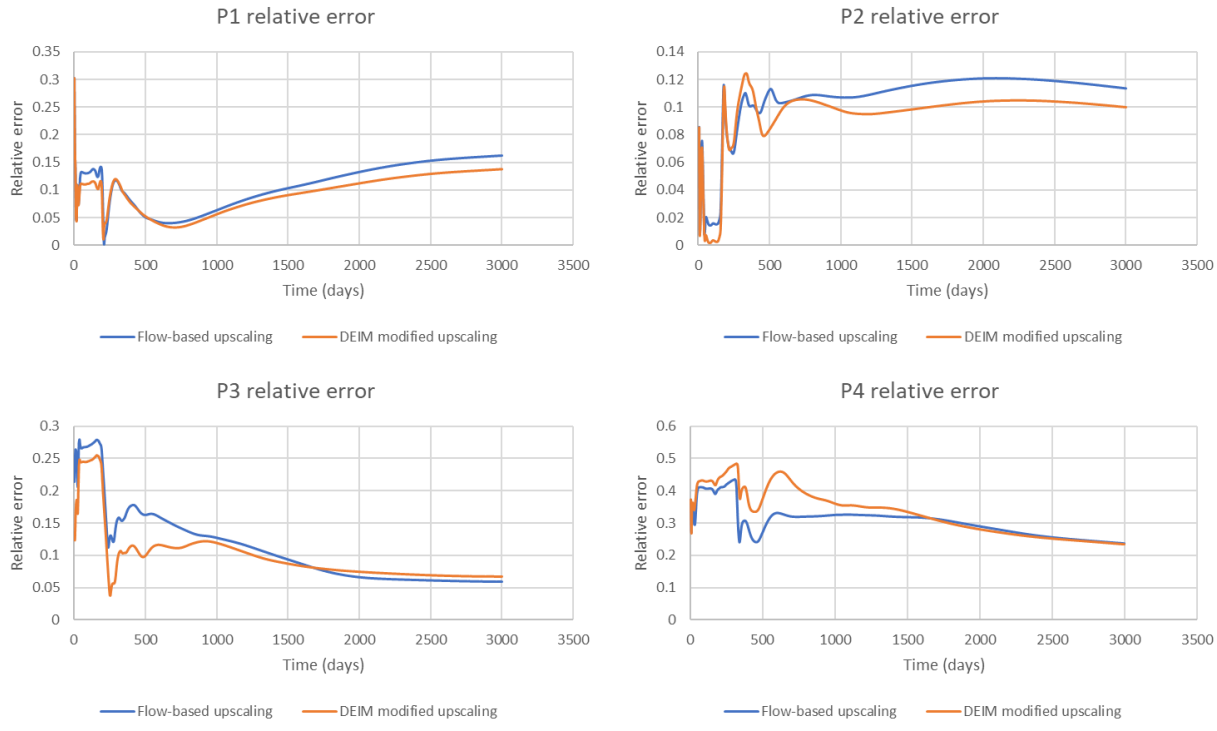

Figure 44 – 3D Model Layer 50-55 oil production rate comparison for the four producers.

Besides the measurement of oil production rate error, other important parameters that evaluate the extent of reservoir characteristic similarity are well block pressure, water saturation, and water cut ratio. Since the 3D cases have numerous well blocks perforated, we only compared the above parameters of 2D cases for evaluation purposes.

Fig. 45 – **Fig. 53** shows each of those measurements for the model of layer 1, 10, and 30 in Tarbet Formation for flow-based upscaling, DEIM-modified upscaling, and most importantly, the comparison of relative error between the two. We can see that in each of these plots, the well block pressures of the DEIM-modified upscaling cases are always consistent with the flow-based upscaling method. Some cases such as P3 of layer 1, and P1, P3 of layer 3 has a mild error reduction in well block pressure around 1%. In the well block water saturation and water cut criteria, the DEIM modified upscaling case has almost exact same relative error as the upscaling method, with some cases having a mildly error reduction as well.

This finding indicates that even with some changes in the upscaled permeability data, the overall reservoir characteristic matching is not jeopardized. The well block pressures, water saturation, water cut all have consistent value with the flow-based upscaling model, while some well blocks have a mild relative error reduction.

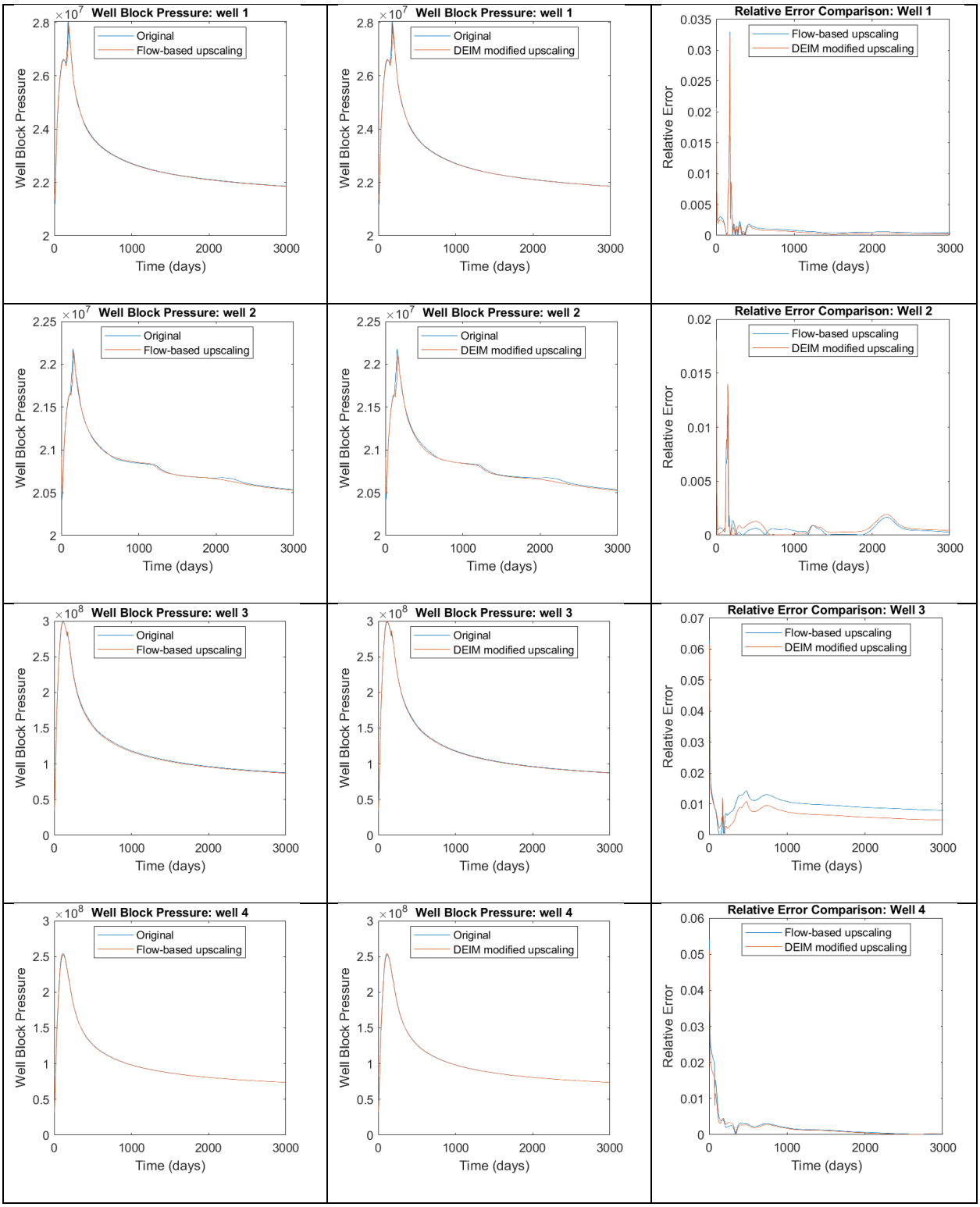

Figure 45 – Layer 1 wells block pressures comparison for the four producers.

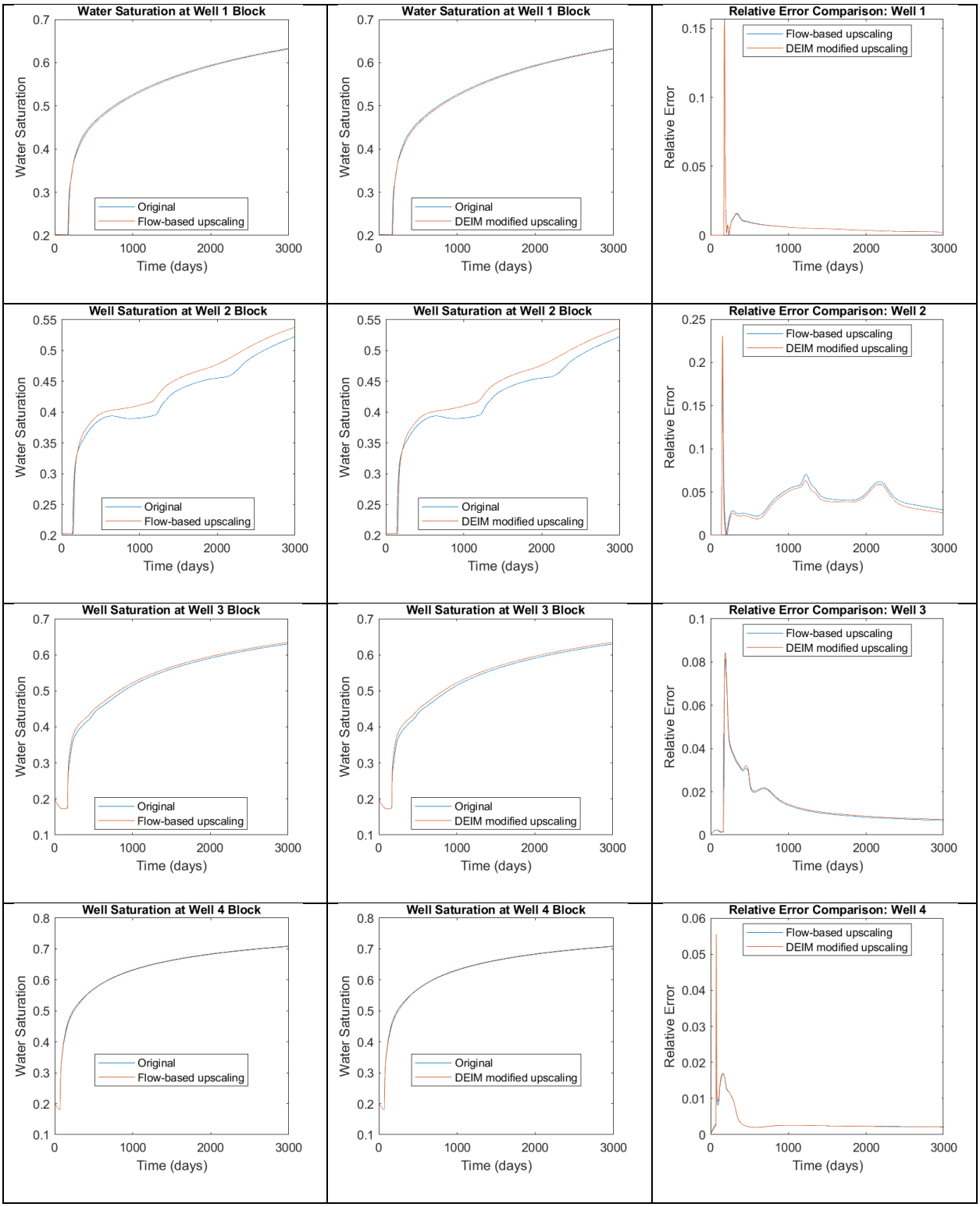

Figure 46 – Layer 1 wells block water saturation comparison for the four producers.

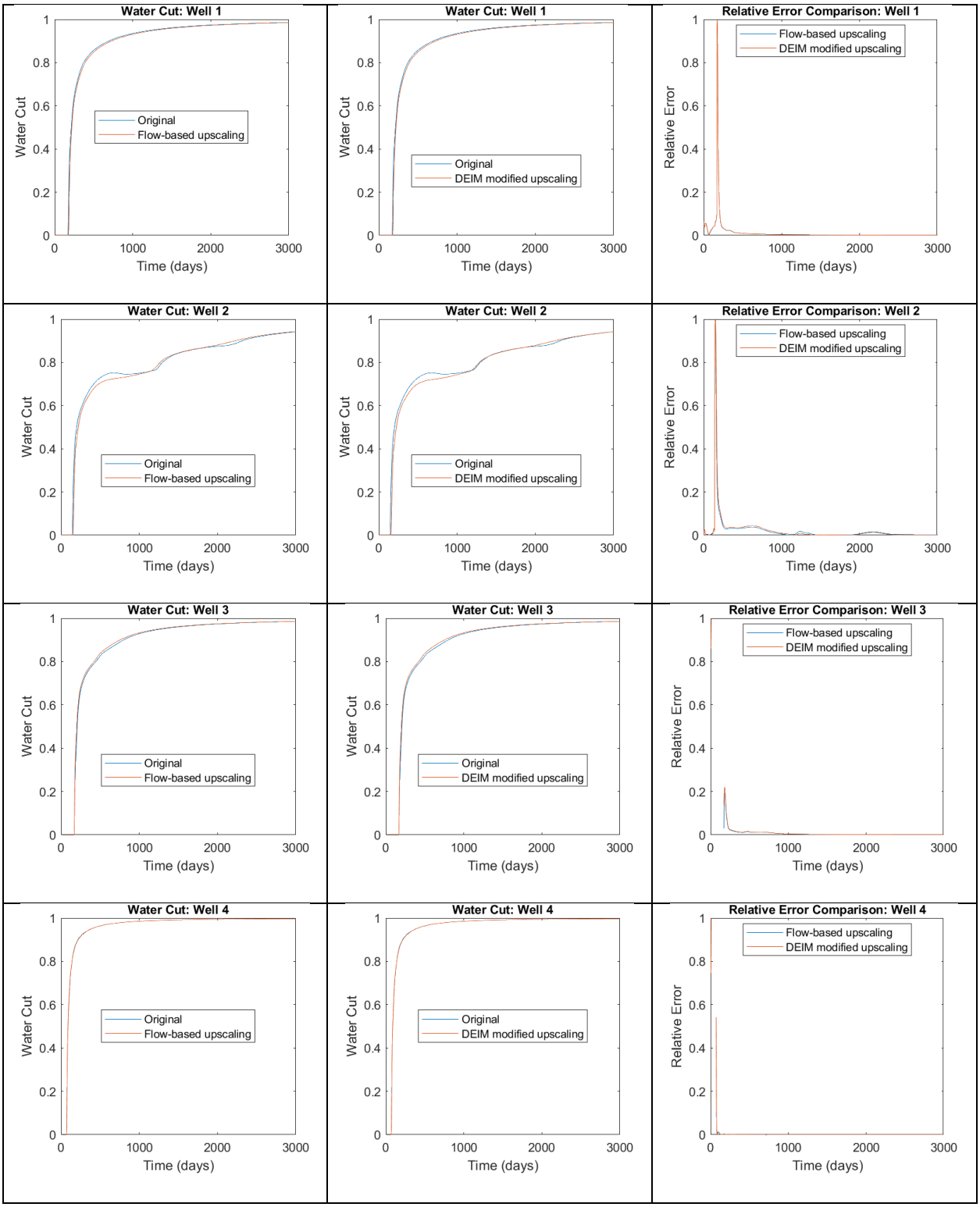

Figure 47 – Layer 1 wells water cut comparison for the four producers.

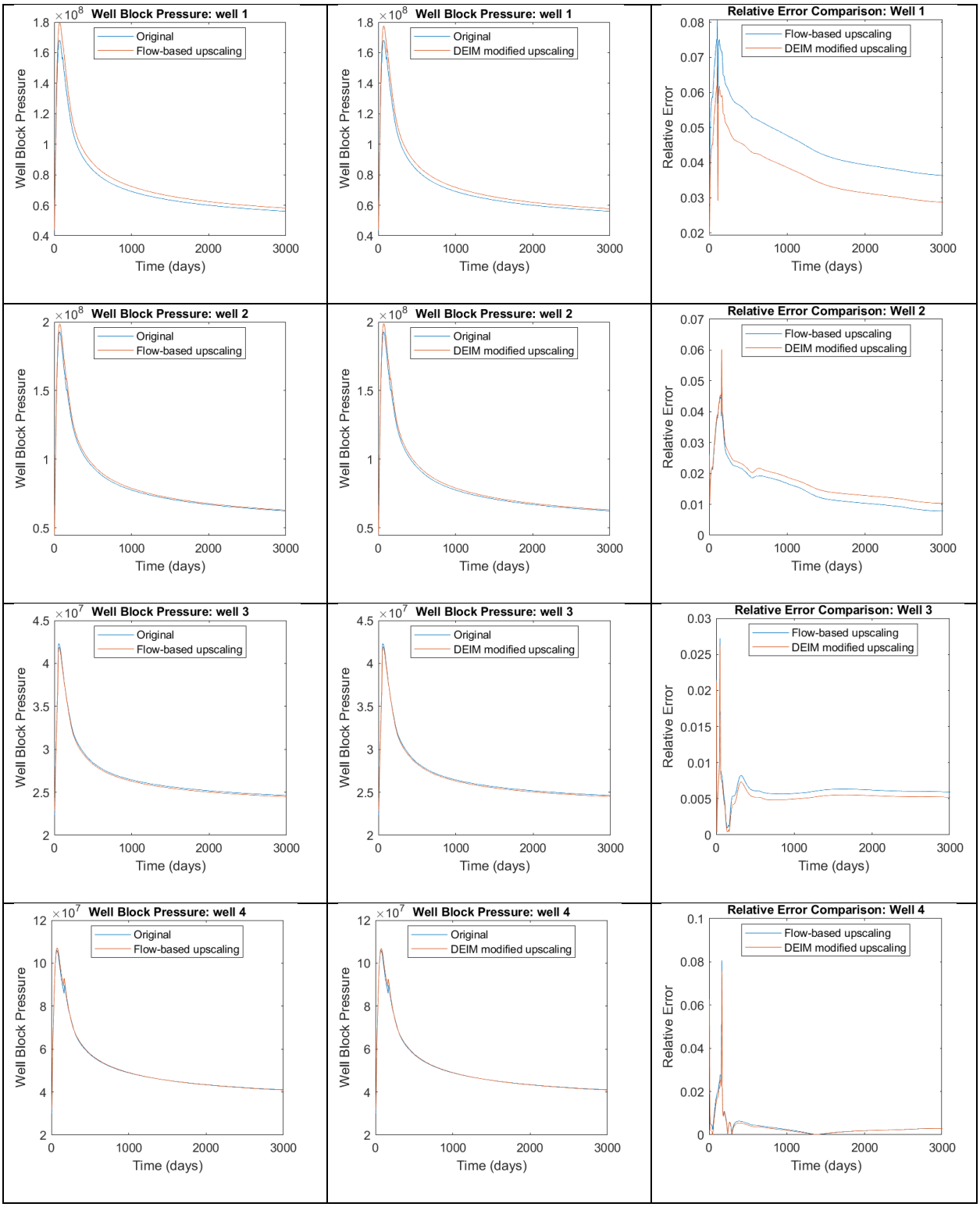

Figure 48 – Layer 10 wells block pressures comparison for the four producers.

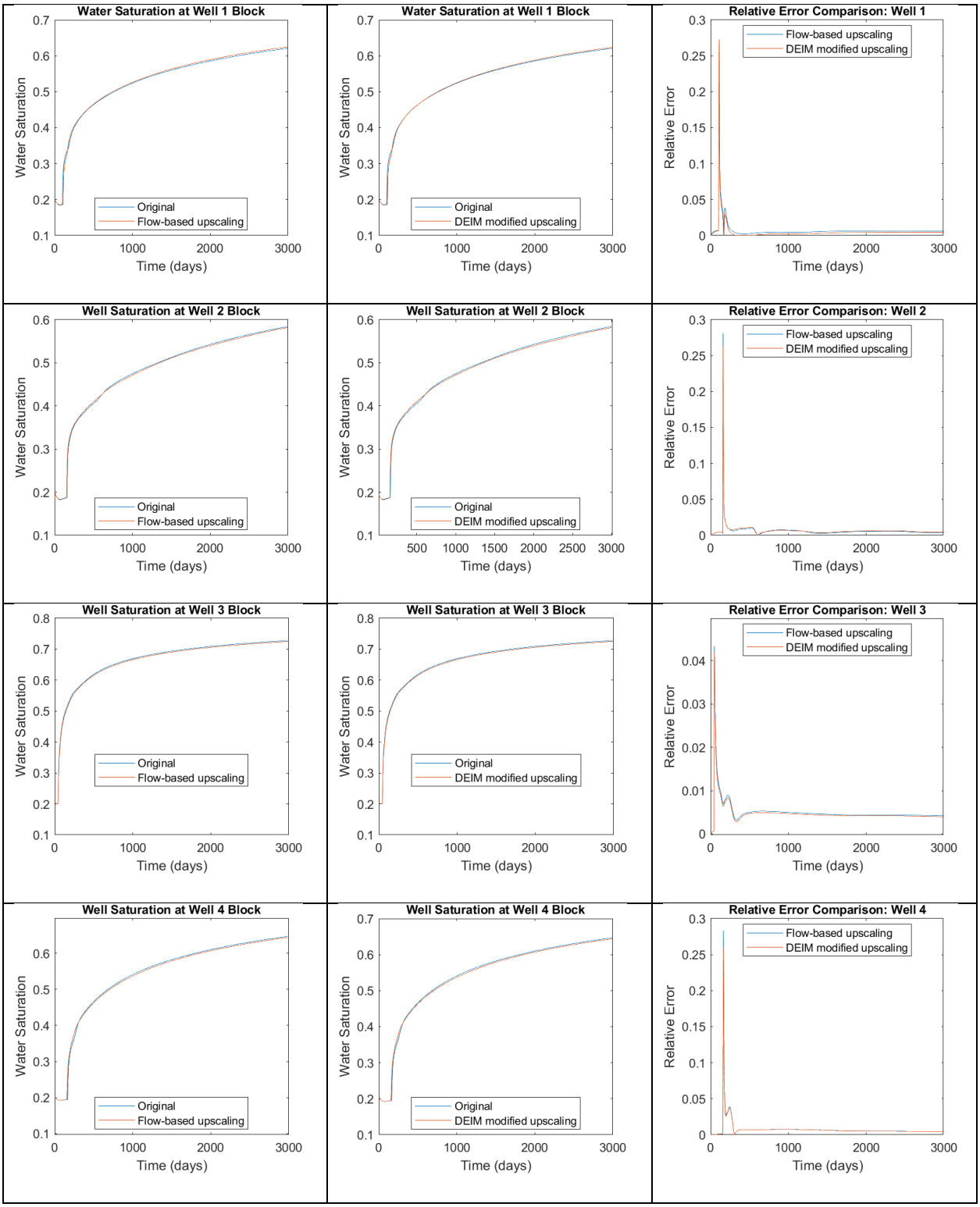

Figure 49 – Layer 10 wells block water saturation comparison for the four producers.

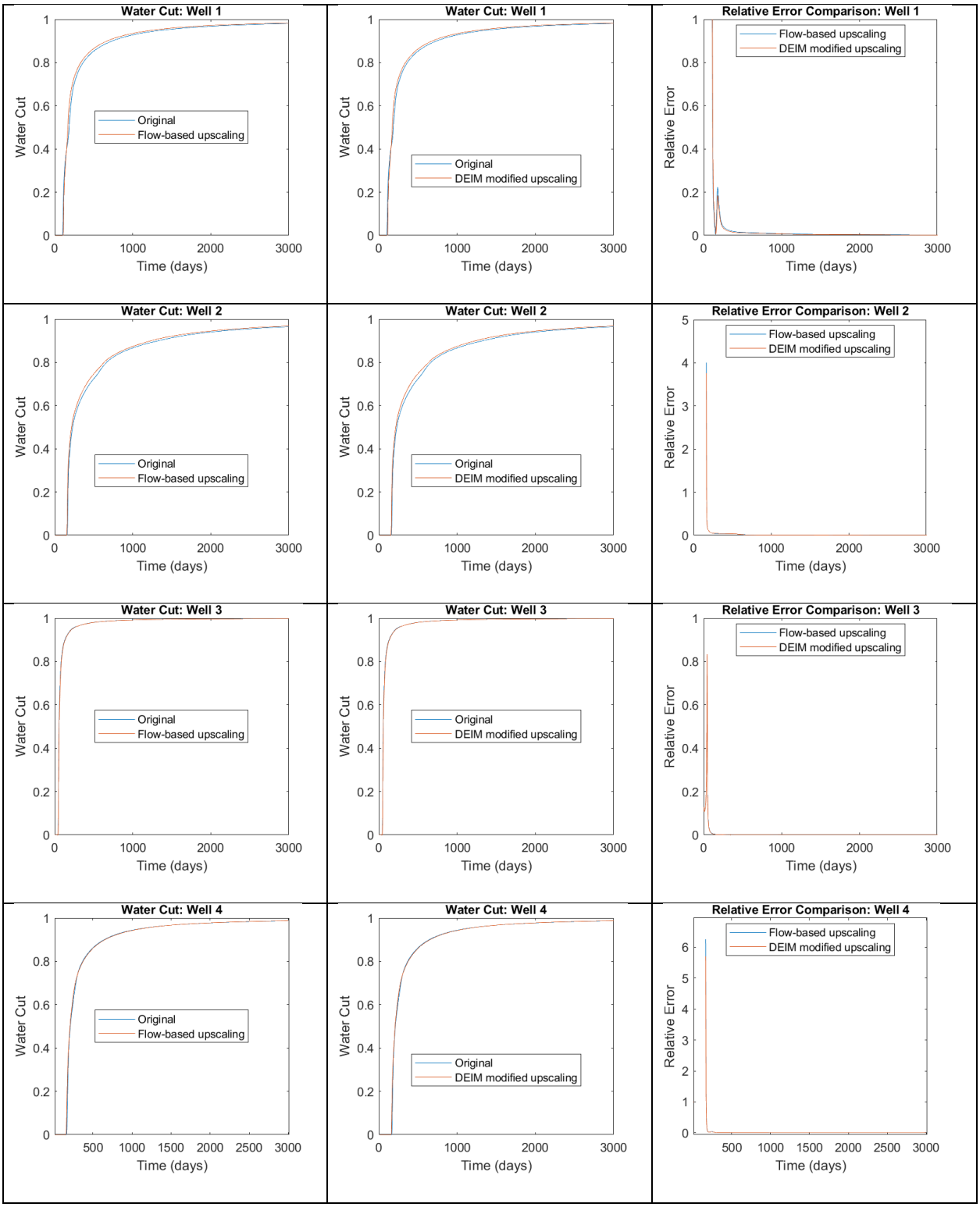

Figure 50 – Layer 10 wells water cut comparison for the four producers.

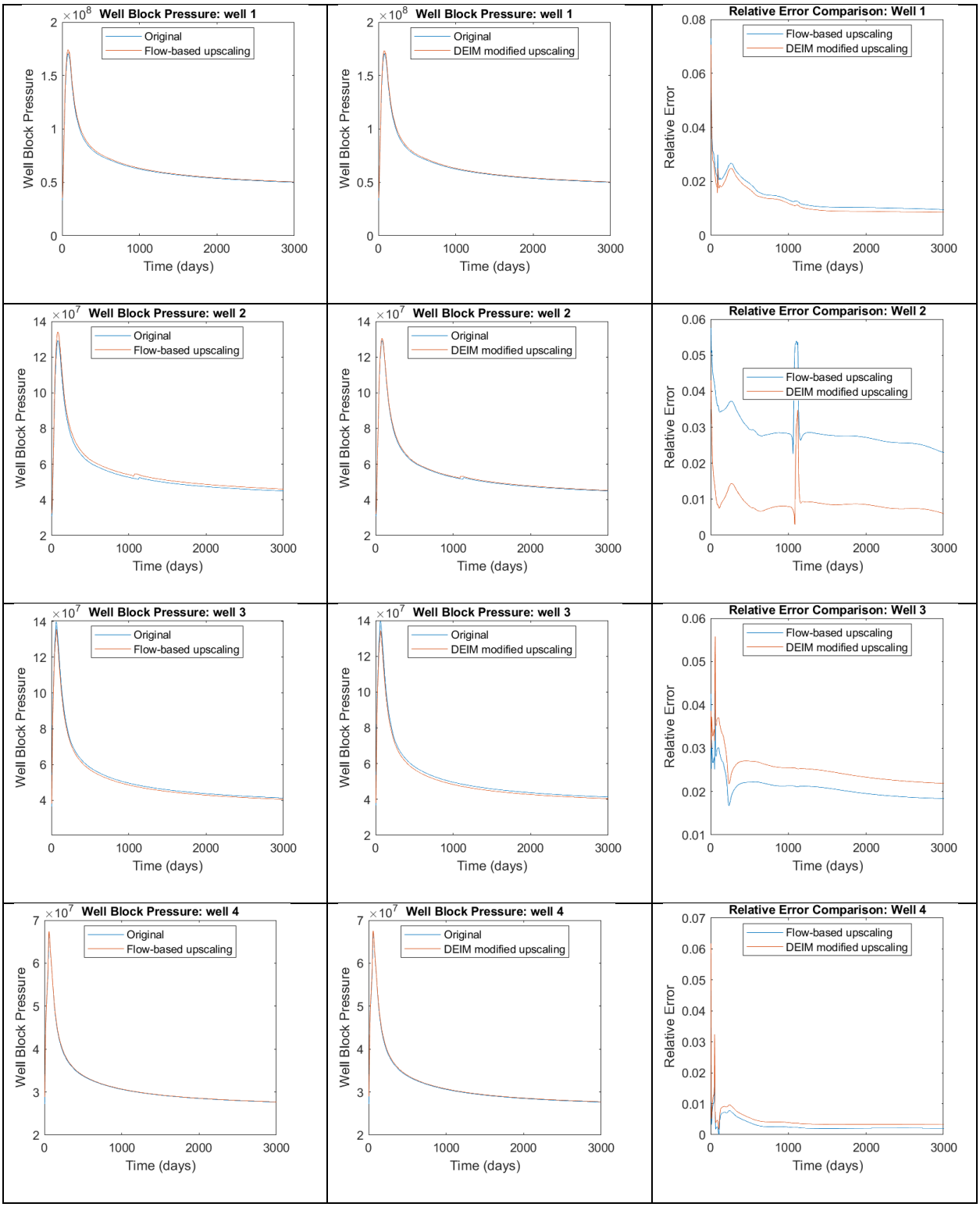

Figure 51 – Layer 30 wells block pressures comparison for the four producers.

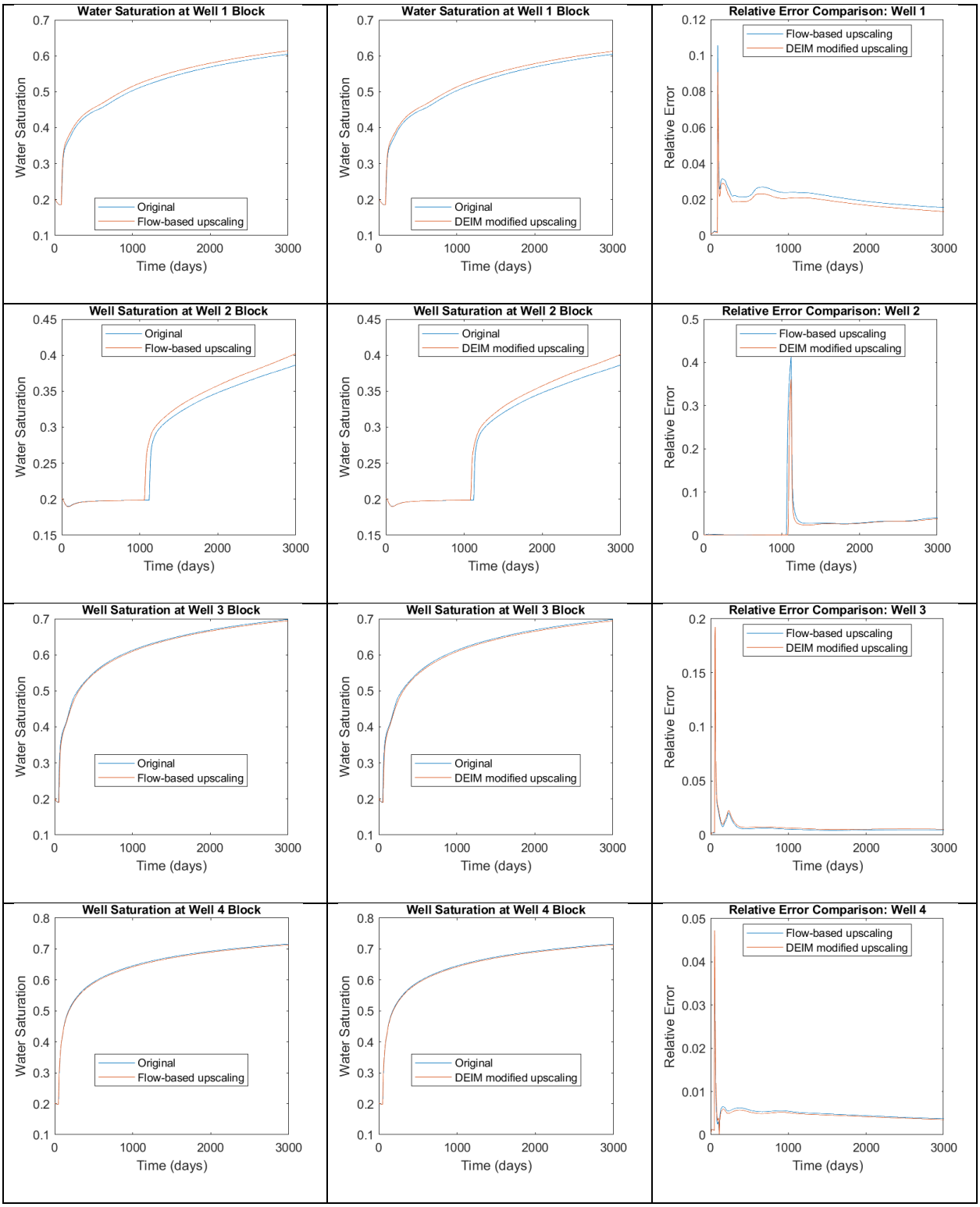

Figure 52 – Layer 30 wells block water saturation comparison for the four producers.

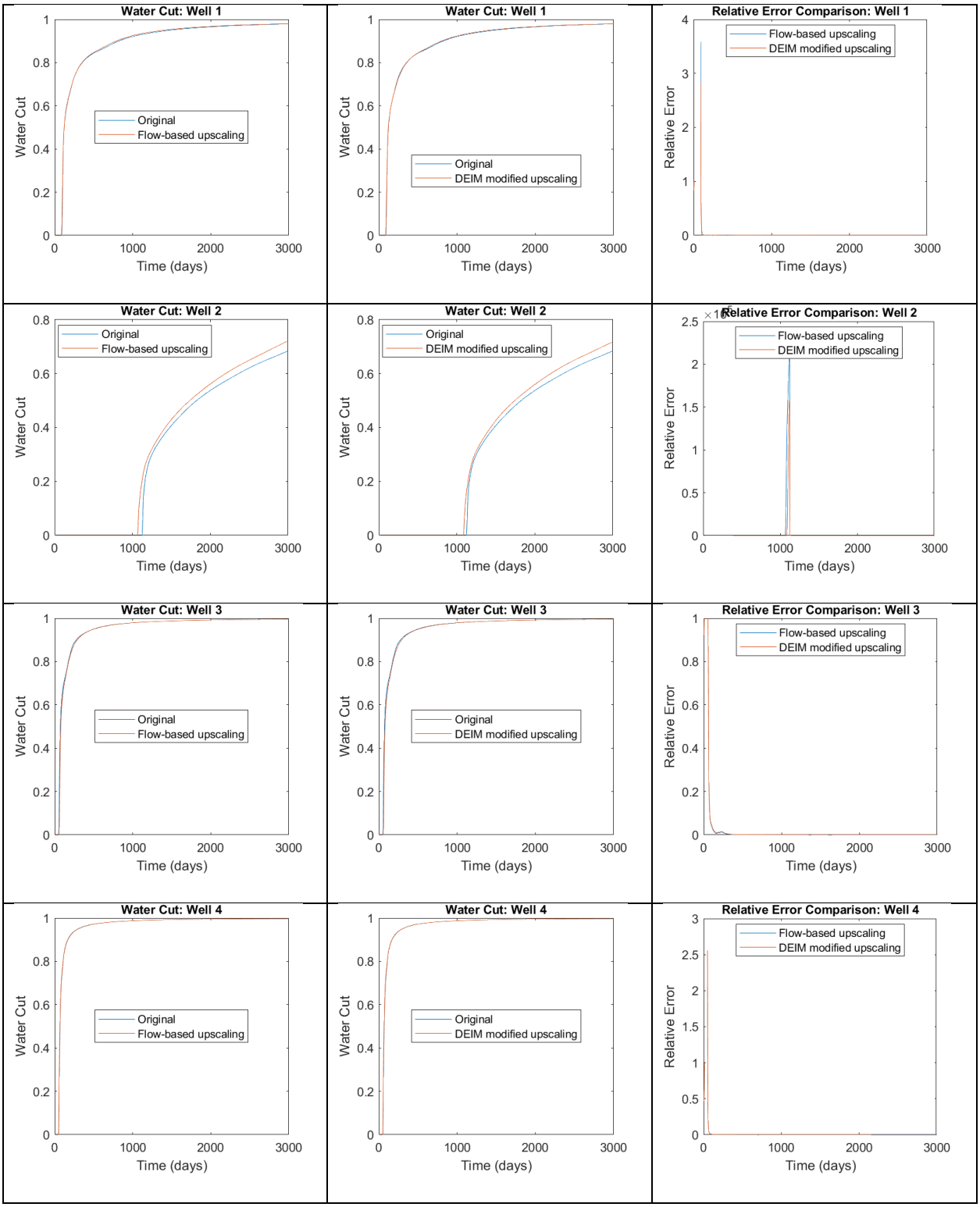

Figure 53 – Layer 30 wells water cut comparison for the four producers.

The measurements for layer 50, 60, and 70 in Upper Ness Formation is demonstrated in **Fig. 54** to **Fig. 62**. Since previously we demonstrated the oil rate matching accuracy is much better in these reservoirs, we expect the well block pressure, water saturation, and water cut be much better as well.

From **Fig. 54** to **Fig. 62**, the well block pressure, water saturation and water cut for 4 wells indeed corroborate our initial promises. The reduction in relative error is more evident, as most of the cases have relative well pressure error reduction, such as P4 of layer 70 has a water cut error reduction of around 3%. Other cases such as the P3 and P4 of layer 60 are consistent with the flow-based ones. Again, the majority test cases exhibit improved or consistent relative error rate reduction than the flow-based upscaling, proving that the combining POD-DEIM index in modifying flow-based permeability yields more accurate reservoir characterization than flow-based upscaling.

Some cases however, exhibits very high relative error in both flow-based upscaling and the DEIM-modified case, such as P2 of layer 50 in **Fig. 55** to **Fig. 57**. The relative error of well block water saturation reaches around 0.6 at the end of production while the water cut ratio close to 1. This discrepancy is due to extremely low oil and water rate in Producer 2. The upscaling process leads to oil rate in that well to rise by a very small amount due to numerical error. However, since the rate is extremely low, this small increment causes water saturation and water cut varying greatly. Such numerical error issue can be mitigated when it is applied in a more realistic, thicker reservoir such that the well production rate is not so low to be affected by numerical error. For example, in layer 30 and layer 60, where each well have a decent oil rate, the well block water saturation and water cut relative error does not show such discrepancy.

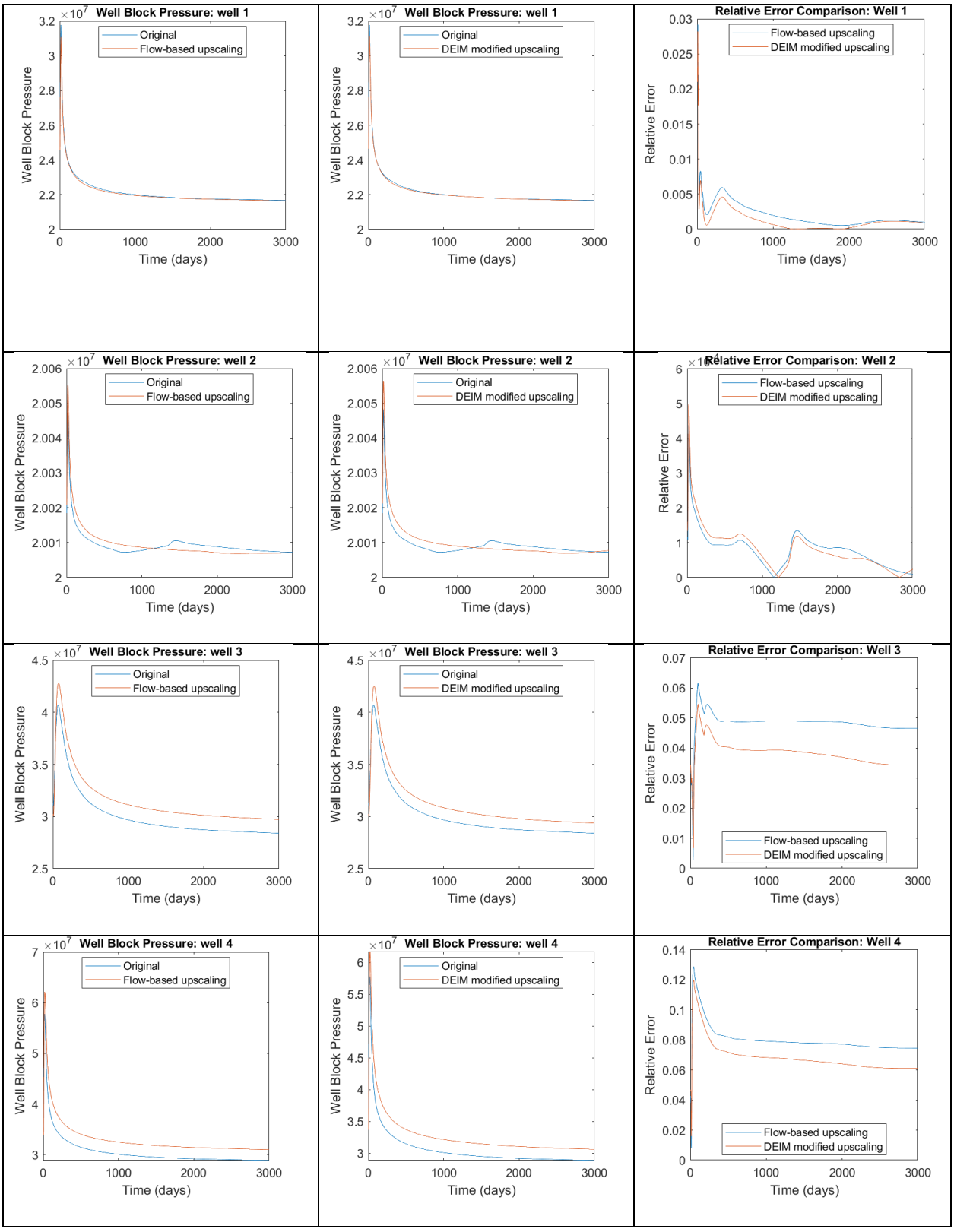

Figure 54 – Layer 50 wells block pressures comparison for the four producers.

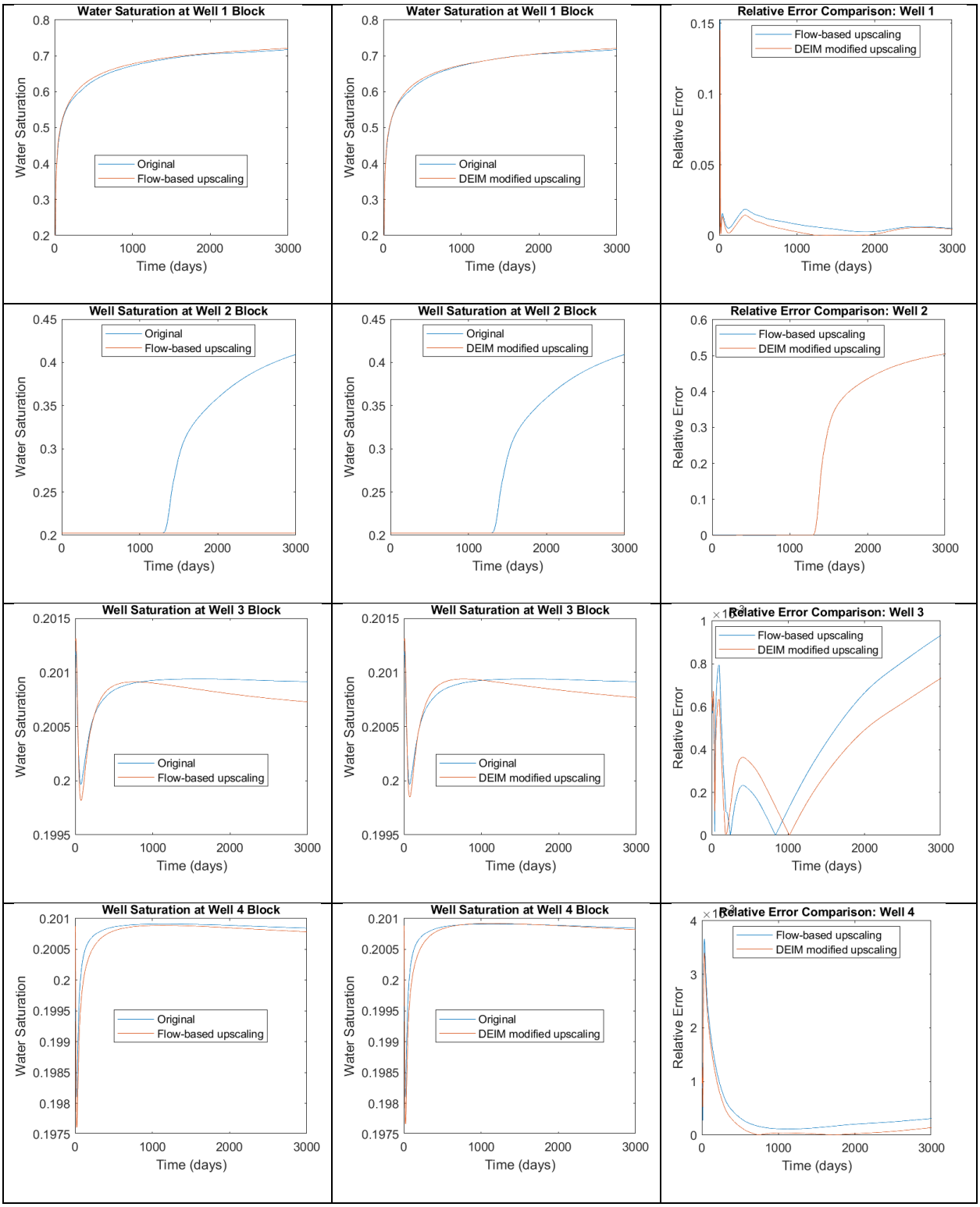

Figure 55 – Layer 50 wells block water saturation comparison for the four producers.

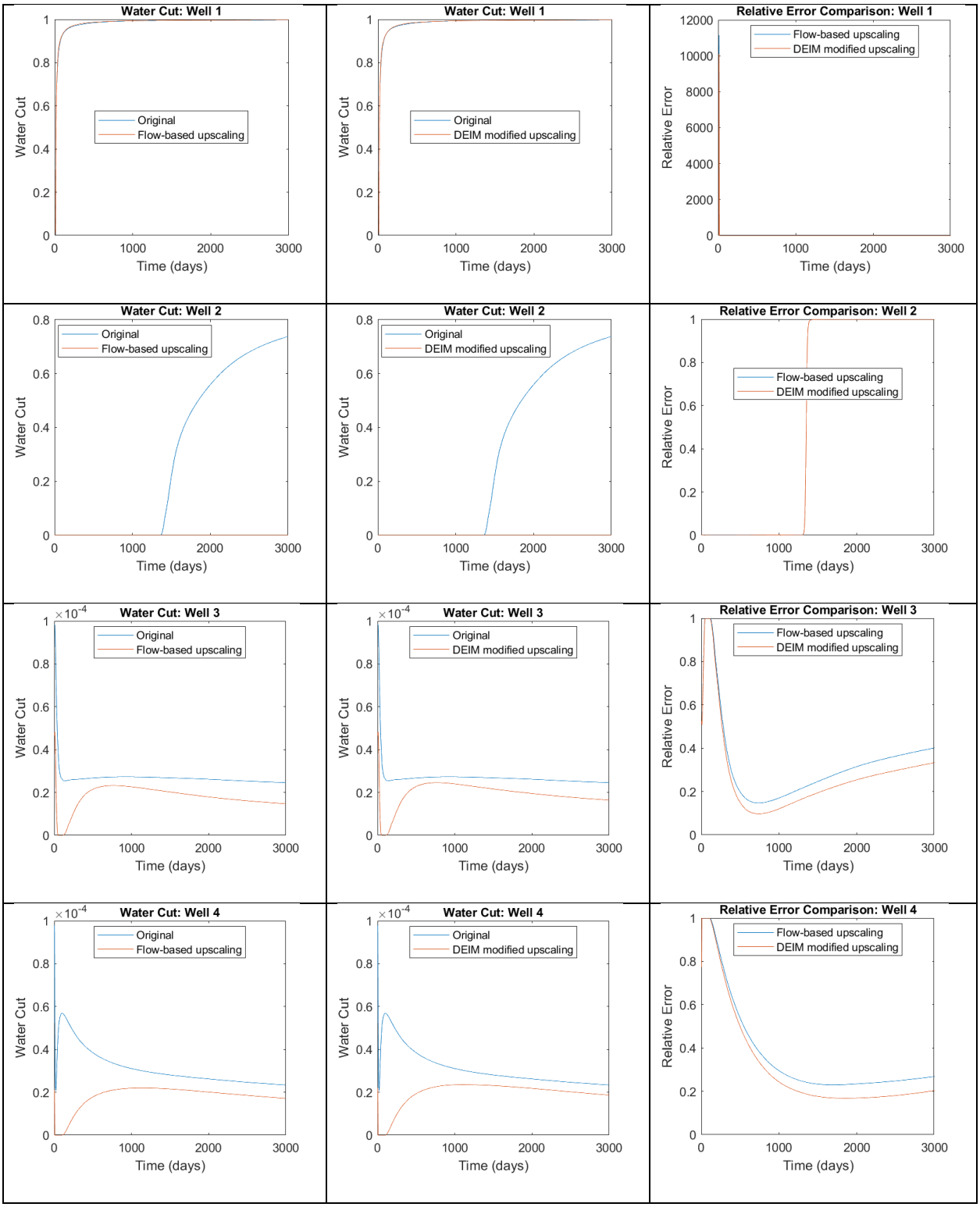

Figure 56 – Layer 50 wells water cut comparison for the four producers.

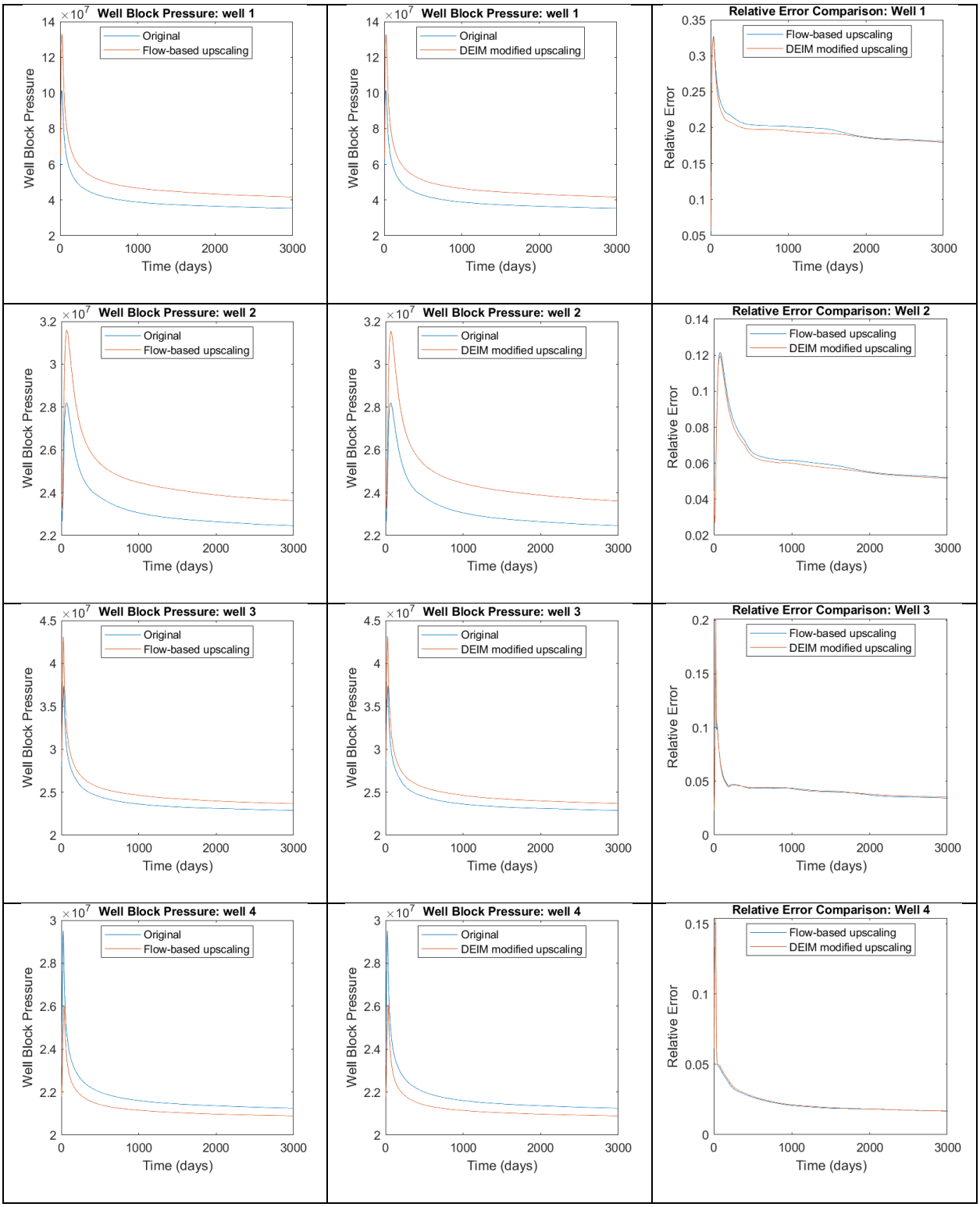

Figure 57 – Layer 60 wells block pressures comparison for the four producers.

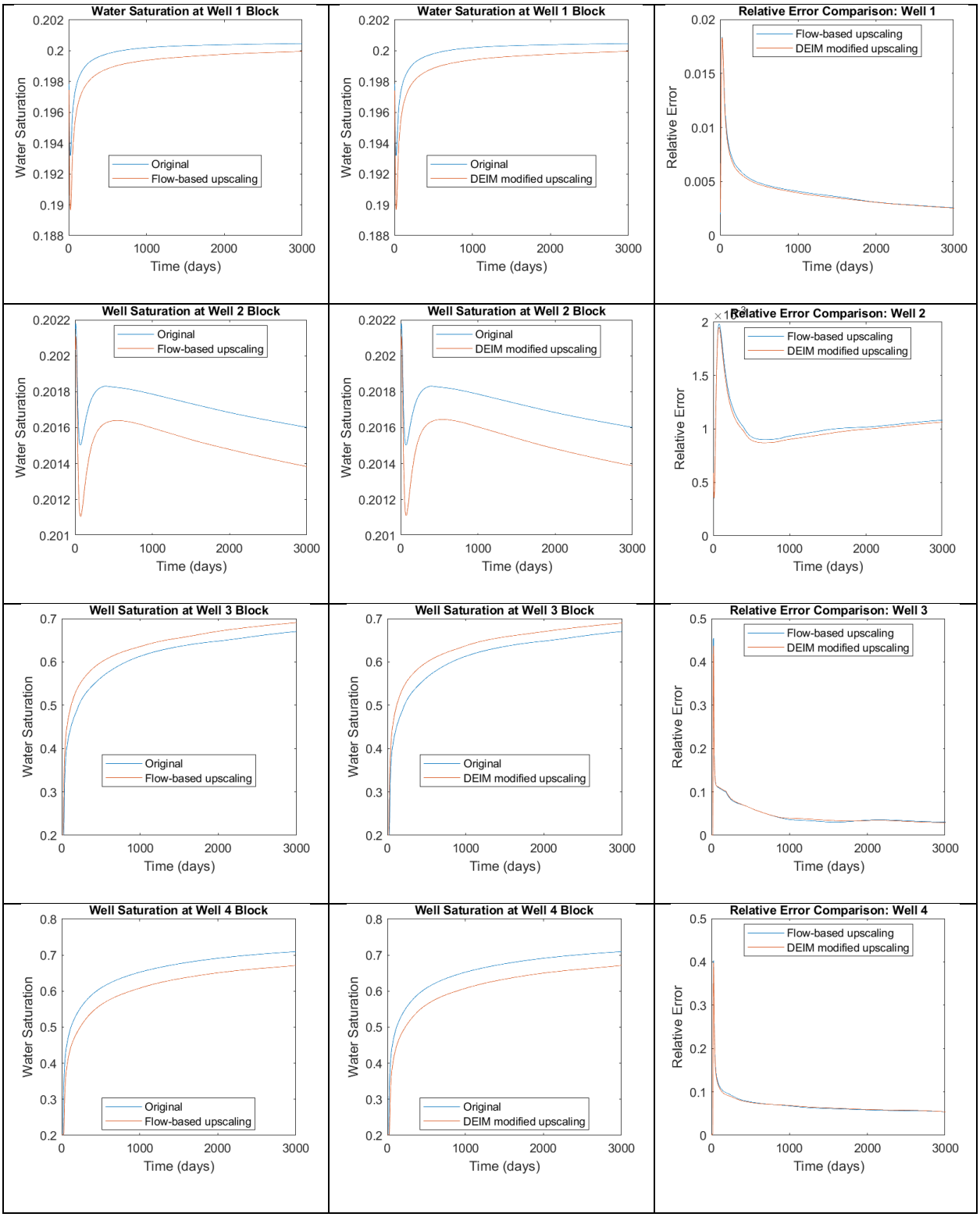

Figure 58 – Layer 60 wells block water saturation comparison for the four producers.

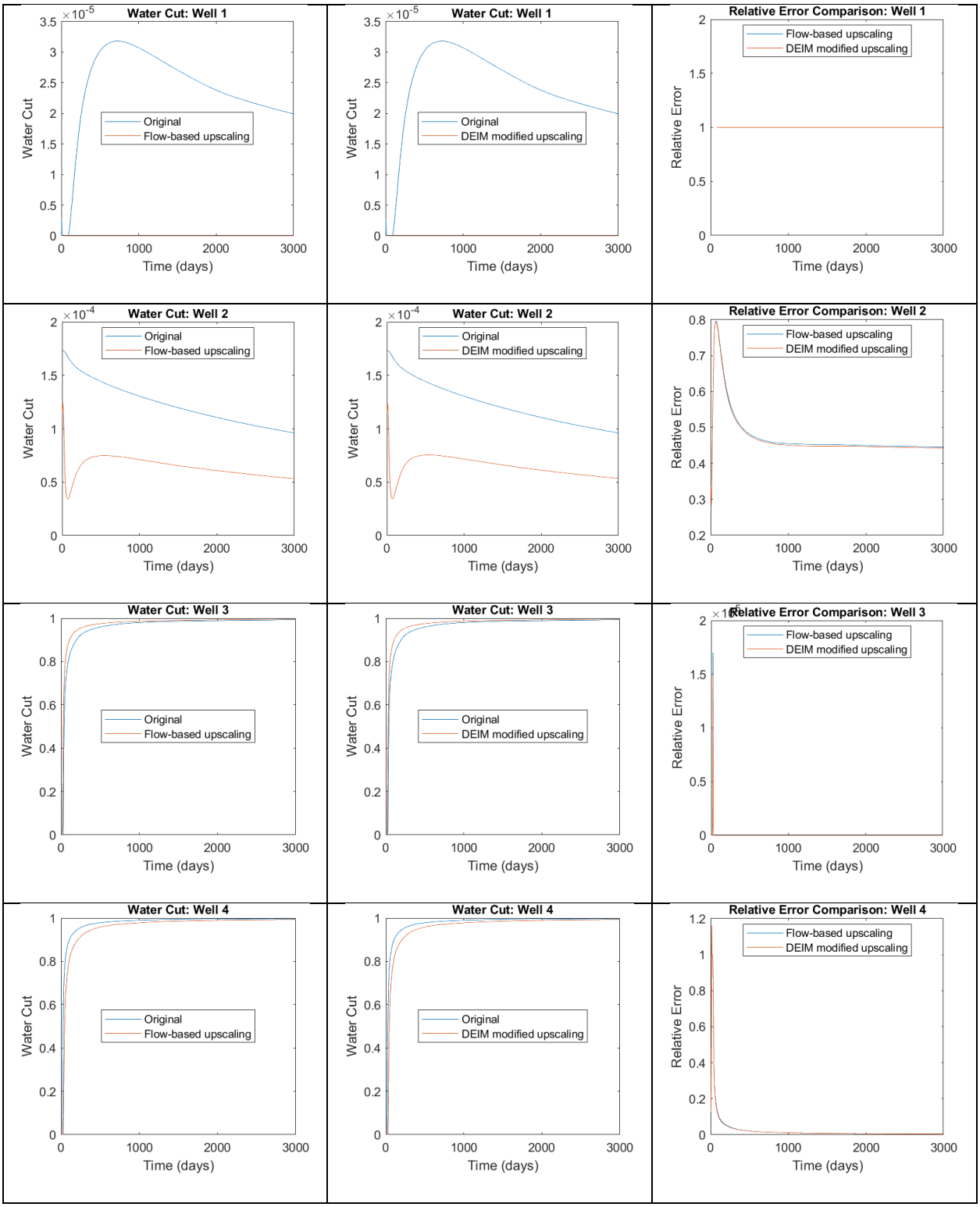

Figure 59 – Layer 60 wells water cut comparison for the four producers.

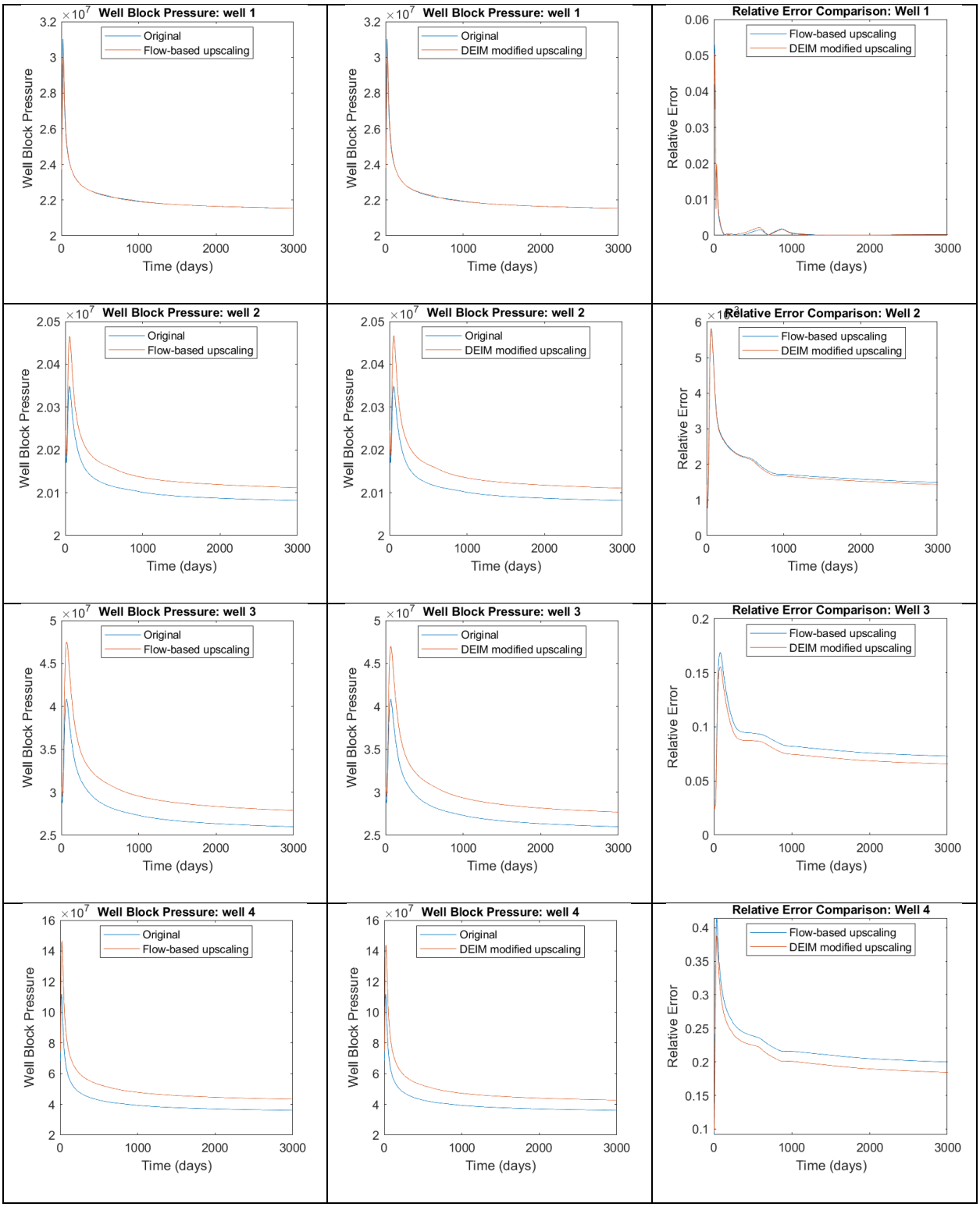

Figure 60 – Layer 70 wells block pressures comparison for the four producers.

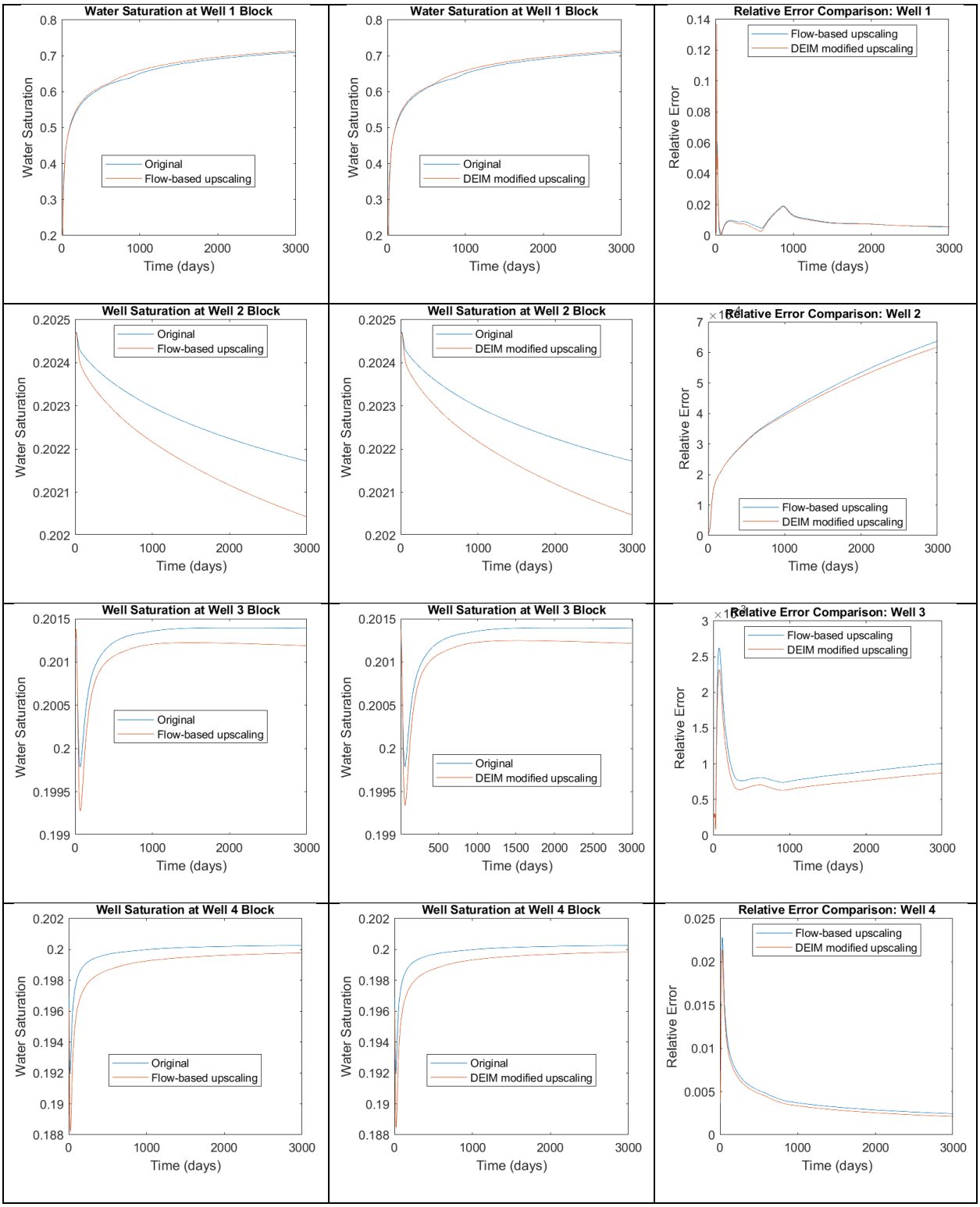

Figure 61 – Layer 70 wells block water saturation comparison for the four producers.

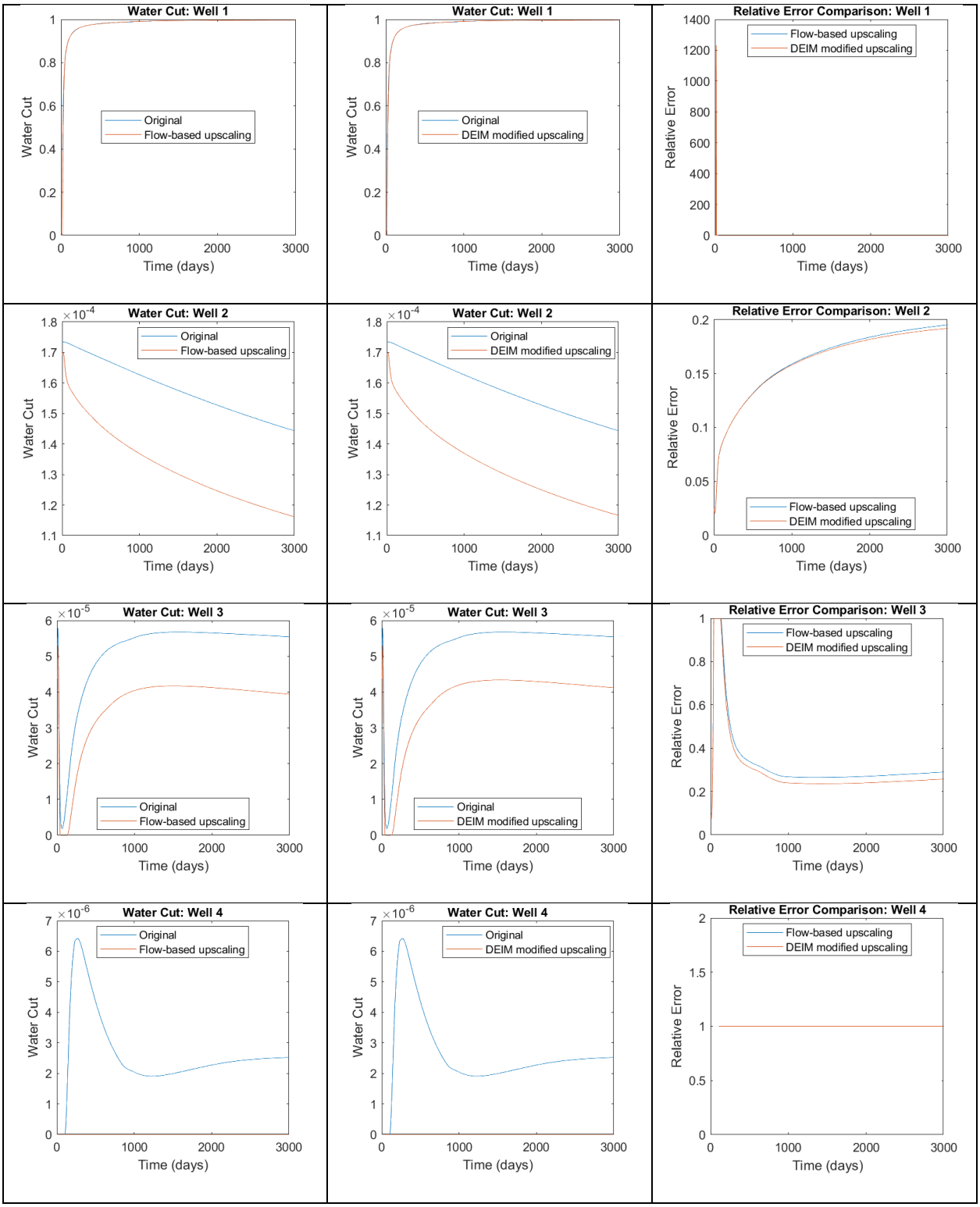

Figure 62 – Layer 70 wells water cut comparison for the four producers.

3.4 Time Reduction and Production Rate Error Comparison

Finally, we analyze the time reduction of these two methods and compare the relative rate error numerically. We compare the online time, which is the time in actual reservoir simulation, and offline time, which is the time to perform upscaling, DEIM index calculation and other parameters used in model reduction. In **Table 6** – **Table 8**, all the time reduction and oil rate error comparison for flow-based upscaling and DEIM modified upscaling are shown. In the 2D model cases, **Table 6** and **Table 7**, both upscaling methods have shown an online reservoir simulation time reduction ranging from 70% to 80%. Whereas in the two 3D model cases **Table 8**, the 2 by 2 by 2 upscaling reduces the online time by over 90%. Comparing the time required to perform offline DEIM index calculation, we conclude that for all cases which have DEIM index of 750, the time required is around 20 seconds, around 2 times than the time required performing flow-based upscaling. This offline time is only a fraction of the online simulation time and needs to be only computed once for a certain production well scheme. Therefore, it is a viable and convenient way to include DEIM index selection in modifying upscaling.

As to the oil production rate error for each well, it is computed with $L2\ norm\ error$ shown in **Eq. 29**. We have boxed the smaller error in green color for visualization. For all cases, at least 3 wells out of 4 have seen an improvement in oil rate production matching with respect to the original full model. The DEIM-modified upscaling mostly has a L2 norm error 1% less than the flow-based upscaling cases, but the actual relative error of reduction of oil rate is around 3% to 5% during production timespan. However, be noted this improvement is only based on 750 DEIM points selection and modification. If we performed a greater number of timesteps, we will be able to obtain a broader range of DEIM index that distributed into other area of the reservoir with lower activity of fluid dynamics, such as zones near water flow path or zones with lower permeability.

Therefore, new overall permeability will have a broader range of permeability difference in compared to the flow-based upscaling base case, thus improving the reservoir characterization and fluid rate matching even more.

In **Table 8** particularly, layer 50, 60, and 70 are all from Upper Ness Formation where there is a distinctive channel feature across the reservoir. Comparing the oil rate matching error in **Table 7** and **Table 8**, and the oil rate relative errors from the previous section, we can conclude that the oil rate error improvement by DEIM selection is better in such complex reservoirs than those from simpler reservoirs in Tarbet Formation. These results prove that DEIM index modification on flow-based upscaling permeability can be extended to more complex reservoir structures and improve the upscaling accuracy for such cases where traditional upscaling techniques cannot provide an accurate model characterization.

$$Production\ rate\ error\ (L2) = \frac{\left|Q_{upscaled} - Q_{original}\right|_2}{\left|Q_{original}\right|_2} \tag{29}$$

Layer 1	Production Oil Rate Error	
	Flow-based Upscaling	POD-DEIM Modified Upscaling
P1	0.0428	0.0428
P2	0.0619	0.0667
P3	0.0205	0.0198
P4	0.0226	0.0206
Overall	0.0207	0.0193

Layer 1		Time(s)	Time reduction
	Full scale	685.7884509	
Online Time	Upscaled (flow-based)	151.5552819	77.90%
	Upscaled (DEIM-modified)	176.5298004	74.26%
Offline Time	Perform upscaling (2 by 2)	10.6963974	
	Perform DEIM (pDEIM = 750)	17.3494	

Layer 10	Production Oil Rate Error	
	Flow-based Upscaling	POD-DEIM Modified Upscaling
P1	0.0879	0.0816
P2	0.0352	0.0349
P3	0.0214	0.0209
P4	0.0274	0.0247
Overall	0.0479	0.0446

Layer 10		Time(s)	Time reduction
	Full scale	516.8444	
Online Time	Upscaled (flow-based)	125.3449	75.75%
	Upscaled (DEIM-modified)	139.9939	72.91%
Offline Time	Perform upscaling (2 by 2)	9.8775	
	Perform DEIM (pDEIM = 750)	18.4975	

Layer 30	Production Oil Rate Error	
	Flow-based Upscaling	POD-DEIM Modified Upscaling
P1	0.0276	0.0254
P2	0.0469	0.0227
P3	0.0464	0.0461
P4	0.0235	0.0226
Overall	0.0245	0.0237

Layer 30		Time(s)	Time reduction
	Full scale	690.8262679	
Online Time	Upscaled (flow-based)	118.669204	82.82%
	Upscaled (DEIM-modified)	148.2933883	78.53%
Offline Time	Perform upscaling (2 by 2)	11.5046643	
	Perform DEIM (pDEIM = 750)	16.6574063	

Table 6 – Oil rate matching comparison and time reduction: Layer 1, 10, 30 from Tarbet Formation.

Layer 50	Production Oil Rate Error	
	Flow-based Upscaling	POD-DEIM Modified Upscaling
P1	0.0985	0.0918
P2	0.3131	0.3417
P3	0.1432	0.1141
P4	0.2289	0.1984
Overall	0.0985	0.0918

Layer 50		Time(s)	Time reduction
	Full scale	527.2722211	
Online Time	Upscaled (flow-based)	108.3111499	79.46%
	Upscaled (DEIM-modified)	139.1828782	73.60%
Offline Time	Perform upscaling (2 by 2)	11.8588015	
	Perform DEIM (pDEIM = 750)	17.4652125	

Layer 60	Production Oil Rate Error	
	Flow-based Upscaling	POD-DEIM Modified Upscaling
P1	0.3991	0.3902
P2	0.4425	0.4317
P3	0.1182	0.1204
P4	0.3652	0.3645
Overall	0.2451	0.2413

Layer 60		Time(s)	Time reduction
	Full scale	442.1532558	
Online Time	Upscaled (flow-based)	104.8366925	76.29%
	Upscaled (DEIM-modified)	115.9039575	73.79%
Offline Time	Perform upscaling (2 by 2)	9.9265666	
	Perform DEIM (pDEIM = 750)	17.8984029	

Layer 70	Production Oil Rate Error	
	Flow-based Upscaling	POD-DEIM Modified Upscaling
P1	0.1447	0.1427
P2	0.3333	0.3264
P3	0.3099	0.2831
P4	0.4458	0.4157
Overall	0.1447	0.1426

Layer 70		Time(s)	Time reduction
	Full scale	565.4184503	
Online Time	Upscaled (flow-based)	110.6569998	80.43%
	Upscaled (DEIM-modified)	145.3010577	74.30%
Offline Time	Perform upscaling (2 by 2)	12.0976986	
	Perform DEIM (pDEIM = 750)	17.4652125	

Table 7 – Oil Rate Matching Comparison and Time Reduction: Layer 50, 60, 70 from Upper Ness Formation.

Layer 1-6	Production Oil Rate Error	
	Flow-based Upscaling	POD-DEIM Modified Upscaling
P1	0.0863	0.0791
P2	0.2417	0.2624
P3	0.3113	0.2768
P4	0.4963	0.4568
Overall	0.0863	0.0782

1-6		Time(s)	Time reduction
	Full scale	8341.79	
Online Time	Upscaled (flow-based)	364.19	95.63%
	Upscaled (DEIM-modified)	421.42	94.95%
Offline Time	Perform upscaling (2 by 2)	51.72	
	Perform DEIM (pDEIM = 750)	18.32	

Layer 50-55	Production Oil Rate Error	
	Flow-based Upscaling	POD-DEIM Modified Upscaling
P1	0.2464	0.2462
P2	0.0633	0.0625
P3	0.2348	0.1522
P4	0.3565	0.3779
Overall	0.0863	0.0785

50-55		Time(s)	Time reduction
	Full scale	7586.79	
Online Time	Upscaled (flow-based)	430.97	94.32%
	Upscaled (DEIM-modified)	522.99	93.11%
Offline Time	Perform upscaling (2 by 2 by 2)	56.96	
	Perform DEIM (pDEIM = 750)	70.54	

Table 8 – Oil Rate Matching Comparison and Time Reduction: 3D cases layer 1-6 and layer 50-55

4. CONCLUSIONS

4.1 Summary

In this research, POD-DEIM model order reduction, conventional flow-based upscaling, and the combined approach of integrating POD-DEIM index onto the modification of flow-based upscaling technique is developed.

To assess the efficiency of POD-DEIM method, a uniform 100 by 100 model is carried out, yielding to a total of 6067 timesteps. The DEIM index is computed with DEIM algorithm performed on the projection matrix from residual snapshots of the full model solution. Different number of DEIM index is computed on the model, and only cases where number of DEIM index greater than 3000 have converged. For cases with lesser DEIM index, the simulation diverges at very early stages.

In upscaling methods, both 2D cases and 3D cases are tested using 2 by 2 upscaling scheme on 2D models and 2 by 2 by 2 upscaling on 3D models. In all models, a two-phase black oil reservoir with no gas content is used, and all the producer and injector wells are set at constant bottom hole flowing pressures and constant rate. Arithmetic, simple harmonic upscaling is carried out to obtain the basic parameters used for modification. Flow-based upscaling generates the base case permeability for modification with DEIM. The oil rate, water cut, water saturation, well block pressure of flow-based upscaling is compared with DEIM-modified upscaling.

Eventually, the new combined method utilizes 750 DEIM index to modify the flow-based upscaling permeability by a newly defined weight-based average that involves the Wiener bound and upscaling coefficient as constraints. The oil production rate matching, well block pressure, water saturation, water cut is compared between flow-based upscaling and the new method.

4.2 Conclusions

To summarize the results of this research, the POD-DEIM standalone case shows that the overall production rate error is less than 10%, but at the cost of performing large amount of timesteps of simulation for a 10000 grids homogeneous reservoir. Another downside of POD-DEIM is the time required for computing each DEIM index, as it grows exponentially. This makes it increasingly difficult to calculate thousands and tens of thousands index, which could require more computational infrastructures. Moreover, a converging POD-DEIM model often requires number of DEIM index at least greater than 30% of total number of grids. Therefore, performing POD-DEIM on large scale reservoir requires large storage of CPU memory. Thus, it is preferable to perform less timesteps, less DEIM index computations while taking advantage of it and combined it with upscaling. In the 10000 cells test case, computing 3000 POD-DEIM indices cost over 350 seconds, but the time grows exponentially as in 4000 POD-DEIM index it takes over 760 seconds, which doubles the time. In large scale reservoir where we would compute thousands or tens of thousands of DEIM indices, computational efforts could be a potential limitation.

In the upscaling part, the traditional flow-based upscaling reduces the computational efforts by coarsening the number of grid blocks. This method shows good oil rate matching with error less than 10% with respect to the full model, especially in less heterogenous reservoirs, such as SPE 10 model layer 1, 10, 30 from the Tarbet Formation. However, in models with complex features such as channels, where in the model layer 50, 60, 70, the oil production rate error is more noticeable, reaching over 20% production matching error in some wells. The time reduction for 2 by 2 upscaling on 2D models is around 70% to 80%, whereas in 3D models, 2 by 2 by 2 upscaling reduces time over 90%. The time required to perform upscaling is only a small fraction of total

simulation time. In 2D cases, around 11 seconds for 60 by 220 grids, whereas it is around 50 seconds for 60 by 220 by 6 3D cases.

To sums up on the combined method, the DEIM modified upscaled permeability does not differs by much compared to the flow-based upscaling. The modified permeability shows a mild reduction in 2D cases relative oil rate error. In channeled reservoirs, the DEIM-modified upscaling reduces the relative oil rate error even more, reaching to 3% to 5% in some wells. In well block water cut, well block pressure and well block water saturation, the new DEIM-modified upscaling also shows a more accurate match to the original model than flow-based upscaling. For 3D cases, 750 DEIM indices cannot effectively populate and capture most area of high fluid dynamic areas. Therefore, the extent of permeability alterations based on these indices are limited. Nevertheless, 3 of the 4 wells in 3D cases are showing descent reduction in relative oil rate production error. It is reasonable to assume it more POD-DEIM indices is computed and applied in the permeability modification process, we would have a more accurate fluid rate matching to the fine scale model and a better coarsen reservoir characterization.

As to the time effort aspect, performing DEIM index calculation is around only 20 seconds for 750 DEIM index. Compared to flow-based upscaling of 10 seconds it is not as fast but can provides better production matching and reservoir characterizations. The online time of DEIM-modified upscaling is very close to that of flow-based upscaling, due to the number of grids is the same. Overall, using POD-DEIM index to alter flow-based upscaling permeability reduces oil production rate error and better characterize coarse scale reservoir properties.

4.3 Recommendation for future work

In this work, only the simplest 2 by 2 (by 2) upscaling is conducted, and the well location, production schemes are identical. For POD-DEIM index, a constant 750 indices are computed and applied in the modification process. The recommendation for future works would be more upscaling schemes, such as 3 by 4, or selective upscaling. Furthermore, different numbers of DEIM indices should be tested out to find what is the optimum number of indices that are used in modification. Mathematically, there could be some connections between DEIM index and by what amount permeability is altered. Thus, a more accurate weight-based alteration could be the focus of future studies.

REFERENCES

Aziz, K., & Settari, A. (1986). Petroleum reservoir simulation. London: Elsevier Applied Science.

Cardoso, M. A. (2009). *Development and application of reduced-order modeling procedures for reservoir simulation*. Stanford University.

Cardoso, M. A., & Durlofsky, L. J. (2010). Linearized reduced-order models for subsurface flow simulation. *Journal of Computational Physics*, *229*(3), 681-700.Tan, X., Gildin, E., Florez, H., Trehan, S., Yang, Y., & Hoda, N. (2019). Trajectory-based DEIM (TDEIM) model reduction applied to reservoir simulation. Computational Geosciences, 23(1), 35-53.

Cardwell Jr, W. T., & Parsons, R. L. (1945). Average permeabilities of heterogeneous oil sands. Transactions of the AIME, 160(01), 34-42.

Chaturantabut, S., & Sorensen, D. C. (2010). Nonlinear model reduction via discrete empirical interpolation. SIAM Journal on Scientific Computing, 32(5), 2737-2764.

Christie, M. A. (1996). Upscaling for reservoir simulation. *Journal of petroleum technology*, *48*(11), 1-004.

Christie, M. A., & Blunt, M. J. (2001, January). Tenth SPE comparative solution project: A comparison of upscaling techniques. In *SPE reservoir simulation symposium*. Society of Petroleum Engineers.

Durlofsky, L. J. (1991). Numerical calculation of equivalent grid block permeability tensors for heterogeneous porous media. *Water resources research*, *27*(5), 699-708.

Durlofsky, L. J. (2005, June). Upscaling and gridding of fine scale geological models for flow simulation. In 8th International Forum on Reservoir Simulation Iles Borromees, Stresa, Italy (Vol. 2024, pp. 1-59).

He, C., & Durlofsky, L. J. (2006). Structured flow-based gridding and upscaling for modeling subsurface flow. *Advances in Water Resources*, *29*(12), 1876-1892.

He, J., & Durlofsky, L. J. (2013, February). Reduced-order modeling for compositional simulation using trajectory piecewise linearization. In *SPE Reservoir Simulation Symposium*. Society of Petroleum Engineers.

Hinze, M., & Volkwein, S. (2005). Proper orthogonal decomposition surrogate models for nonlinear dynamical systems: Error estimates and suboptimal control. In Dimension reduction of large-scale systems (pp. 261-306). Springer, Berlin, Heidelberg.

King, M. J., & Mansfield, M. (1997, January). Flow simulation of geologic models. In *SPE Annual Technical Conference and Exhibition*. Society of Petroleum Engineers.

Lie, K. (2019). Part IV Reservoir Engineering Workflows/ 15 Upscaling Petrophysical Properties. In *An introduction to reservoir simulation using MATLAB/GNU Octave: User guide for the MATLAB reservoir simulation toolbox (MRST)* (pp. 558-596). Cambridge: Cambridge University Press.

Tan, X., Gildin, E., Florez, H., Trehan, S., Yang, Y., & Hoda, N. (2019). Trajectory-based DEIM (TDEIM) model reduction applied to reservoir simulation. Computational Geosciences, 23(1), 35-53.

Tiwary, D. K., Bayuk, I. O., Vikhorev, A. A., & Chesnokov, E. M. (2009). Comparison of seismic upscaling methods: From sonic to seismic. *Geophysics*, *74*(2), WA3-WA14.

Van Doren, J. F., Markovinović, R., & Jansen, J. D. (2006). Reduced-order optimal control of water flooding using proper orthogonal decomposition. *Computational Geosciences*, *10*(1), 137-158.

Vakili, A., & Jansen, J. (2008). Control-Relevant Upscaling. *Europec/EAGE Conference and Exhibition*. doi:10.2118/113647-ms

Yang, Y., Ghasemi, M., Gildin, E., Efendiev, Y., & Calo, V. (2016). Fast multiscale reservoir simulations with pod-deim model reduction. *SPE Journal*, *21*(06), 2-141.